

2022

Wire Arc Additive Manufacturing for Stainless Steel-Nickel Superalloy Bimetallic Components

Tianhao Zhou

Follow this and additional works at: <https://ro.uow.edu.au/theses1>

University of Wollongong

Copyright Warning

You may print or download ONE copy of this document for the purpose of your own research or study. The University does not authorise you to copy, communicate or otherwise make available electronically to any other person any copyright material contained on this site.

You are reminded of the following: This work is copyright. Apart from any use permitted under the Copyright Act 1968, no part of this work may be reproduced by any process, nor may any other exclusive right be exercised, without the permission of the author. Copyright owners are entitled to take legal action against persons who infringe their copyright. A reproduction of material that is protected by copyright may be a copyright infringement. A court may impose penalties and award damages in relation to offences and infringements relating to copyright material.

Higher penalties may apply, and higher damages may be awarded, for offences and infringements involving the conversion of material into digital or electronic form.

Unless otherwise indicated, the views expressed in this thesis are those of the author and do not necessarily represent the views of the University of Wollongong.

Research Online is the open access institutional repository for the University of Wollongong. For further information contact the UOW Library: research-pubs@uow.edu.au



UNIVERSITY
OF WOLLONGONG
AUSTRALIA

Wire Arc Additive Manufacturing for Stainless Steel-Nickel Superalloy Bimetallic Components

This thesis is presented as part of the requirement for the conferral of the degree:

Master of Research

By

Tianhao Zhou

Supervisor:
Huijun Li

School of Mechanical, Materials, Mechatronics and Biomedical Engineering

Faculty of Engineering and Information Sciences

University of Wollongong

March 2022

Abstract

Nickel superalloys have commonly been used in the aerospace, maritime platform, and nuclear industry; because of their high mechanical performance, high thermal creep strength, high corrosion resistance and oxidation resistance, it is one of the best choices for severe environments such as high temperature, high pressure, and corrosive environment. However, due to its high fabrication cost, it is unnecessary to build all the workpieces up with nickel alloys; an appropriate method for manufacturing dual-layer structure with nickel superalloys and body materials has great potential for reducing the material cost without compromising the overall performance.

In addition, the high mechanical properties give nickel alloys an edge in industrial production. However, it also limits the manufacturing process of nickel alloys as well—the high strength makes the conventional “subtraction” manufacturing process a difficult task, especially for joining dissimilar materials that require a more accurate shape of the part. Additive manufacturing (AM) processes can build a workpiece with complex geometry. With several AM processes evaluated, the Wire arc additive manufacturing (WAAM) process is considered the best choice for manufacturing these high-strength alloys joined with dissimilar materials for producing quality bimetallic parts.

In this study, a series of nickel alloy and stainless steel (commonly used material in manufacturing) bimetallic walls were successfully fabricated via the Gas-shielded metal arc welding (GMAW) process with an interweaving building strategy. The as-built walls have no obvious macroscopic defects, but optical microscopy can observe hot cracks. The microstructure and cracking behaviour on the cross-section of as-built samples have been thoroughly analysed. The result shows microstructure and hardness of as-built specimens are similar to that of the samples fabricated by other AM

Abstract

processes, and it is also revealed the number of cracking of IN718-SS316 bimetallic material are strongly related to welding parameters such as interpass temperature, cooling method, torch angle and heat input (Wire feed speed & Traveling speed).

Acknowledgments

I wish to express my sincere appreciation and gratitude to my supervisor, Prof. Huijun Li, for his valuable guidance, support, inspiration, close supervision, and good friendship during my master's career at the University of Wollongong (UOW). The assistance he provided in my studies this year is critical for successfully completing my work.

I would like to express my warmest thanks to Dr Yuxing Li, Yan Ma, Zhijun Qiu, Binta Wu and Bosheng Dong for their valuable discussion, good friendship, and encouragement.

I am deeply grateful to the UOW Welding and Industrial Automation Research Centre staff and Australia's Nuclear Science and Technology Organisation for their expertise and extensive use of facilities. A special thanks to Matthew Franklin and Michael Grantham for their support.

I would also like to convey sincere appreciation to all the Faculty of Engineering and Information Science members at UOW and Engineering Enquiry Centre staff for assisting in administration works.

A special thanks to Wenxue Li and my parents for their encouragement and mental support cheered me up throughout my study.

Finally, I wish to express my sincere thanks to my friends and groupmates for their support and encouragement during my Master of Research career.

Certification

I, Tianhao Zhou, declare that this thesis submitted in fulfilment of the requirements for the conferral of the degree Master of research (Material Engineering) from the University of Wollongong, is wholly my work unless otherwise referenced or acknowledged. This document has not been submitted for qualifications at any other academic institution.

Tianhao Zhou

8th March 2022

List of Names or Abbreviations

List of Names or Abbreviations

3DP	3D printing
AISI	American Iron and Steel Institute
AM	Additive manufacturing
ANSTO	Australian Nuclear Science and Technology Organization
ASTM	American Society for Testing and Materials
A-TIG	Activated flux tungsten inert gas welding method
BCT	Body-centred- Tetragonal
BJ	Binder Jetting
BM	Base metal
CAD	Computer-aided design
CBN	Cubic Boron Nitride
CC-GTAW	Constant current gas tungsten arc welding
CEM	Composite Extrusion Modelling
CLs	Gas-based coolant-lubricants
CMT	Cold metal transfer
CMT-PADV	Cold metal transfer pulse advanced
CP-GTAW	Conventional pulsed gas tungsten arc welding
DED	Directed Energy Deposition
DMLS	Direct metal laser sintering
EBF ³	Electron beam freeform fabrication
EBM	Electron beam melting
EBW	Electron beam welding
EDM	Electrical discharged machining
EDS	Electrical dispersive spectroscopy
ESR	Electro-slag Remelting
FCC	Face-centred-cubic

List of Names or Abbreviations

FGM	Functionally graded material
FSW	Friction Stir welding
GCP	Geometrically close-packed phases
GMAW, MIG	Gas-shielded metal arc welding
GTAW, TIG	Gas tungsten arc welding
GTCAW	Gas tungsten constricted arc welding
HAZ	Heat affected zone
HCP	Hexagonal Closest Packed
HIP	Hot isostatic pressing treatment+ aging
IC	Investment Casting
INC	International Nickel Company
LBW	laser beam welding
LBW	Laser beam welding
LC	Laser consolidation
MJ	Material Jetting
MAO-GTAW	Magnetic arc oscillation TIG welding
OM	Optical microscope
PCBN	Polycrystalline cubic boron nitride
PP	Precipitation
PREN	Pitting resistance equivalence number
PVD	Physical vapour deposition
PAW	Plasma arc welding
SA	Solution treatment+ aging
SAC	Strain age cracking
SE	Stress equalising
SEM	Scanning electron microscope
SFE	Stacking fault energy
SLM	Selective laser melting
SLS	Selective laser sintering

List of Names or Abbreviations

SMAW	Shielded metal arc welding
SMC	Special Metals Corporation
SPT	Small punch test
SS	Solid solution
SV	Stress relieving
TCP	Topologically Close-Packed
UC	Ultrasonic consolidation
UHFP-GTAW	Ultra-high frequency pulsed gas tungsten arc welding
UTS	Ultimate tensile strength
UOW	University of Wollongong
VAR	Vacuum Arc Remelting
VIM	Vacuum Induction Melting
WAAM	Wire arc additive manufacturing
WEDM	Discharge Machining
YS	Yield strength

Table of Contents

Abstract.....	I
Acknowledgments	III
Certification.....	V
List of Names or Abbreviations	VI
Table of Contents.....	X
List of Tables, Figures, and Illustrations	XIV
Figure Caption	XIV
Table Caption.....	XVI
Chapter 1 Project Statement.....	1
Chapter 2 Literature Review	3
2.1 Superalloys	3
2.1.1 Introduction	3
2.1.2 Mainly used superalloys in manufacturing.....	5
2.1.3 Strengthening mechanisms	9
2.2 Nickel-based Superalloys	11
2.2.1 Introduction	11
2.2.2 Producing nickel superalloys	15
2.2.3 Processing Ni-based superalloys	19
2.2.4 Microstructure of nickel alloys.....	38
2.3 Inconel Superalloys	45
2.3.1 Elements in Inconel alloys.....	45
2.3.2 Mechanical properties of Inconel	47
2.3.3 Corrosion and oxidation resistance of Inconel	57
2.4 Stainless Steel	63
2.4.1 Introduction	63
2.4.2 Categories of stainless steel.....	64
2.4.3 Characteristics & Properties of austenitic stainless steel.....	68
2.5 Wire Arc Additive Manufacturing	75
2.5.1 AM and AM for Metals	75

Table of contents

2.5.2 WAAM	77
2.5.3 Joining dissimilar metals by WAAM	80
2.5.4 Common defects in WAAM parts and improvement	82
Chapter 3 Research Approach and Methodology.....	127
3.1 Materials	127
3.2 Experimental Equipment	127
3.3 Metallography.....	129
3.3.1 Preparation.....	129
3.3.2 Optical microscope (OM).....	130
3.3.3 Scanning electron microscope (SEM)	131
3.3.4 Electrical dispersive spectroscopy (EDS).....	132
3.4 Mechanical Properties	132
3.4.1 Vickers hardness testing	132
3.4.2 Small punch test (SPT)	132
Chapter 4 Material Selection	136
4.1 Introduction	136
4.2 Experimental Procedures	136
4.3 Results and Discussion	137
4.3.1 Macrostructure.....	137
4.3.2 Microstructure of specimens	139
4.3.3 Observation of cracks	142
4.3.4 Microhardness	145
4.4 Conclusion	147
Chapter 5 Hot Crack Investigation	151
5.1 Introduction	151
5.2 Experimental Procedure	151
5.3 Results and Discussion	154
5.3.1 Macrostructure.....	154
5.3.2 Microstructure	155
5.3.3 Observation of hot cracks	157
5.3.4 SEM-EDS observation	161

Table of contents

5.3.5 Mechanical properties.....	163
5.4 Conclusion	170
Chapter 6 Summary and Future Research	171
Reference	173

List of Tables, Figures, and Illustrations

Figure Caption

<i>Figure 2.1.1. Illustration of Simple cubic, Body-centred cubic, Face-centred cubic metallic crystal structure.....</i>	<i>4</i>
<i>Figure 2.1.2. Comparison of Stress rupture strength between different materials in a high temperature</i>	<i>5</i>
<i>Figure 2.1.3. The comparison of the stress rupture of three different kinds of superalloys (Precipitation, Carbide, Solid solution strengthened alloys).....</i>	<i>6</i>
<i>Figure 2.1.4. The comparison of yield strength between nickel-based superalloy and steel..</i>	<i>7</i>
<i>Figure 2.1.5. Two types of solid solution strengthening (Substitutional and Interstitial)</i>	<i>9</i>
<i>Figure 2.2.1. The schematic of the WEDM system</i>	<i>28</i>
<i>Figure 2.2.2. An image of metallic contaminant on the nickel alloy surface after air exposure[72]</i>	<i>31</i>
<i>Figure 2.2.3. Microstructure of etched Inconel 718 etched by Kalling II reagent under the observation of Optical Microscope [93]</i>	<i>42</i>
<i>Figure 2.2.4. a) The Optical microscope image b) the SEM image of Super cast 247A Superalloy [94].....</i>	<i>42</i>
<i>Figure 2.2.5. The SEM image of as casted superalloy 17 [95]</i>	<i>43</i>
<i>Figure 2.2.6. The SEM image of carbides [96]</i>	<i>43</i>
<i>Figure 2.2.7. SEM images of needle-like TCP phases in nickel-based superalloy [96].....</i>	<i>44</i>
<i>Figure 2.3.1. Distribution of microhardness of welded Inconel 718 joint.....</i>	<i>53</i>
<i>Figure 2.3.2. The high-temperature performance of Inconel 718 bar [108].....</i>	<i>55</i>
<i>Figure 2.4.1. Comparison of impact strength in temperature between (a) austenitic steel, (b) duplex steel and (c) ferritic steel.....</i>	<i>71</i>
<i>Figure 2.4.2. Relative creep rupture strength (100,000 hrs.) comparison between a series of stainless steels [172].....</i>	<i>74</i>
<i>Figure 2.5.1. Categories of main AM process for metal and the proportion in the market (2020).....</i>	<i>77</i>
<i>Figure 2.5.2. Interrelationships between materials and defect tendency in WAAM [181]....</i>	<i>83</i>
<i>Figure 2.5.3. The typical image of (a) Solidification cracking and (b) liquation cracking [220]</i>	<i>87</i>
<i>Figure 3.2.1. Illustration of GMAW welding system in this study.</i>	<i>128</i>
<i>Figure 3.2.2. Illustration of (a) double welding torch and (b) the principle of the twin welding torch.....</i>	<i>129</i>
<i>Figure 3.3.1. Struers automatic polisher Tegrapol 21</i>	<i>130</i>
<i>Figure 3.3.2. The preparation of small punch test samples</i>	<i>130</i>
<i>Figure 3.3.3. Leica DMR optical microscope.....</i>	<i>131</i>
<i>Figure 3.3.4. JEOL 6000 operating Scanning Electron Microscope.....</i>	<i>131</i>
<i>Figure 3.4.1. MATSUZAWA Vickers automatic hardness tester</i>	<i>132</i>
<i>Figure 4.3.1. Three thin wall samples (a) Inconel 718 (IN718)-stainless steel 316 (SS316), (b)</i>	

List of Tables, Figures, and Illustrations

<i>Inconel 625 (IN625)-stainless steel 316 (SS316), (c) Monel 400 (M400)-Mild steel (LCS)..</i>	<i>137</i>
<i>Figure 4.3.2. The image of three samples and their cross-section cuts</i>	<i>138</i>
<i>Figure 4.3.3 (1). The representative microstructure in both SS316 and IN718 sides of Wall 1</i>	<i>139</i>
<i>Figure 4.3.3 (2). The representative microstructure in both IN625 and SS316 sides of Wall 2</i>	<i>140</i>
<i>Figure 4.3.3 (3). The representative microstructure in both LCS and M400 sides of Wall 3</i>	<i>140</i>
<i>Figure 4.3.3 (4). Microstructure of nickel alloys sites in as-built walls under 50*10 magnification</i>	<i>141</i>
<i>Figure 4.3.4 (1). Image of cracks in Inconel 718-stainless steel 316 wall observed via Optical Microscope (etched)</i>	<i>142</i>
<i>Figure 4.3.4 (2). Image of cracks in Inconel 625-stainless steel 316 wall observed via Optical Microscope (etched)</i>	<i>143</i>
<i>Figure 4.3.4 (3). Image of cracks in Monel 400-Mild steel wall observed via Optical Microscope (unetched).....</i>	<i>143</i>
<i>Figure 4.3.5 (1). Hardness distribution from the bottom to the top in the cross-section of Wall 1 (SS316/IN718).....</i>	<i>145</i>
<i>Figure 4.3.5 (2). Hardness distribution from the bottom to the top in the cross-section of Wall 2 (SS316/IN625).....</i>	<i>145</i>
<i>Figure 4.3.5 (3). Hardness distribution from the bottom to the top in the cross-section of Wall 3 (LCS/M400).....</i>	<i>146</i>
<i>Figure 5.3.1. Six walls under different welding parameters and conditions.</i>	<i>154</i>
<i>Figure 5.3.2. The representative microstructure in both SS316 and IN716 sides of Wall 6</i>	<i>155</i>
<i>Figure 5.3.3. Microstructure of wire and arc additively manufactured (a) SS316 [237] and (b) IN718 [238].....</i>	<i>156</i>
<i>Figure 5.3.4. The representative microstructure in the interface of Wall 6.</i>	<i>156</i>
<i>Figure 5.3.5. Distribution map of existing micro-cracks of WAAM built six walls</i>	<i>158</i>
<i>Figure 5.3.6 (1). Microstructure of hot cracks exist in Wall 4.....</i>	<i>159</i>
<i>Figure 5.3.6 (2). Microstructure of hot cracks exist in Wall 6.....</i>	<i>160</i>
<i>Figure 5.3.7 (1). (a) SEM image of the observed interface area in Wall 6; (b) SEM-EDS elemental maps—elemental distribution at the interface in Wall 6; (c) Composition of elements in the observed interface area in Wall 6.....</i>	<i>162</i>
<i>Figure 5.3.7 (2). Line analysis of the elemental distribution near the crack existed at the interface.</i>	<i>163</i>
<i>Figure 5.3.8 (1). Vickers hardness comparison from top to bottom of Wall 5</i>	<i>164</i>
<i>Figure 5.3.8 (2). Vickers hardness comparison from top to bottom of Wall 6</i>	<i>165</i>
<i>Figure 5.3.9 (1). Diagram of SPT data of specimens from Wall 5.....</i>	<i>166</i>
<i>Figure 5.3.9 (2). Diagram of SPT data of specimens from Wall 6.....</i>	<i>166</i>
<i>Figure 5.3.10. Determination of elastic-plastic force</i>	<i>167</i>
<i>Figure 6.1. The as-fabricated IN718-SS316 bimetallic cylinder.</i>	<i>171</i>

Table Caption

<i>Table 2.2.1. Classification of nickel alloys.....</i>	<i>12</i>
<i>Table 2.2.2. The constituent elements of some forms of carbides [49].....</i>	<i>41</i>
<i>Table 2.3.1. The mechanical properties of typical Inconel alloy 718 at room temperature ..</i>	<i>48</i>
<i>Table 2.3.2. The mechanical properties of typical Inconel alloy 625 at room temperature ..</i>	<i>49</i>
<i>Table 2.3.3. The effect of different welding methods on mechanical properties of Alloy 718 [120]</i>	<i>50</i>
<i>Table 2.3.4. Vickers hardness value of Inconel 718 specimens under different annealing conditions [135]</i>	<i>54</i>
<i>Table 2.3.5. Comparison of corrosion rate (miles per year) between different austenitic alloys [141]</i>	<i>59</i>
<i>Table 3.1.1. Elemental components of materials used in this study.....</i>	<i>127</i>
<i>Table 3.3.1. Metallography polishing process of as-fabricated samples.....</i>	<i>130</i>
<i>Table 4.2.1. Welding parameters of fabricated bimetallic walls.....</i>	<i>137</i>
<i>Table 5.2.1. Comparative experiments plan with modified working parameters</i>	<i>153</i>
<i>Table 5.2.2. Welding parameters and heat inputs of as-fabricated walls.....</i>	<i>153</i>

Chapter 1 Project Statement

Background

Superalloys are a kind of metal with high performance at a high temperature due to their unique components and microstructure [1]. Unlike ordinary metallic materials, they behave a high level of mechanical performance, creep resistance, thermal and oxidation resistance even near their melting point, which makes them a reliable material that can be used in severe environments such as aerospace, submarine area, and nuclear industries.

As its name reveals, a nickel-based superalloy is a superalloy whose main element is nickel. It has been developed in the last century and is getting widely used as engine parts, gas turbines, vessels, etc. It is one of the most concentrated superalloys because of the superior performance and outstanding advantages over other superalloys—lower cost, higher performance than Co-based alloy, and more stability than Iron-based superalloys (prone to generate detrimental phases due to its complex elemental compositions). However, the processing has become an issue due to its perfect performance—its high strength may lead to mechanical degradation or even structural deformation of built parts [2].

Stainless steel is one of the most significant materials from industries to our daily life; there is a kind of stainless steel—the austenitic stainless steel in the big family can be used in severe environments similar to the function of superalloys, although it has a lower cost than that of the superalloys, it also has poorer performance than that of the superalloys.

Problem statement

Both stainless steel and nickel-based superalloy have their different usage in manufacturing industries—steel as the main body and nickel alloy as the material of the severe-environmental-tolerance part. However, joining those two kinds of materials

has become challenging due to their different performances [3].

Wire arc additive manufacturing (WAAM) is a processing method in additive manufacturing (also called 3D printing) family, the basement of it is direct energy deposition (DED), and the principle of it is using arc to melt the metallic wire onto the top of the product and so achieve the objective of building complex 3D shapes. As a newly existing producing process, WAAM has several advantages over other building processes, such as the reduction of the cost of building materials, the ability of building multiple materials, and the high flexibility of designing parts.

Compared with other welding processes, Friction welding have a limited shape for the building material. Diffusion bonding requires a long production time; Electron beam welding requires a vacuum environment, which is not economical-friendly than other welding methods. WAAM is an excellent method that can be used for nickel-based superalloys. The WAAM process technically avoids the high mechanical performance of nickel-based superalloys, thus preventing the possibility of degradation in processing.

Aims and objectives

This study aims at building a defect-free nickel superalloy-stainless steel bimetallic part with a complex geometry by WAAM with a layer-by-layer interweaving building strategy. The most feasible welding parameters are investigated. The mechanical performance and metallography of as-built specimens were examined and compared with standard metallic materials and Ni-Fe bimetallic parts built by other AM processes.

Thesis outlines

This thesis starts from the literature review, which introduces detailed knowledge and information about researched materials that author learned from literatures, including processing, production, strengthening mechanism, characteristics and properties, followed by an introduction of AM process, which leads to the description of WAAM and recent studies of joining dissimilar materials.

Project Statement

Then, the following experimental procedure chapter comprehensively introduced all the equipment and sampling paths used in this study. Subsequently, two groups of experiments named “material selection” and “crack investigation” are listed in the following chapters, which exhibit two main steps accomplished by this study. The experimental results, including feasibility examination, microstructural observation, cracking quantification and qualification, are displayed and analysed in this thesis.

Chapter 2 Literature Review

2.1 Superalloys

2.1.1 Introduction

The usage of metallic materials can be traced back to the Bronze Age all over human history; it has been proven that the metallic materials own a series of advantages: its fusibility allows people to use them widely in work and daily life, the high mechanical performance of it highly promotes the enhancement and evolution of human races. In modern society, metallic materials can be seen from a can of coke to an artificial satellite in aerospace everywhere in our daily life. There are several common metals get used in the world. The first one is iron and steel, the most common metal in both industry and daily life, and they are mainly used in constructing the main framework of buildings such as houses and bridges owing to their high strength and low cost. Aluminium is the second most-produced metal has relatively wider usage than iron and steel, owing to its low density and high corrosion resistance. It can be used widely in the vehicle and aerospace area, demanding lighter building materials. The second-largest usage of aluminium is as conducting material in the industry due to its good conductivity and low density, making it a common choice of electrical appliances. Other metallic materials like copper and zinc are not commonly used metals, but they still have their specific application; copper is the most valuable material as conducting wires due to its high conductivity and softness. It is also a decorating material because of its unique colour of it. Zinc is a kind of metal that can be used in the electrochemical areas—as a significant material of batteries or protective coating for other metals.

However, despite normal utilisation, several needs of high-performance metallic materials have been concerned by industries. They are needed by some of the severe environments like aerospace, submarine, and nuclear systems. Those extreme environments are always of a high temperature (over 500 °C), so the demand for the

high mechanical performance of materials in such a high temperature has been processed by those industries as well, which means the metallic materials used in that particular environment should own a high level of thermal stability—a good performance even near to their melting point, creep deformation resistance—good resistance to degradation in quite a period, and corrosion resistance—owing to severe operating environments such as corrosive hot gases and sea-water, those kinds of alloys who own those outstanding properties and able to work in extreme environments are always superalloys.

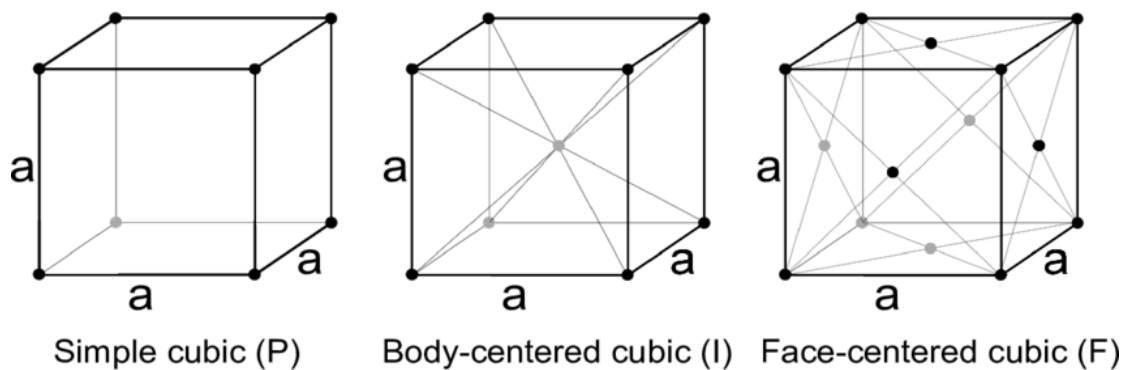


Figure 2.1.1. Illustration of Simple cubic, Body-centred cubic, Face-centred cubic metallic crystal structure

It is reasonable that superalloys can work in a severe environment, the first is the crystal structure is face-centred-cubic (FCC) austenitic, as shown in figure 2.1.1[4], which provides considerable plasticity and toughness to the material; the second is the existence of secondary phases—causing precipitation strengthening to the material that contributes a high-temperature strength to the alloy, as shown in Figure 2.1.2, the high level of oxidation and corrosion resistance of superalloys, however, is not only provided by their basement elements (nickel, iron, Cobalt, etc.) but also several specific secondary elements such as aluminium, chromium and molybdenum.

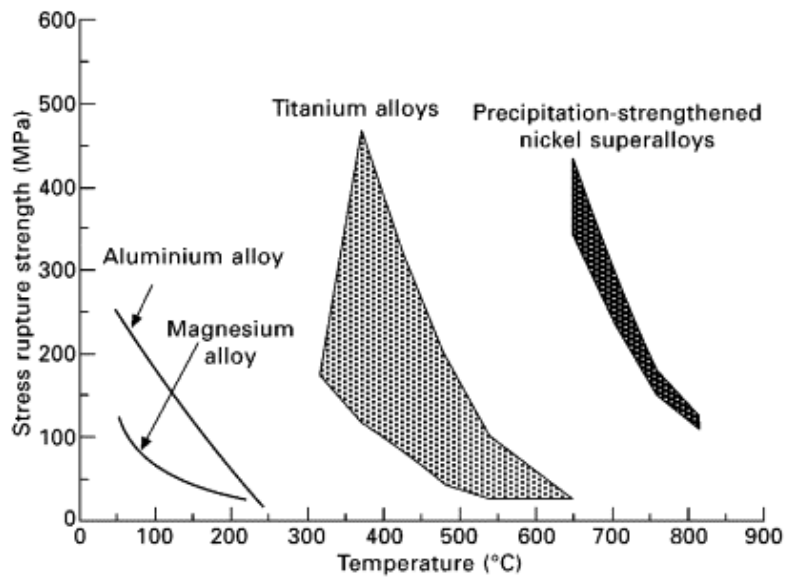


Figure 2.1.2. Comparison of Stress rupture strength between different materials in a high temperature

2.1.2 Mainly used superalloys in manufacturing

There are a considerable number of superalloys already existing in the industry to meet the market's need; some typical series of commercial superalloys such as Inconel, Hastelloy, Waspaloy, etc., have played an essential role in aerospace, nuclear process, and marine industry. The big family of superalloys can be categorised based on their body elements: nickel-based, Cobalt-based, and Iron-based superalloys. Figure 2.1.3 below shows the comparison of stress rupture between three different kinds of typical superalloys [5].

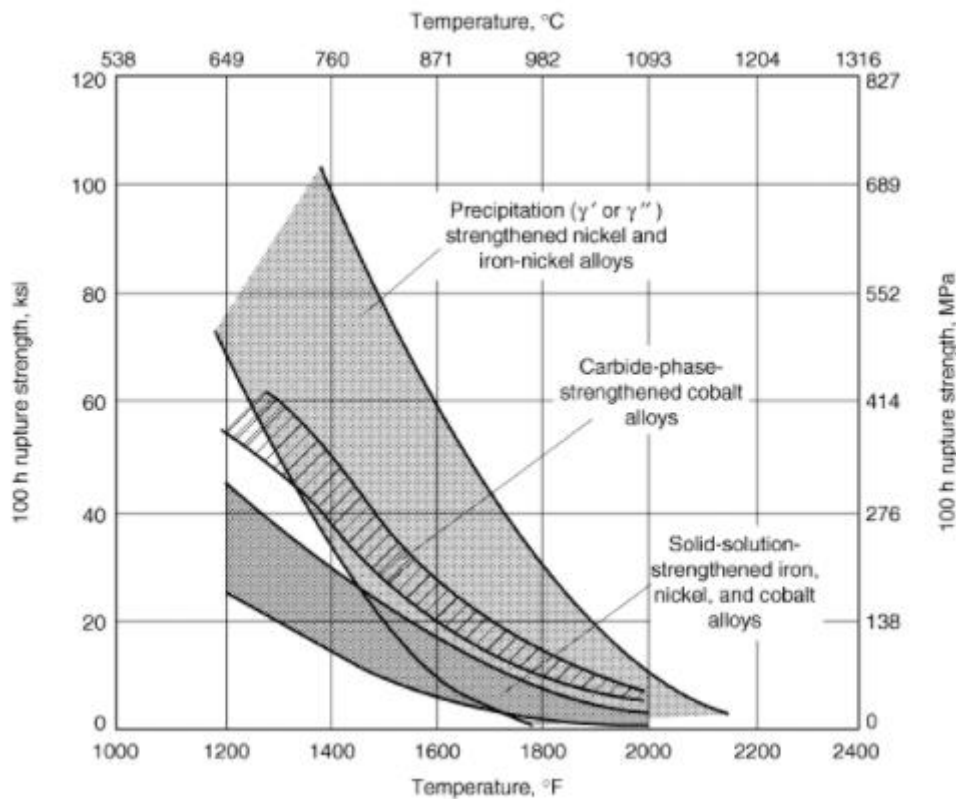


Figure 2.1.3. The comparison of the stress rupture of three different kinds of superalloys (Precipitation, Carbide, Solid solution strengthened alloys)

As the most essential and popular superalloy, nickel-based superalloys have been widely used in turbine engines due to their perfect mechanical properties and corrosion resistance in their working temperature (able to be above 800°C) [6]. Due to their superior performances, nickel-based alloys are the most suitable choice for a high-temperature environment. However, despite those perfect properties, there are also several shortcomings in the nickel superalloy. Its excellent mechanical properties (as shown in Figure 2.1.4[7]) make the processing process an arduous task—an inadequate method can lead to a degradation of mechanical properties or even deformation of metallic structure[2]. Therefore, it is necessary to scrutinise this kind of superalloy and investigate an appropriate processing method. One type of specific nickel-based alloy called Inconel® will be discussed in other sections.

Cobalt-based superalloys are a kind of alloy mainly comprised of cobalt, which has a good characteristic of high strength, corrosion resistance, high wear, and heat

resistance. They are always suitable materials in some challenging environments. The reason for the high performance of Cobalt-based alloys is the same as nickel-based alloy, the Gamma (γ) phase (with the introduction of secondary elements[8]) and Gamma Prime (γ') phase (provided by L12 structure of Co_3Ti or Face-centred-cubic Co_3Ta [9]) caused the solid-solution strengthening that provides corrosion resistance and thermal resistance respectively, the Carbide Phases provides precipitation hardening to the material. There are also topologically Close-Packed (TCP) phases inside the alloy—which is considered an issue to the properties of the alloy. However, although many benefits have been discovered from Cobalt-based superalloys, the nickel-based alloys, which keeps similar advantages as Co-based alloys, have almost totally replaced the occupation of Co alloys in the market. Compared with nickel-based alloys, Cobalt alloys have a much higher price but a lower range of applications than the former. Although they behave a much higher strength at high temperatures, it is not convincing that industries choose a far more expensive material for manufacturing. The most significant value of Co-based superalloys nowadays is as a research material to provide theoretical support to other superalloys in recent studies.

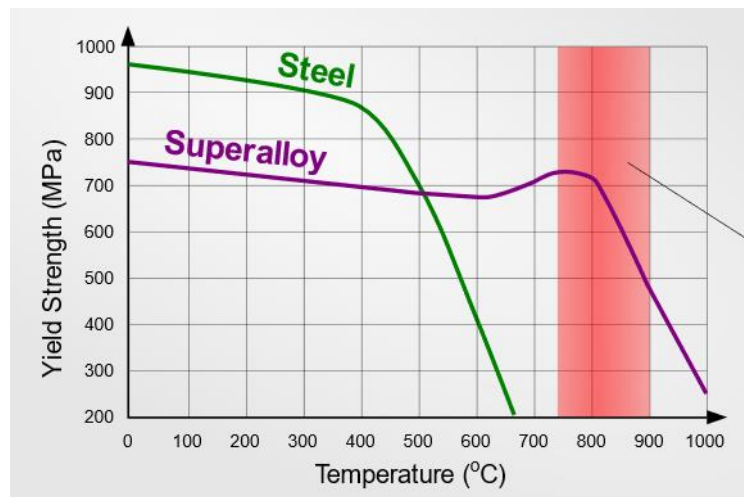


Figure 2.1.4. The comparison of yield strength between nickel-based superalloy and steel

The third kind of superalloy is Fe-based superalloys, and they are exactly Iron-nickel based alloy—Fe as the main element (35%-50%) and nickel as the secondary element (25%-45%). They are formed from austenitic stainless steel, based on FCC

matrix and strengthened by solid-solution and precipitation strengthening[10]. Using Fe in superalloys, some of the steel alloys' performance has a similar creep and oxidation resistance as nickel-based alloys. Still, the application of Fe makes the material more economical and simplify the production process. The principle of the high performance of Fe-nickel based alloy is also similar to that of the nickel-based superalloys, Gamma (γ) phase and Gamma-prime (γ') phase—leads to solid solution strengthening and precipitates strengthening that enhanced the corrosion resistance and thermal resistance, respectively, which makes them a decent kind of materials for severe environments. However, only a few kinds of Iron-based alloys can be seen as superalloys; those who own a base matrix of FCC such as Nitronic[®] and Multmet[®] can be considered as superalloys. Some researchers have also revealed that compared to nickel-based alloys, the severe environments may cause a negative impact in Iron-based alloy—when exposed to water vapour at a high temperature, the lifetime of alloys can be reduced [11]. In addition, owing to the matrix element of Fe, its stability is not as high as nickel and Cobalt-based alloys, the components in Fe superalloys are also sophisticated. They always comprise a higher proportion of detrimental phases such as η (Ni₃Ti), σ (Fe_xCr_y), G (Fe₆Ni₁₆Si₇), μ (Fe₇Mo₆) and laves phase than that of the other two superalloys.

It is noticeable that differentiated by the microstructure and processing method, another kind of newly existing metallic material was introduced—single-crystal superalloys, which is categorised by their microstructure, is a kind of alloy produced by directional solidification techniques. This technique causes an absence of grain boundaries and leads them to a superior creep and thermal fatigue resistance than the standard polycrystalline alloys, the lack of some specific elements such as B and Zr provides a higher incipient melting temperature, which significantly increases the tensile strength and decreases the creep-rupture properties of the material [12]. However, its unique structure makes the repairing process a challenging task. It is difficult to avoid the loss of crystal structure and the solidification cracking along the grain boundaries[13], leading to a catastrophe in manufacturing.

2.1.3 Strengthening mechanisms

Superalloys have such superior performance. They can play a role in severe environments because of the strengthening of alloys—solid solution, grain boundary and precipitation (including carbide-phase) strengthening, caused by the phases generated inside the materials [14].

First of all, the solid solution strengthening will be introduced by the following text, and it is a kind of strengthening method caused by the size of alloying atoms. As shown in Figure 2.1.5, the large-sized atoms lead to a Substitutional solid solution strengthening—the large atom replaces the lattice positions of solvent atoms, and the small-sized atoms (up to 57% of the radii of the solvent atoms) leads to Interstitial solid solutions form—small enough to inside the interstitial sites of lattice [15]. Many studies have examined that the strength of metallic materials depends on the propagation speed of dislocation of the crystal lattice. With the introduction of solute atoms, the dislocation of metallic material has been blocked so that the tensile stress of the material has increased [16]. The solid solution strengthening is mainly caused by the elements of Cr, W, Co, Mo, Re and Ru etc. in the superalloys, and it almost happens in all kinds of alloys—for improving the strength of a pure metal [17], it is the primary strengthening mechanism of Inconel 625.

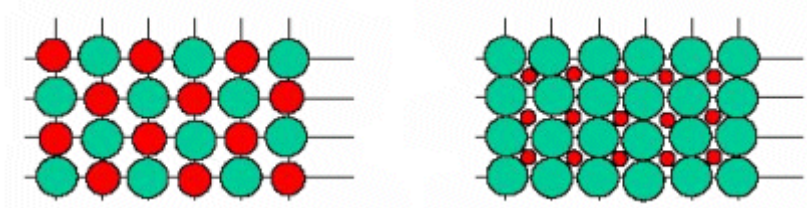


Figure 2.1.5. Two types of solid solution strengthening (Substitutional and Interstitial)

Grain boundary strengthening, also called Hall-Petch strengthening, mainly happens in Iron-nickel based and nickel-based superalloys. It is based on reducing the average grain size of the material. The dislocations always occur in the grain but never exceed the grain boundary, which means every grain boundary is a barrier to slip. In

contrast, a large number of dislocations may cause stress onto the adjacent grain, eventually leading to a deformation of the adjacent grain. By reducing the grain size, the number of grain boundaries increases, so does the energy required for dislocation of material has increased by the increased amount of grain boundaries, then transfer to the adjacent grains, finally the dislocation of the material has been impeded [18]. The yield strength of the material has been improved. However, some researchers have found that the grain boundary pro weakened the material at a high temperature. Based on several experimental observations, such as at a fine nanocrystalline grain size less than 10 nm, the material will weaken at even room temperature [19].

Precipitation strengthening is a variety of strengthening methods that can increase the yield strength and elasticity of superalloys. It involves three steps, Solution annealing—treat the metallic material with a high temperature (marginally under the material's eutectic point) solution to precipitate the metastable phases and alter the inhomogeneities into homogeneities, Quenching—using water, oil and gas to rapidly cool down the material after annealing, a metastable, oversaturated and single-phase solid solution has generated after this process, Aging—the quenched material will be heated up to a specific temperature (depends on the material) after treated by the constant temperature in a particular time, the single-phase solid solution will precipitate, transfer into a two-phases material, the primary phase is known as the matrix phase [20, 21]. After treatment, the metallic material has been strengthened by those tiny particles—the movement of dislocations and defects in a crystal's lattice has been impeded. Precipitation strengthening always happens in nickel or Iron-nickel based superalloys; it is the main strengthening phase of Inconel 718 because the Nb existed in the alloy, contributes Ni_3Nb precipitates [14].

In conclusion, the strengthening mechanisms are the most significant reason for superalloys' high performance and the basis of using superalloys in severe environments.

2.2 Nickel-based Superalloys

2.2.1 Introduction

Nickel-based superalloys have been reached, developed and applied for over 50 years from now on, and they are mainly used at the gas turbine where the temperature is typically over 500 °C [22]. The nickel superalloy is also the best choice for the hottest engine components—usually able to reach 800 °C (which exceed 70% of its melting temperature) in the aircraft because of its outstanding creep and rupture resistance in a high temperature of it. In contrast, other materials like Ti and Al (used in cooler parts of the engine) may rapidly creep just above 150 to 350 °C [23]. Owing to its high mechanical properties and thermal stability, nickel-alloy has become a kind of “hot” material that attracts the attention of AM industries [24].

There are a few mechanisms of why nickel alloy can be used in a high-temperature environment. One of the significant reasons is that the nickel displays an FCC crystal structure as the matrix phase of the alloy, which provides the alloy toughness and ductility owing to the bonding of the outer d electrons providing extensive cohesive energy to the alloy. In addition, the FCC structure also provides a stable thermal performance to nickel—makes it durable from room temperature to its melting point and avoids the expansions and contractions caused by the phase transformations, which extremely validates its application for high-temperature parts. Moreover, the FCC metals always have a low diffusion rate—driving a relatively low rate of thermally activated deformation and enhancing the microstructure stability at a gradually increasing temperature of the material [25]. Other transition metallic materials which have the same FCC structure as nickel, however, are relatively dense and extremely expensive (platinum series metals such as Pt, Ru, Ir as an example) or toxic (such as Os and Tc), although Cobalt has been applied for superalloys for an extended period, it has a higher cost but similar performance than that of the nickel-based superalloys [26].

Another reason is the strengthening in alloys; the performance of nickel alloy has

been enhanced by solid solution strengthening and precipitate strengthening. As introduced in the previous section, the elements like Cr, Mo, etc., in nickel alloy provide a significant enhancement to the thermal durability of the material. The precipitates comprised of secondary components and carbide increase the material's strength and ductility [20].

Nickel-based alloys have not been systematically categorised yet. Still, they are always being identified by the trademarks followed by the unique number (and letter), each numbering corresponds to a specific kind of alloy, such as Inconel 718, Hastelloy X, Nimonic series and Incoloy series etc. The nickel alloys can be divided into four classifications based on their components they are commercially pure nickel, Solid-solution strengthened, precipitate-strengthened, and specialty alloys, except the commercially pure nickel, some of the alloys in other three categories (especially in the third—Precipitation strengthened alloys) can be considered as superalloys, as shown in the table below [27].

Table 2.2.1. Classification of nickel alloys

Nickel alloys			
Commercially pure	SS strengthened	PP strengthened	Specialty
Pure Ni	Ni-Cu	Ni-Al-Ti	Ni-Al intermetallic
	Ni-Mo	Ni-Cu-Al-Ti	Oxide disperses strengthened
	Ni-Fe	Ni-Cr-Al-Ti	
	Ni-Cr-Fe	Ni-Cr-Nb	
	Ni-Cr-Fe-Mo	Ni-Fe-Cr-Nb-Al-Ti	
	Ni-Cr-Mo-W		
	Ni-Cr-Co-Mo		

The commercial pure nickel contains 99% (wt.) nickel. Two alloys represent the entire pure nickel family—nickel 201 and 200. These materials have poor strength and hardness. They are initially used in a corrosion environment due to their corrosion resistance. They also have good weldability, but they are prone to gain porosity when

welding, thus the cleanliness and the addition of Ti and Al are significantly crucial for their applications in electrical and magnetostrictive areas [27].

Solid solution (SS) strengthened nickel alloys are based on the solubility of other alloying elements in the nickel matrix. Cu, as an example, is an element that is completely solid soluble in nickel so that the production of the alloy can be formed as a total single-phase alloy. In addition, those elements also have a high level of hardening coefficients so that the creep strength of the matrix can be improved. Except for Cu, high solubility elements should include all the elements from Groups VA and VIIA, and some elements from IIA and IVA, Groups IB to VB should be considered. Throughout complete analysis via various conditions such as atom size and chemical compatibility, the most appropriate solid solution strengthening formers are tungsten, molybdenum and titanium, which have a high melting point and high hardening efficiency. However, they have a relatively low solubility in nickel, for some of the high soluble elements such as tantalum, niobium, and vanadium also appear in alloys but still in a very small dose. Still, their strengthening efficiency are not outstanding, but although the elements like chromium have a smaller strengthening efficiency than the formers, their solubility is high [28]. Single addition elements existed in alloys are allowable, but not proper for a superalloy—simple Ni-Cu alloy is highly weldable, but it is also prone to generate porosity if the proper deoxidising and shielding gas are not applied, the nickel alloy who only additions Fe (INVAR[®] series) owns the lowest coefficient expansion all over the nickel alloys. Thus, the cooperation of these elements (including Cr, Mo, W) should occur in a solid strengthened alloy, which brings them a good corrosion resistance to corrosive environments. Those elements make the classifications of solid solution strengthened alloys various well [27].

Precipitation (PP) strengthened alloys always contain additional Ti, Al, and Nb to form precipitates, which increases the dislocation motion resistance and thus improve the strength of integral alloy after proper heat treatments. In most cases, the elements

in solid solution strengthening should not form precipitates (except chromium). They are achieved by those “low coefficient” but still added elements. It is possible that solid solution strengthened alloys are further precipitation strengthened for a higher performance [28]. Usually, the precipitates are coherent with the matrix—the precipitates are usually called Gamma prime (γ') or Gamma double prime (γ'') phases, and the matrix is Gamma (γ) phase (will be introduced in other sections). Throughout history, the first kind of precipitation strengthened nickel alloy is the nickel-chromium alloy (known as X-750). It is strengthened by the gamma prime phase and behaves an excellent oxidation resistance and high-temperature performance near the melting point. However, it owns poor weldability—usually suffers a severe strain age cracking (SAC) when welding or direct aging without annealing. To enhance the weldability of the alloy, the second nickel-chromium generation was invented to prevent SAC. They are strengthened by the gamma double prime phase, owing to the formation speed of the gamma double prime being lower than that of the gamma prime, and the SAC could be prevented via post-weld heat treatment. The most popular precipitation strengthened nickel alloy is Alloy 718 (Inconel 718), used for gas turbine shafting in aerospace and pressure controllers. It has widely known because of its high performance in a high temperature and high corrosion, oxidation resistance because of the superior properties provided by the gamma prime and double prime phases, and that is also the reason why most of the precipitation-strengthened alloys are referred to as “superalloys” [27].

There is, however, expected precipitate strengthened alloys, another kind of alloy that may reach the height of superalloys—specialty alloys, for example, alloy MA6000 exhibits a tremendously high temperature creep resistance and stability, which is achieved by the cooperation of precipitate strengthening and oxide dispersion strengthening from itself—different from the majority of other nickel alloys, the strengthening factors are fine dispersion oxide particles. Another example is nickel-Aluminides, which comes from NiAl and NiAl₃ compound. It also has a high performance and corrosion resistance. However, the weldability of it is extremely poor,

while the induction of additional elements like B, Cr, Mo, Sc etc. (Borides instead the role of carbides) makes the Ni-Aluminide an applicable alloy that can reach the level of “superalloy” (IC-221M alloy as an example) [27, 29].

2.2.2 Producing nickel superalloys

Initially, the conventional production of nickel-based superalloys is casting—just as ordinary metallic materials; however, the random orientation of grains caused by casting has become a severe problem to the performance of alloys. Thus, grain refinement methods have become a prominent topic among metallurgical researchers. At first, directional solidification was developed as a refinement strategy in the 1970s, the principle of it solidifies the melted metal from the bottom to the top with a controlled specific temperature gradient and solidification rate, whereas approach the aim of removing perpendicularly oriented grains—hence align the structure of crystal [30]. In the 1980s, the refinement has updated to the single crystal casting process, which is still in use nowadays, it has the same fundamentals as that of directional solidification, but one thing different is the removal of misoriented grains that happens before the casting process—the grain selector has been applied in this process, the selector turns tightly, thus limits the numbers of crystal orientation, so the metallic material can only constitute with single grain after casting, which significantly limits the possibility of deformation [31].

The production of nickel-based superalloys starts with a metal ingot’s contribution with a suitable component. The production process contains a three-step melting program. Each step's purpose is to reduce the segregation of the elements, abolish tramp and detrimental elements (Oxygen, Sulphur, etc.), and flatten the microstructure of the metallic ingot, respectively [31]. After the large ingot has been produced, it will be left at a specific high temperature to get it annealed, which minimises the probability of segregation and enhances the performance of the metallic compounds (as mentioned before, the precipitation strengthening happens during annealing). After the cast and wrought process, the ingot has been deformed because of the hydraulic presses, which

reduce the diameter and break the microstructure of the bar to start with. Then the ingot will be formed into a metallic disk and go through the forging process.

However, with the increase of the complexity of the elements in the alloy, which provides higher strength, casting and wrought has become a challenging task for those upgraded alloys. The researchers discovered another way of producing it called “powder processing”. The powder processing is initiated by melting the triple melt ingot into a crucible. Then the molten metal has been atomised by pure argon gas that blows through the liquid metal when it falls. After the atomised metal goes through a series of sieves to get an average diameter, after being condensed at a high temperature (>1000°C) and high pressure (about 100 MPa), the metal will achieve a shape that is similar to the final part [32].

The processing of nickel-based superalloys is based on several routes. The materials are formed as large ingots initially, then being remelted and come through one of the three processes: investment casting, wrought processing, or remelt into powder form and wrought processing afterwards. The following section will introduce several remelting superalloys, which can be applied to nickel-based superalloys and other kinds of superalloys.

2.3.2.1 Main melting process

Investment Casting (IC) (or lost-wax casting) is a conventional melting process, which can be historically traced back to 5000 years ago. For superalloys, the goal of casting complex metallic parts can be achieved by an investment casting process, which is almost impossible for a conventional way—cutting a complicated geometry part out from a giant block. An investment process usually contains several steps: the first step is mould preparation, which can be accomplished by master pattern production, mould creating, assembling, ceramic applying and dewaxing. After the ceramic mould has been obtained, the mould would be preheated to a specific temperature to remove moisture and remaining wax. After pouring the metal, the metallic part will be successfully produced, divesting the mould and some modifications [33]. The produced

metallic part is as accurate as the requirements, with a smooth surface and no flash or parting lines. Also, almost any kind of material can be used in this process.

Vacuum Induction Melting (VIM) is fundamentally a melting process using electric currents to melt the material in a vacuum surrounding (for preventing impurities and low melting point contaminants). It was initially considered as a melting method for specialised and exotic alloys but consequently became commonplace with the development of special alloys. It is an appropriate melting method for those alloys that contain Nb, Ti, and Al inside. The VIM process is also considered the upgraded version of Investment Casting, which prevents some of the disadvantages of IC, such as avoiding oxidation, removing dissolved gases, and getting the components controlled of final alloy [34]. The process starts with the selection and preparation of the crucible. A well-selected crucible can significantly improve the quality of the material, then is the preparation of casting material, which coarsens the metal ingot but with a lower level of impurities because the processing time can be elongated, after being melted by the vacuum induction furnace, the refined bars can be directly getting used into casting with the material remained—the electrode processed by VIM will be remelted by secondary melting process (as introduced below) and also being converted into ingots. After the thermomechanical treatment is applied, the produced parts are refined and finally able to use [35].

2.3.2.2 Remelting process

The Vacuum Arc Remelting (VAR) process is one of the secondary remelting methods after the VIM process. At first, the cylinder generated from VIM will be put into an enclosed cylinder crucible; with a certain level of vacuum is applied, the electrode will be brought into the crucible with a few molten metals lying on the bottom of the crucible. After being melted by the arc generated by a high Direct current (for several kiloamperes) applied between the material and the bottom of the crucible, the arc may happen between the electrode and sidewalls of the crucible that the electrode

needs to be lowered to maintain a certain height. Its diameter also needs to be larger than the crucible [36]. To gain a defect-free metallic part, the current, cooling water and the arcing gap should get adequately controlled [37]. The main advantage of the VAR process can be summarised as the improvement and refinement of the material's structure.

Following the VIM process, Electro-slag Remelting (ESR) is another secondary remelting method. In the ESR process, the prepared electrode is melted by the heat generated by the electric resistance of the electros slag (always the mixture of CaF_2 , CaO and Al_2O_3) in the mould, a low voltage but high ampere current goes through both the electrode and slag, which keeps the slag remains molten. With the liquid metal run through, the refinement of the material is achieved by the fallen droplets of the electrode. Finally, the material solidifies at the bottom of the molten pool into the cooled copper crucible [38]. Unlike the VAR progress, the ESR can control the final composition of the material, which can be accomplished by reactions with the electros slag [39].

The main difference between ESR and VAR is the participation of the active electros slag. The chemical components usually would not be changed dramatically but can be slightly adjusted by electros slag, which the VAR process cannot achieve. However, hydrogen contamination in the ESR process should be controlled strictly because removing hydrogen contents is difficult in ESR, a considerable limitation of the ESR remelting process [40]. The objective of the VAR process is to produce high homogeneous materials [39], which is an unreachable direction for the ESR process. Furthermore, the material that went through the ESR process is free of inclusion, which VAR can hardly achieve, but the VAR is more effective than ESR in controlling segregation [41]. Thus, the remelting process should be selected prudently depending on the user requirement and the material's properties (components, impurities).

2.2.3 Processing Ni-based superalloys

2.2.3.1 Heat treatment

Heat treatment (also called heat treating) is a group of processes that heat the metal to a specific temperature (should not reach the melting stage) and then let the metal cool along a controlled way to gain required mechanical properties [42]. It is a way of specialising the superalloys by changing the properties of the metallic material. After producing solid material, the heat treatment is applied because all superalloys must be heat-treated for a specific time (such as cogging and forging). Furthermore, some chemical processing (coating as an example) also requires a high temperature to ensure the ongoing chemical reactions. The modification also involves the heat of the microstructure of the material. Thus, the heat treatment is logically a sequence step after producing and is also the premise of generating these specialised superalloys [5].

The heat treatment methods vary due to the different compositions for different superalloys. However, the heat treatment can also be different for a specific superalloy to obtain specialised properties. The following contents introduce several heat treatment methods usually applied for processing nickel-based superalloys.

Stress-relieving (SV) is used to eliminate or decrease the stress inside the work-hardened alloys, which is accomplished by applying a temperature of 425 to 870°C that remove the stress but does not cause the recrystallisation of the grains [43]. However, eliminating residual stress may cause an unreversible negative impact on the superalloy's high-temperature performance and corrosion resistance. It needs to be weighted between them [5].

Stress equalising (SE) is a method that can balance the stress for the cold-worked superalloys whose mechanical performance is reducing, always being used in coil springs, wire forms, and flat spring stampings. Stress equalising is a relatively low-temperature heat treatment, which causes the “partial recovery” that considerably

increases the proportional limit slightly improves the material's hardness and tensile strength. The material's electrical conductivity returns to its characteristic value with balanced stress. The temperature of the Stress equalising process, however, also depends on the composition of the superalloy. For nickel-based superalloys, the temperature should range from 230 to 315°C, but for commercial use, the temperature should be controlled above 275°C, which leads to no detrimental results to the material even with an extended treatment time [44].

Annealing, as a typical heat treatment method among alloys, can also be used in processing nickel-based superalloys, the principle of it is to heat the material to a high temperature (usually 700-1200°C for nickel superalloy), with the temperature maintained for some time, then the temperature cools down. Annealing fully recrystallises the material's microstructure and maximises its softness, so it is just a method for those wrought materials that are non-hardened. The solution annealing should be applied for a hardened nickel superalloy [5]. There are three steps in annealing progress; the first step is recovery—leads to a softening of the material by removing dislocations and the interval stress caused by them, the second step is called recrystallisation, several grains nucleate and sprout to replace deformed old grains, after the recrystallisation being finalised, the final step grain growth happens, which coarsen the microstructure of the material and may lead to a catastrophe to the strength of the material, the missed strength can be regained via hardening process though [45].

Solution annealing, as mentioned before, is an ideal heat treatment method (first part of the age hardening) for hardened alloys. It is a high-temperature treatment method that puts the already formed carbides back into the solution, transforming the material into the structure of single phase to generate a coarse grain size after rapid quenching to a room temperature by oil or water at the end of the annealing for avoiding the generation of precipitations, so that the mechanical or electrical properties of the material can be improved. After Solution annealing, the hardening process (age

hardening/precipitate hardening) is required, making the hardening decide the alloy's final precipitates. It is critically related to the hardness, strength, toughness etc., based on the composition, size, and quantities of the precipitations generated by the following aging process [46].

Age hardening (also called precipitation hardening) comprises three steps: solution annealing, quenching, and aging. The material is heated up and quenched rapidly and then goes into the precipitation process, which causes precipitates from the oversaturated matrix phase. This process can generate several phases (Gamma prime and Gamma double prime). The temperature-controlled in this process may range from 600 °C to 1000 °C. For some materials (primarily for wrought superalloys), multiple aging is required for gaining a more advanced property. The aging steps can be two (double aging) or more (yo-yo aging). The temperature should be sequentially lower than the former aging step in a single precipitation hardening process [5].

Generally, the heat treatment procedure of nickel-based superalloys includes solution or full annealing, quenching and aging hardening.

2.2.3.2 Machining and surface finishing

Machining is a technique that alters raw materials into an accurate component that reach the requirement. The machining usually contains turning, milling, drilling and grinding. As a high-performance alloy, the machining of nickel-based superalloys has become difficult for a standard cutting method. It is owing to its high strength, operation temperature and cutting force. However, the heat conductivity of nickel alloy is relatively low, leading to the generated heat not being dispersed via cutting workpiece and chips effectively. A failure might happen with the heat accumulation inside the component or the cutting parts. Thus, finding suitable machining to gain well-machined components is an arduous task. The machining process for a specific material can be affected by two critical factors: The selected tool material and the cutting parameters [47, 48].

2.2.3.3 Effect of cutting tool materials

The geometry and shape of the cutting blade significantly impact the tool life and the machined surface of the component. For example, a rhomboid-shaped ceramic blade does not suit nickel superalloys—the part is poorly performed, and the age of the tool is shortened, but for a square or round shaped tool, they perform a more extended tool life a better surface than the former one. That is because the included angle in square and round tools are larger, which tends to increase the contact area between tool and chip and the edge strength of the cutting blade so that the stresses and the cutting temperature at the cutting location [49].

A machining operation can be affected for a variety of reasons. It is the cutting tool, the smallest but the most significant. The selection of the material of the cutting blades should include the following requirements: good wear resistance, high hardness and strength, high thermal hardness and shock properties, and stable chemical properties in an elevated temperature [49].

Several material categories have been used in machining nickel superalloys; examples are demonstrated below. High-speed steel and cemented-carbide blades are a cutting tool used for several decades, one of the most reliable choices for machining. Multilayer coated (such as TiN, TiCN, TiN) carbide blade prepared by physical vapour deposition (PVD) is also a suitable choice for cutting nickel-based superalloys [50]. Ceramic is also a common cutting material, the Silicon nitride- and alumina-based ceramics can be successfully used for machining [51, 52]. Another reliable choice is the Cubic Boron Nitride (CBN) (known as the second hardest material of all the materials) cutting blade that is principally used for cutting ferrous materials, has also shown an excellent performance in cutting nickel alloys—even better than that of cemented carbides, however, the cost of it is relatively higher than others [5].

2.2.3.4 Effect of cutting parameters

The machining process should consider several cutting parameters, such as cutting

depth, cutting speed, feed rate, etc. Both of them play vital roles machining process by affecting the performance of machined components and machining tools [53]. For example, the standard cutting speed for nickel-based superalloys by cemented carbide tool ranges from 10 to 30 m/min. In contrast, the speed is far higher than 30, then severe flank wear and notching will happen in the tool nose. With the speed increases, the notching occurs more seriously, leading to a premature failure of the entire edge [49]. As a machining magazine [54] mentioned, when machining nickel superalloy, a high mechanical and thermal pressure will be put on the cutting blade so that forcing down the speeds and feeds of cutting, issues like built-up edge, work hardening, temperature diffusion and notching will generate during the machining process, they have “an aggressive abrasive effect on the carbide cutting edge, all excellent formulas for wearing out cutting tools fast”, with a sensitive parameter—cutting speed, which affects the life of tools.

Although a high cutting speed results in a cutting tool failure, the feed rate and cutting speed should be controlled, a few studies demonstrate that in a low speed, high feed rate machining process, the tensile property of residual stress should be controlled increased. The peak value of compressive residual stress in-depth ascended as well. The surface roughness will increase with the feed rate, and for a constant cutting speed and feed rate, a more profound cutting procedure always means a higher cutting force. While an increase in feed speed always leads to a higher cutting speed and consequently leads to a lower cutting force [53]. Furthermore, the nickel composition in the alloy is also an important parameter. When the nickel content is 60%, the recommended carbide tool speed is 13 m/min. In comparison, the cutting rate will increase with a lower content nickel in the alloy—for an alloy containing 45% Ni, the recommended speed is 20m/min [55].

On the other hand, the surface finish of the machined part can be tremendously affected by the feed rate—followed by different parameters such as nose radius and cutting velocity. Also, the feed rate is an important parameter that affects tools life, surface roughness and cutting force. It is noticeable that a deeper cutting depth or a

larger chip can result in a worse surface finish, and the feed rate affects the surface more than the depth, which means the productivity should be controlled (mainly Feed rate and cutting speed) while machining nickel superalloys to get an appropriate surface finish [56].

2.2.3.5 Cutting fluids

Cutting fluid contains coolant and lubricant designed explicitly for metalworking. In the machining process of nickel-based superalloys, the cutting fluids are neglectable. They have been used for decades to improve the machinability of the alloy by lubricating several contact areas (e.g., rake face and chips, machined part and rake face) to remove the accumulated heat from the cutting zone machining [57]. A proper selection of cutting fluids is vital for keeping the machining process working, as it can influence cutting forces, tool life, machining accuracy, power efficiency, and surface integrity. Those who own a more significant lubrication effect are usually used in a severe machining condition—low-speed machining as an example, but for coolants, they are generally used in high-speed machining—always a company with low cutting force and a high machining temperature [58]. The miscibility can categorise the cutting fluids in water—those who can dissolve in water are water-soluble fluids and those who cannot are non-water-soluble (or oil-based fluids) and with an additional gas-form fluid [58].

Water-miscible fluids—as mentioned before, is a water-soluble cutting fluid, the main effect of them is removing heat generated in the contact area—be as a coolant, it is desired that the coolant should have a high level of thermal conductivity and specific heat water has the most specific heat capacity in nature and also with a low cost, which makes it the most favourable coolant. However, water is a little corrosive to metals (especially for ferrous metal) and owns poor lubrication and even tend to wash out the remained lubricants (for sliding surfaces in the cutting machine) so which leads to a worn device [58].

To overcome these issues, additives are added into the fluids so that branches into soluble oil (added organic oil with emulsifiers), synthetic (with a series of additives such as high-pressure additives, corrosion inhibitors and so on) and semi-synthetic fluids, both of them have their advantages: soluble oil fluids are multifunctional—own lubrication, corrosion-resisting, and cooling effects at the same time, synthetic fluids are free of mineral oil—the functionality of them depends on the additives added inside, semi-synthetic cutting fluids contain both mineral oil and chemical additives, they have both of the characteristics of the former two fluids—considered as an intermediate choice [59]. However, the disadvantage of water-based fluids is also considerable—the growth of bacteria or fungi in the water can be a severe issue impacting the lifespan of the services, additives like bactericides are needed to be added into the water-miscible fluids.

Oil-based or neat-oil cutting fluids is a kind of alternative coolant that has been widely used in machining. They are mineral oils and usually contains several additives (always other lubricants and extreme pressure compounds) to gain a more advanced property [60]. The initial usage is as lubricants to lubricate the moving parts/the tool-chip contacting surface by reducing the coefficient of friction and the heat generated by friction. By reducing friction, the cutting forces can be decreased, and the possibility of tool wear can be limited. The application of oil-based fluids curtails the corrosion and oxidation of both the machined surface and machining tools.

Based on their composition, there are two types of oil-based fluids in the market, categorised into naphthenic mineral oils and paraffinic mineral oils. Their characteristics can be enhanced by the added additives (such as fatty lubricants and extreme pressure additives). Although mineral oils provide outstanding lubrication and corrosion resistance, they cannot be used in a high working load and working temperature—they generate mist and smoke and even tend to be kindled, leading to a disaster. Thus, the application of pure oil-based fluids is limited in cutting easy-to-cut materials such as Al, Mg and Mild steel [58]. However, the compounded oils are

reliable choices for nickel superalloys—it favours a low speed but high load machining owing to its ability to chemically react with the surface (which should not cause a surface degradation), and that leads to a formation of thin lubricating film onto the surface, so that reduces the friction [61].

Gas-based coolant-lubricants (CLs) are usually in the gas form from room temperature. They are used as air form or cooled-pressured fluids form in the machining process. Mainly used CLs are air, nitrogen, Ar, He or carbon dioxide, which can also be in conjunction with a traditional fluid—enhancing their lubrication capability in droplets or mist form [59].

The most common use of gas as coolant is in the dry cutting process—gases are used to cool the tool and the workpiece [62]. However, due to the poor thermal conductivity of gases, researchers have investigated several ways of enhancing them. The most successful one is compressed gas-based CLs—it can penetrate the interface of chip-tool, which is even better than any other traditional cutting fluids. It has been proved by Brandao et al. [63] that compared to other forms of gas (comparison between dry air, chilled air, and compressed air), the compressed air caused significantly reduced thermally induced dimensional variations of the workpiece.

For nickel-based superalloys, the liquid nitrogen can be considered as a good gas-based CL, as Hong et al.'s research [64] demonstrates: the life of rake and flank face of the carbide tool used in machining Ti–6Al–4V superalloy was prolonged up to 3.3 times more by applying liquid nitrogen as a cutting fluid, that is achieved by the ability to reduce heat and chemical reactivity of the machining part of the applied liquid nitrogen so that the possibility of tool wear has been reduced. Also, those gaseous coolants (inert gases like Nitrogen, Argon, Helium etc.) can provide an inert surrounding for preventing the oxidation of the surface and cutting tool at a high temperature.

2.2.3.6 Electrical discharged machining (EDM)

EDM is a machining process specially designed for machining hard-to-cut

conductive materials (usually metals). The principle is using a controllable spark (occurs between the workpiece that spoiled in a dielectric liquid and electrode) to machine the material, the electrode can be considered as the cutting tool, and the dielectric fluid is for conducting electricity (initially is an insulator, become conductive while a specific voltage applied). The spark that exists in the machining process has a frequency of 2000 to 50000 sparks per second, which makes the spark seems like it occurs simultaneously, but actually, only one spark exists per instant. They remove the material both from the electrode and the workpiece. With the dielectric liquid being applied for controlling the spark gap and cooling down the temperature, the machining process can proceed.

Differentiating from the conventional machining process, there is no contact between the cutting tool and the workpiece in EDM, making EDM have no tool force. Thus the tool wear rarely exists in an EDM system, making it a perfect machining process for nickel-based superalloys who usually require a high workload and workforce in a conventional machining way [65].

Based on the spark erosion machining, a more advanced innovative method called Wire Electrical Discharge Machining (WEDM) has already been applied in engineering—producing sophisticated parts such as turbine blades, fuel injector nozzles etc. [66], in a WEDM process, the electrode is in a wire form, and the electrical sparks generate from it, the workpiece is separated by the flushing of the dielectric fluid, a voltage has been added in amid the wire and works material, with the supply of the dielectric presence, the work part is melted by the sparks and with the wire continuously running, the machining of material taken place (as shown in the image below) [67].

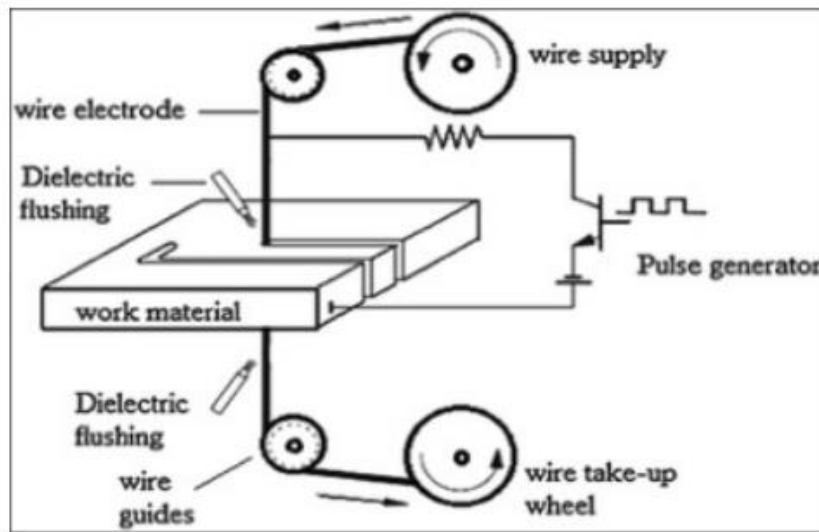


Figure 2.2.1. The schematic of the WEDM system

Several researchers have investigated the WEDM method's availability for machining nickel-based superalloys. Priyaranjan Sharma et al. [68] have used Inconel 706 as a specimen and get a few parameters controlled to produce a perfect machined part. With the investigation of the various performance of the performed IN 706, it has been proved that WEDM can machine nickel-based superalloys, and no microcracks are found on the surface. Other microstructures that may impact the overall performance, like microvoids and micro globules, can be controlled by reducing pulse on time and incrementing servo voltage. Further theoretically research has been finished by Binoj et al. [69], the Inconel 718 has been used as machining material, by adopting WEDM as machining method, they have built a model of parameters such as Pulse On-Time and Pulse off time etc. with the help of Taguchi's method, theoretically supports the future industries for enhancing the production rate and product quality of the Inconel 718's machining process.

2.2.3.7 Surface integrity, surface cleaning and surface finishing

While the machining process finished, the completed workpiece should have owned the required shape and thickness. However, the surface of the machined material may not be in a suitable qualification, and a poor surface quality may negatively impact

the mechanical properties of the material (e.g., fatigue strength, corrosion resistance and coefficient of friction). It has been proved that the nickel-based superalloys are sensitive to even tiny changes among their microstructure owing to the high strength in a high temperature and high tendency to work hardening [70]. Several significant changes while machining can be induced residual stresses; hardness changes (due to work hardening); the existence of microcracks (or macrocracks, especially in grinding); severe defects (like tears, laps, and crevices); plastic deformations; metallurgical transformations (the effect of the high temperature); and chemical changes (such as oxidation reaction and diffusion) [49]. The factors that influence surface integrity can be various. It can be because of the characteristic of the machined material—hard-to-cut materials with a high hardness may lead to a rough surface. Also, another reason can be the facts of the machining process—tool variables (like tool material, rake angle etc.) and cutting conditions (parameters mentioned before) [2].

The surface cleaning and finishing are introduced to improve the machined nickel surface feature based on the above. The cleaning process is aimed at erasing contaminants from the surface, the impurities may include some simple substances (such as oil, grease, cutting fluids) that solvents or emulsifiers can easily remove, but there also can be a series of complex compositions: metallic contaminants, tarnish or oxides, which also should be removed owing to the severe consequence caused by them (such as surface attack or even scrap of the fundamental component) [5]. It is noticeable that those compositions are not always harmful, such as tarnish, which is a thin oxide film that is generated on the surface, they usually do not harm the final part that made of nickel superalloy, they can even be helpful—it can prevent further oxidation of the material and also can block the diffusion from other alloys, the removal of them always take place before welding or brazing. The oxides/scales are also not that detrimental—the oxidation resistance of nickel superalloys is partially based on the generated Cr_2O_3 and Al_2O_3 oxides. However, those oxides are not strong enough—or not thick enough to protect the material, so in further operations, their removal is required [71]. The metallic contaminations are not always harmful as well, they are generated from the

accumulation of other metals' traces induced by the contact between the material and cutting tool, forming dies or fixtures. In some cases, they should not affect the surface, but they can also be very dangerous in some instances—based on specific components, for example—the Zn traces (come from drawing dies) on the surface of Inconel X-750 can rarely negatively impacts the features of it, but a tiny little particle of aluminium will quickly ruin the corrosion resistance and mechanical integrity of the affected area of Inconel—by blending in the Inconel in an elevated temperature, the same principle happens on the copper who also degrades the features of the affected material. Thus, removing Metallic contaminants is inevitable—for avoiding degradation at an elevated temperature [5].

Thus, appropriate surface cleaning methods should be considered for attaining a better characteristic. Based on the difference of each kind of contaminant, there are a few methods that aim at surface cleaning—they can be categorised into physical and chemical removal processes. For metallic pollutants, there is a different solution for them—by avoiding the attachment of them, it is said that the use of lubricants can effectively reduce or prevent the metallic contaminants in cutting or forming operations, which is the most preferred method for industries because lubricants can be removed easily—if they have not been heated up before the removal process. For those metallic contaminants that are unavoidable, the testing method should be applied to test the existing contaminants' severity. The physical appearance of the material after specific processes (such as chemical treatment or heat treatment) can reveal the contaminants—but some procedures like heat treatment will harm the material—as mentioned before, so it should be avoided unless the absence of pollutants is proved. Furthermore, chemical detection can also be applied—it can be achieved by using specific chemical solvents so that the contaminants can be marked by specific colours (different colours for different elements). In addition, except physical or chemical testing methods, metallographic examinations can also reveal metallic contaminants, such as bend test (the elasticity of the material may be severely impacted by contaminants) or hardness test (a high loss of hardness in the affected zone can be

determined) [5].

Metallic contaminants can be removed physically—dry or wet abrasive blasting with the help of metal-free abrasives is always a good choice for dealing with those impurities, but the shaped requirement, the surface finishing and the allowance of material loss should also be concerned for judging the feasibility of this method. The metallic contaminants can also be removed chemically—they are more commonly used methods than the physical one, aiming at different elements. The removal methods are also different. One of the typical methods of removing iron, zinc, and thin films is firstly making the material vapour degreased or alkaline treated. After being immersed in a 1:1 water and nitric solution for 15 to 30 minutes, the material is washed and dried with the process finished [5, 71].

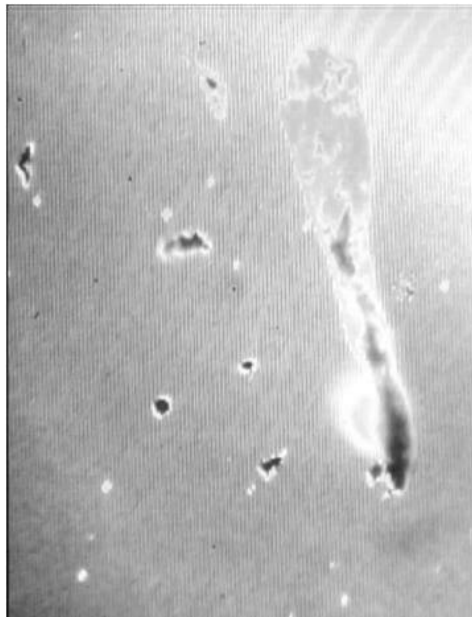


Figure 2.2.2. An image of metallic contaminant on the nickel alloy surface after air exposure[72]

For tarnish, the physical method of removing them is almost the same as that of the metallic contaminants. At the same time, the physical processes can also result in the removal of some metals or even degradation of surface finishes. So, chemical methods are needed for some situations. The flash pickling, which is more common than abrasives for removing tarnishes, a typical flash pickling solution contains 23% nitric acid, 4% hydrofluoric acid and 73% water. The material will be put into this solution

for 1~5 mins at a temperature of 52 °C, and a warmed part before the flash pickling process is preferred to increase the speed of reactions—usually warmed by hot water flushing and drying is required after the pickling progress. Flash pickling occurs very fast (that is why it is called flash pickling), so the gain should have been cared to avoid over-pickling or etching [5].

With the removal of oxide/scale, the oxide tarnish films can generate from the heat treatment in a reducing atmosphere. They can sometimes be removed by the tarnish-removing process mentioned before. However, the oxide in the surface of superalloys is usually integral and indomitable. They can be formed by contact with air, carbon monoxide or water. Because of the effect of oxide-forming components (elements like Ni, Cr, Al, etc.), the pickling process should be chosen to remove them. Scale is generated by the heat treatment process, which exposes the material in the air—such as hot-forging and hot-forming. In addition, some special environments like oxidising atmospheres, high sulphur contained fuels, or air exposure in furnaces can result in a heavy scale onto the surface of Ni superalloys. Usually, scale occurs in all gradations, they have a spongy and dull appearance and can cause fine cracks inside them. They may also break and fall from the surface—with the rough underneath material left. The removal methods, same as that of other removals, can be classified into mechanical or chemical removal. For oxide/scale, the most commonly used approaches are abrasive cleaning, acid pickling and molten salt descaling [5].

Abrasive blasting cleaning is achieved by using dry aluminium oxide, silicon carbide also is a reliable choice for removing oxide/scale, but they are more expensive than Al oxide. For those stubborn scales, the following acid pickling process is required. That enables the use of metallic shot and grit—with the help of pickling, the metal contaminants can be eliminated. Another abrasive blasting—known as wet blasting, is happened by abrasive silica particles mixed with water, a slurry will be produced for the removal of scale, the surface-treated by wet abrasive blasting is always suitable for welding, brazing or further inspections, further washing or flushing are seldom required because the cleanliness of the surface is significantly improved by this cleaning method.

Furthermore, another conventional and direct method can also be used for removing tiny scale or discolouration—using a wire brush [5, 71].

A scale conditioning process should be applied to soften, reduce, and modify the scale required by the following acid pickling process. The conditioning bath consists of alkaline solid solution (sometimes with complexing and chelating compounds inside) that can solute some of the scales but not all of them. Following further treatment with a solution containing highly oxidising substances (such as KMnO_4), the organic components residue on the surface (usually incompletely burnt carbon or polymerised residues) can be eliminated by the chemical reaction with the oxygen released by these oxidising substances. Acid pickling happens to follow the conditioning step. It loosens the attachment between scales and makes them either breakaway or too loose to attach onto the surface so that the high-pressure water can descale them. The acid pickling solution usually consists of dilute nitric acid or hydrofluoric-nitric acid. Both are strongly corrosive acids, so the time pickling process should be controlled to prevent metal loss or surface degradation owing to the etching effect of those acids. Another technological process for the scale removal is achieved by a salt bath (fused caustic soda)—it is more expensive than acid pickling because of the maintaining cost of salt bath in idle time, especially for an intermittent producing process wasting. But its efficiency is generally high, which can remove up to 80% of the oxide and scale on the alloy's surface. Thus, the industry is increasingly concerned with the salt bath for a higher efficiency [5].

Surface finishing changes the surface of a produced item for unique properties that meet the requirement. The finishing processes can be categorised into two groups: the workpiece's effect, removing or reshaping finishing and adding or altering finishing [73]. For the surface finishing of superalloys, there are pretty many methods that are not required to apply to them—although some of them are generally widely used in common materials such as steel and other metals, one of the reasons is because of the high corrosion performance of them in any temperature and environment—makes normal surface finishing process not that important, another reason is that the

application of superalloys does not require a refined, polished surface for a cosmetic reason so that the polish finishing is also not recommended in most cases [5]. Some typical finishing processes for superalloys such as electroplating, coating, polishing and shot peening is required for several specific usages. An essential reason for applying surface finishing is coating. Commonly, a natural oxide coating will be generated by the superalloy itself, which is the principle of their high corrosion and oxidation resistance. The coating program aims to create a dense, tenacious oxide that enhances the material's corrosion resistance by providing more Al and Cr to ensure the formation and regeneration of protective oxide. Electroplating is not a typical surface finishing process for superalloys, but sometimes, the plating of Cr, Cu, Ag or Ni may happen for the following procedure (such as brazing, depositing, correcting or repairing). Another intention of finishing is polishing, which can be achieved by silicon carbide paper and conducted to gain a required surface finish and remove some of the light scale/oxide from the part for other welding and brazing. Shot peening is constantly being used for enhancing the mechanical properties of blades (turbine blades, compressor blades and so on) by introducing a particular pattern of residual stress. It is a finishing process for specific usages [5, 73].

2.2.3.8 Welding and Joining

For all kinds of materials, their weldability is an important property, the effect of high-temperature gains the localised coalescence. As the most common, effective and economical way of joining metals, the welding processes have also been widely used in processing superalloys—methods like gas tungsten arc welding (GTAW or TIG), gas-shielded metal arc welding (GMAW or MIG), electron beam welding (EBW), shielded metal arc welding (SMAW), laser beam welding (LBW) and friction stir welding (FSW) [74]. For those superalloys which are precipitation or solid solution strengthened, the most commonly used welding methods are arc welding, electron beam welding and laser welding. The following text introduces three kinds of representative welding methods from different main categories, and their comparative research and

characteristics are discussed.

Gas tungsten arc welding (TIG) is a method that immensely suits nickel-based alloys owing to its versatility in joining metals, allowing welding to process anywhere. The TIG process generates an arc between the workpiece and the tungsten electrode. The shielding gas comes from the electrode to prevent the welded metal from oxidation, with the deposition of molten metals, the materials are directly welded onto the workpiece without any loss because welding spatter rarely happens in the TIG process. An essential influencing parameter is heat input, followed by welding speed and gas flow rate. An inappropriate choice of parameters may cause severe defects in the microstructure or even a collapse of the built metal or make the material unable to form at all [75].

Other researchers have found that the parameters like weld heat input, cooling rate and post-weld heat treatment are the key to controlling the formation of laves phase—a phase significantly impairs the mechanical properties of the material, which is generated by the micro-segregation of alloying elements (like Nb, Ta, Mo etc.), caused by the insufficiency of the solubility because of their sizeable atomic radius, for welding nickel superalloys, a high cooling rate is recommended according to Radhakrishna et al. [76]. A similar conclusion is also examined by Manikandan et al. [77]. The formation of the laves phase is reduced by the maximum instantaneous cooling rate by combining compound current pulse mode and enhancement on the shielding argon or helium in their experiment. In addition, controlled heat input is also recommended by Xin Ye et al. [78] for avoiding hot cracks, they have found that a higher heat input makes the hot cracks prone to emerge, so that a lower heat input combined with a crater grinding is suggested, and also pre-welding homogenisation heat treatment—which can decrease the liquation sensitivity of the heat-affected zone (where the hot cracks commonly generate) [75].

Electron beam welding (EBW) is a welding technique that the consolidation of materials is achieved by the concentrated beam comprised of high-velocity electrons flow colliding into the welding joint. The affecting parameters of this method are heat

input (almost for all of the welding techniques), beam feed rate and the oscillation frequency of the electron beam.

Thanks to the research of Richards et al., the effect of parameters in EBW has been investigated to eliminate microcracks. They have found that a higher current density with a lower welding speed will lower the number of cracks, however, the heat input is almost maintained compared with other groups in their experiment [79]. As Richards et al. investigated, a large number of liquid film migration happens in Heat affected zone (HAZ) while welding so that the micro-fissures are reduced. Other parameters such as pre-weld heat treatment, post heat treatment and heat input have also been proved to be closely related to the microcracks [80-82].

Laser beam welding (LBW), always used in the automation industry, is a welding technique that joins the workpieces by laser, heats the metallic material surface and joins them by the thermal conductivity of the material themselves. The CO₂ and Nd-YAG laser are the most used in the joining process for nickel-based superalloys. Similar to the former two welding techniques, parameters like heat input, laser welding speed, and laser power are the significant impact factor of the welding process. The outputs' geometries and mechanical properties are generally influenced [75].

There is some completed research that pioneers have done. In 1996, Gobbi et al. found that the post welding of Alloy 718 plate can be achieved by high power CO₂ CW laser welding, and the uniform bead profiles can be accomplished by Nd-YAG laser. They also found that the grain size of the welded material should get controlled (ASTM 10 or finer) to avoid the microcracks (which is related to the delta phase and NbC phase) appearing at the delta phase band so that an over-1000-post welding solution treatment has been applied to precipitate the delta phases, while after the 1038°C-heat treatment, the laves phase dissolved completely with the NbC phases left in the fusion zone—thus the micro fissuring are prevented [83]. The same conclusion has been proven by Reddy et al. [84], they have tried three groups of different conditions—direct aging, 980°C solution treatment + aging, and 1080°C solution treatment + aging for eliminating laves phases, a 980°C temperature could not dissolve laves phase completely but a 1080°C

environment can. However, although the laves phase does not exist in the latter group, Reddy et al. have found that the grain of the base metal has significantly coarsened so that the material's properties have been negatively impacted. It is considered that the solution treatment + aging of 980°C group is the best—the property has been improved at least.

Besides those former standard welding techniques, friction stir welding (FSW)—is solid-state welding met that hod, has massive usage in shipbuilding, trains and aerospace areas. Different from other ordinary welding methods, FSW does not melt the workpiece material in the welding process, the friction between surfaces achieves the joining—the workpieces are heated by the friction with the rotating tool, which softens the workpiece material so that those hot, soft metals can be forged mechanically by the applied pressure, much like the joining of clay to some extent. Due to the speciality of joining progress (no metal melted and solidified in progress), defects like cracks and porosities rarely happen in FSW, so the overall property of the production is better than other arc welding techniques. However, the flexibility of FSW has been limited. Initially, this technique was used for welding metallic materials, but in recent years, several applications in joining polymers and dissimilar metals have been investigated by researchers [85]. The main affecting parameters of FSW are tool speed and feed rate of the workpiece, as same as other welding performance, the mechanical performance of the workpieces can be affected.

Sato et al. [86] have investigated a more advanced friction stir welding process by applying polycrystalline cubic boron nitride (PCBN) tool into welding. It turns out that the microstructure of Inconel 600 has changed—the grain structure is more refined than the base metal so that a higher mechanical property has been formed in the stir zone, but the corrosion resistance slightly decreased in the HAZ and part of the stir zone. Song et al. [87] research have demonstrated the relationship between defect and welding speed, they have discovered in the welding process of Inconel 600 plates, a 150 to 200 mm/min welding speed is recommended for a defect-free workpiece, and also, same as the previous study, the mechanical properties of the workpiece have been

improved (10% higher tensile, 20% higher hardness) owing to the grain refinement compared with raw materials.

2.2.4 Microstructure of nickel alloys

In the solidification process of melted alloy, several phases will be solidified with the descent of temperature, both of them determines the properties of the material, some of them are beneficial, but some of them are detrimental, such as a fine grain microstructure provides high tensile strength and fatigue life. Yet, a coarse grain microstructure benefits the high-temperature behaviour of the superalloys. In addition, the size of precipitation that exists in the material significantly impacts its yield strength because of the reciprocal action between the dislocation and precipitates in the material [88]. The phases can be categorised into three types—geometrically close-packed phases (GCP), topologically close-packed (TCP) phases and carbides, GCPs are usually suitable for the properties of the material, but the TCPs, however, are always inimical. The following text will introduce phases that exist in Inconel alloys, their composition and their properties.

2.2.4.1 Phases

The matrix phase of Inconel series superalloys is the gamma phase, which is contributed by austenitic Face-centred cubic (FCC) nickel. It is a nonmagnetic and coherent phase which is the basement and background of other phases, usually containing a considerable amount of solid solution elements—that is where the solid solution strengthening happens in the material.

Gamma prime (γ') phase is one of the secondary phases in the GCP category, which is coherent to the matrix phase, it is the main strengthening phase of most of the nickel-based superalloys, and the main component of it is $\text{Ni}_3\text{Al}(\text{Ti})$, similar to that of matrix phase, the structure of Gamma prime phase is also FCC, but the size of its crystal lattice is a bit different from Gamma phase, the shape of it is various (from the sphere in some old-type nickel alloy to cubic in newly developed alloys). Its size depends on the

exposure time and temperature in processing and usually depends on the ratio of γ'/γ lattice mismatch. When the ratio is high, some uncontrollable other phases like η (Ni_3Ti) or δ (Ni_3Nb) phases will be generated under a temperature above 700°C [14].

Gamma double prime (γ'') phase is coherent to the Gamma prime phase and belongs to the GCP family, which behaves like a series of small disks comprised of Ni_3Nb . Its microstructure is Body-centred-Tetragonal (BCT), the main strengthening phase of Inconel 718. With a high temperature being applied, the Gamma double prime phase will be dissolved [89].

η (eta) phase is also a member of GCP, with a Hexagonal Closest Packed (HCP) structure and comprised of Ni_3Ti , which can be found in the superalloys that with a high titanium/aluminium ratio and being exposed for a long period, it may form both intergranular and intragranular as cellular and Widmanstätten patterns respectively.

δ (delta) phase in the nickel alloys has an orthorhombic structure, usually found at overaged nickel superalloys. Its constituent is the same as that of the Gamma double prime phase—both of them are Ni_3Nb , but the δ phase is not coherent with the Gamma series phase. Fortunately, the strength is not weak, so they can be added to alloys to refine the grains on purpose.

σ (sigma) phase is a TCP phase that negatively impacts the mechanical properties of superalloys, which appears as irregular small balls and always elongated. As the worst phase over the three kinds of TCP phases, it is not that a typical pernicious phase appears in nickel-based superalloys.

Laves phase is another detrimental phase to the mechanical properties of Inconel alloys, which has abnormal properties of both mechanical and chemical aspects, which is attractive to metallurgy researchers for developing potential applications. The laves phase's appearance is the same as that of the σ phase, globule shaped and always elongated, but after being treated by a long-time exposure, its shape will be formed as platelets [14].

The last kind of TCP phase is the μ phase, generally being observed in an alloy that owns a high component of Mo or W, mainly composed of the elements of Mo, Re, W,

Cr, Co, Nb etc., it severely damages the stress rupture strength of the superalloy in a high temperature [90].

Overall, the Inconel series superalloy was strengthened by a series of beneficial phases under the supplement of the matrix phase, but a series of detrimental phases can also ruin their properties. It has become a challenging task for researchers to avoid damaging phases. The already existing research has revealed that both the strengthening phases and detrimental phases have a solid relationship to the components of alloy, for those alloys that have Al and Ti inside, the strengthening precipitate of it is Gamma prime (γ') phase, for those who have Nb inside, the strengthening precipitate of it is Gamma double prime (γ''), as for detrimental phases, the σ phase existed based on Cr, the laves phase usually based on Fe, usually appears in iron-based superalloys. The formation of the μ phase always existed in the area where W or Mo are enriched [14]. Thus, the component of elements and also the distribution of elements should be controlled via refining the processing to avoid detrimental phases.

2.2.4.2 Carbides

Carbides are another kind of precipitations in Inconel alloys, string-like clumps' appearance makes them easy to find in observation, there is a series kind of carbides that depend on different performing processes and components, but they can be categorised into MC, $M_{23}C_6$, and M_6C (M=metal elements, C=carbon) three categories [91]. The carbides in superalloys are always beneficial, which can enhance the alloy's mechanical properties, one of the strengthening mechanisms of carbide is that the carbides placed in grain boundaries and inter-dendritic regions can prevent the sliding of grain boundaries—considered as providing precipitation strengthening to the material, another strengthening mechanism is that the carbides are capable of tying up certain elements for halting the engender of detrimental phases [92]. The figure below shows the composing elements of some of the carbides.

Table 2.2.2. The constituent elements of some forms of carbides [49].

Carbide Form	
MC	W, Ti, Nb, Ta, Mo, Hf
M ₂₃ C ₆	Cr, Mo, W
M ₆ C	Mo, W, Nb

The MC carbides are the primary carbon source for the alloys when a relative chemical reaction happens. They have an FCC microstructure and are usually considered one of the most stable composites in nature. They can be formed in the liquid alloy or after the solidification process at a high temperature, which exists along the grain boundaries or within the grains in blocky or script morphologies [49].

M₂₃C₆ carbides usually can be found in high-chromium composed alloys, they are formed by low-temperature heat treatment (760–980°C) and also can be produced from the degeneration of MC carbides or the soluble carbon residue in the matrix. The alloy’s properties can be significantly affected by the form of those carbides—when they are at a discrete particle form in grain boundaries, the rupture strength of the alloy can be considerably increased by inhibiting the grain boundary sliding. However, when the M₂₃C₆ carbides form cellular structures films, the properties can be adversely affected [49].

M₆C carbides can be formed from the MC’s degeneration and high-temperature heat treatment, are usually appears in the alloys that own a relatively high molybdenum content, dislike M₂₃C₆ carbides, the M₆C carbides behave higher thermal stability and more practical usefulness as precipitation in the grain boundary to controlling the grain sizes [49].

2.2.4.3 Microstructure

As elements constitute the phases, that refined microstructure (as shown in the image below) exists in the nickel-based superalloys, which are being observed underneath OM (optical microscope) or SEM (scanning electron microscope) for higher magnification.

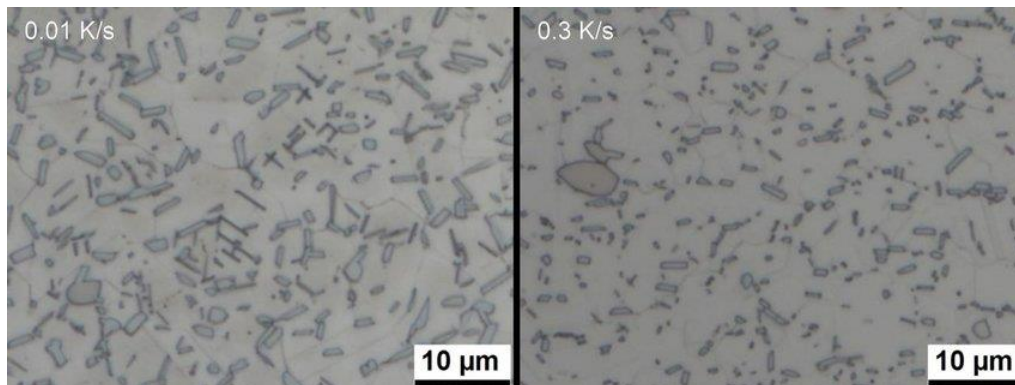


Figure 2.2.3. Microstructure of etched Inconel 718 etched by Kalling II reagent under the observation of Optical Microscope [93]

The metallography of nickel-based alloy has been observed via OM by Christian Rowolt et al. [93], the matrix phase and some dendritic structure can be seen for this image.

The image below from the OM observation can only distinguish some mass structures, such as dendrites and apparent defects. Higher magnification equipment like SEM should be applied to investigate the detailed structure.

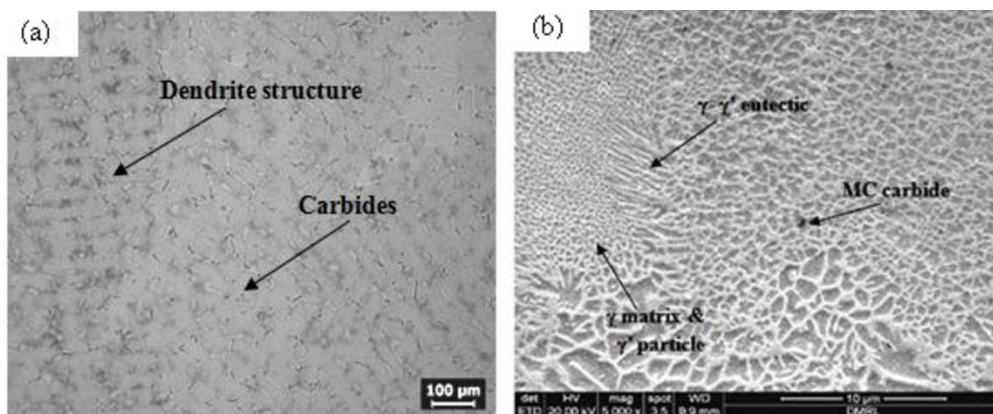


Figure 2.2.4. a) The Optical microscope image b) the SEM image of Super cast 247A Superalloy [94]

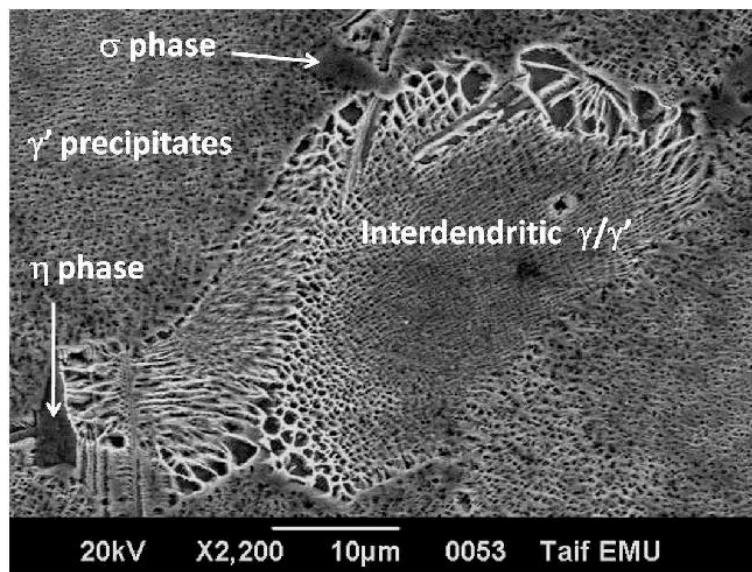


Figure 2.2.5. The SEM image of as casted superalloy 17 [95]

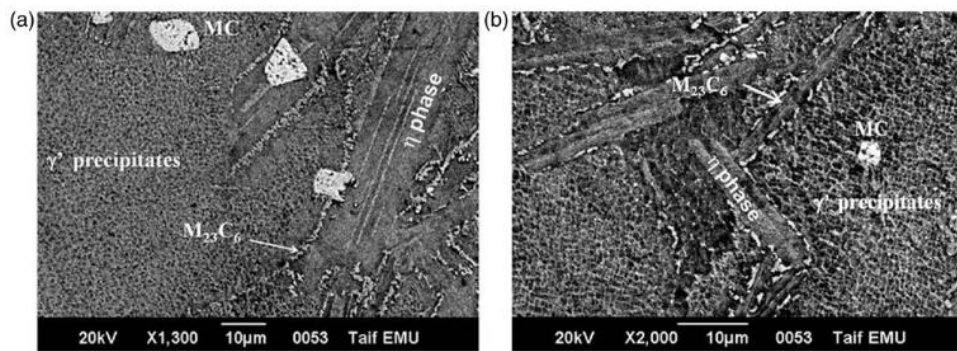


Figure 2.2.6. The SEM image of carbides [96]

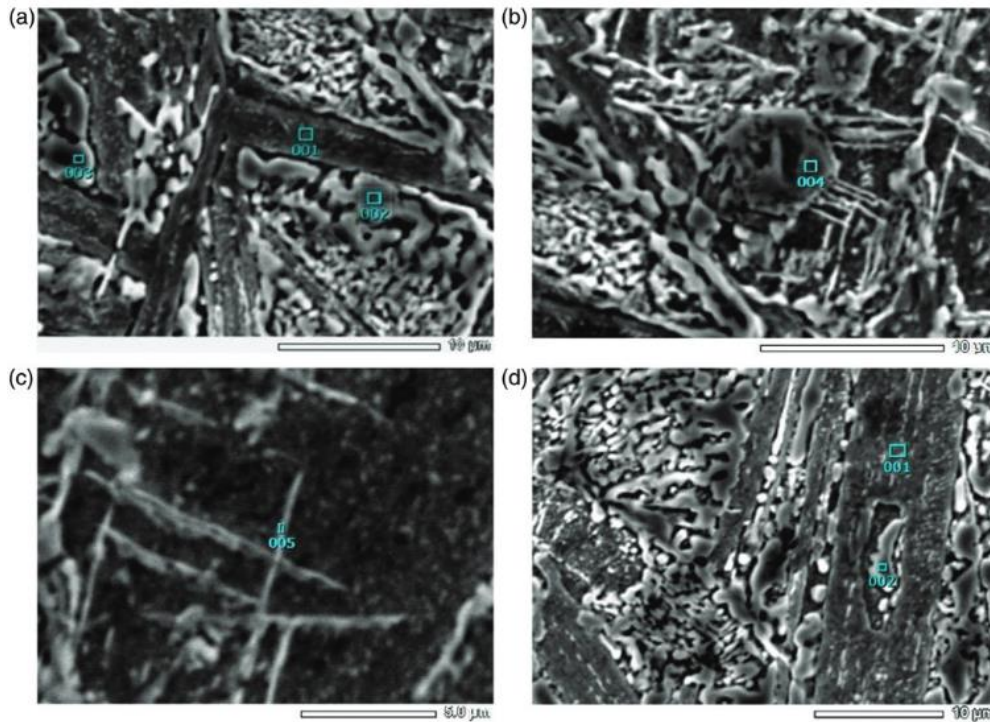


Figure 2.2.7. SEM images of needle-like TCP phases in nickel-based superalloy [96]

Those images have shown some of the detailed microstructures (phases, carbides) of nickel-based superalloys, which can be determined and explored by EDS (Energy Dispersive X-Ray Spectroscopy) via their elemental distribution.

2.2.4.4 Microstructure and properties

It is noticeable that there is a strong link between the microstructure of nickel-based superalloys and the mechanical properties of them, to some extent, the finer the grain size, the higher the tensile and fatigue life, which is caused by the dislocation movement that leads to grain orientation and stress concentration alongside the slip plane, but on the other hand, coarse grain size may enhance the creep and fatigue strength in a high temperature [97]. Also, different compositions like precipitations can virtually impact the yield strength of the material, that is because of the effects between precipitates and dislocations, as for small-sized precipitates, the dislocation cutting (the dislocation cut through precipitates, so that introduces more precipitate-matrix interface) occupies the dominant position, for large-sized precipitates, the main effect is dominated by

dislocation bowing (bowing around the particles) that around the precipitates, as shown in the equation below.

$$\begin{aligned}\omega &= G * b/L - 2r \text{ for cutting} \\ \omega &= r * \vartheta * \tau/b * L \text{ for bowing}\end{aligned}$$

G for the shear modulus, b is the magnitude of the Burgers vector (depending on the material), L for the distance between precipitates, r is the radius of the precipitates, τ for the strength of the material and γ is the surface energy [97, 98].

2.3 Inconel Superalloys

As one of the most commonly used superalloys, Inconel is a series of nickel-chromium based austenitic alloy[99], which has been of interest for a considerable period, ranging from the early 20th century, Inconel[®] was invented by International nickel Company (INC) in the year of 1932, firstly was used in Whittle jet engine [100] and developed by a series of companies, the trademark is now held by Special Metals Corporation (SMC) [101].

2.3.1 Elements in Inconel alloys

The composition of Inconel is sophisticated, the main element is nickel, the second most element is Cr, other elements such as Fe, Mo, and Ta, their proportion is depending on the materials and both of them have their properties, which makes the usage of different Inconel alloys various.

Nickel, as the main element, is the basis of nickel-based superalloys, occupies more than 58% of the components in Inconel series alloys. As the fundamental element, nickel provides a face-centred-cubic (FCC) basic structure combined with other elements in solid solution, serves a matrix phase to other precipitates, provides ductility to the material[102]. Moreover, the nickel itself also provides an outstanding corrosion and oxidation resistance because of the chemical properties of nickel—superior resistance to alkali environment and good resistance to acid and oxides[103].

Chromium is the second most element in Inconel series superalloys (except

IN718), which is an element that provides the superalloy with a superior oxidation resistance by generating Cr_2O_3 oxide film on the surface of alloys[5]. Another utilisation of chromium is solid solution strengthening. As mentioned before, owing to the radii difference between nickel and chromium, the γ solid solution can be strengthened by dissolved chromium atoms, which enhances the high-temperature durability of the material[104]. In addition, chromium also plays a significant role in precipitation strengthening. Those dissolved chromium atoms can develop a series of carbides with carbon, with the participation of active refractory elements (such as Ti, Nb, Ta, Hf etc.), the MC-type (M=metal, C=carbon) carbides have been formed, with the effect of heat treatment, the carbides are decomposed into $\text{M}_2\text{3C}_6$ or M_6C low carbon and high chromium compounds, which strengthen the material by providing yield strength and elasticity to it [105].

Molybdenum is an element that only exists in Inconel 617, 625 (wt. 8~10%) [106, 107] and 718 (wt. 2.8~3.3%) [108] among the Inconel family. Molybdenum is an element that provides corrosion resistance to the material due to its excellent chemical properties of itself—it only reacts to concentrated HNO_3 , Aqua regia, hot and concentrated H_2SO_4 , and boiling HCl but no reacts with any alkaline solutions in room temperatures [109], a similar effect is provided by W (tungsten), but the proportion of it is not as high as Mo. The strengthening mechanism of Mo is the same as that of chromium, providing solid solution strengthening and precipitation strengthening to the material[5]. In addition, Mo also provides a Grain Refinement Effect, the more the content of Mo, the fine the grain size of the alloy, which makes the material being strengthened [110].

Iron is also a common element not only used in the Inconel series but also almost in all kinds of alloys. Its price and weldability make it an excellent choice for a commercial alloy to reduce costs [109]. Furthermore, Iron also plays a role in solid solution strengthening, which provides the alloy with higher tensile strength. However, the addition of Iron can negatively impact the mechanical properties of the alloy by contributing topologically close-packed (TCP) phases with other elements, which

contains σ phase (FeCr, FeCrMo etc.), μ phase (Fe₂Nb, Fe₂Ti etc.) and laves phase ((Fe, Co)₇(Mo, W)₆ etc.) [111].

Other metallic elements that occupy a few mass proportions in the alloy also appear in the Inconel family, both of them have similar functionality—precipitation strengthening, some of them have other functions, such as Cobalt—generating MC type carbide and strengthening the alloy [112], Niobium and Tantalum—only existed in Inconel 625, 718 and X-750 [107, 108, 113], the Niobium reduces the generation time of the protective form of alloy, so that provides corrosion resistance [114] and both the Nb and Ta are a significant component of MC-type carbides—causing precipitation strengthening[115], and so does Titanium. Other elements like Manganese can improve the weldability and oxidation resistance, and aluminium provides high-temperature corrosion resistance by generating tight adherent alumina films. The copper improves the material's resistance to reducing acids[44].

Despite metallic components, there are also several non-metallic atoms in the alloy. Some of those minor elements positively impact the alloy, but some may harm the alloy. Carbon and Boron are used to form carbides or borides, a compound with metallic atoms, as mentioned before. Other elements like Silicon, Sulphur, Phosphorus etc., can reinforce the alloy by promoting the formation of the carbides[116]. However, they also can be detrimental to the grains. As OP Sinha et al. have investigated, the grain boundary can be disastrously affected by high localised tramp elements [117].

In conclusion, the elements in the Inconel series superalloy are various. Most of them are engaged in strengthening the alloy, providing it with better mechanical and chemical properties. However, some of them also can be detrimental and negatively impact the alloy. Thus, the manufacturing process of superalloys should be concerned with avoiding detrimental phases.

2.3.2 Mechanical properties of Inconel

The mechanical properties of alloys are the exhibition of physical properties of them while a force has been applied onto the material, the major categories of

mechanical properties of metallic materials that are concerned in manufacturing are Strength (under an external load, the ability to withstanding destruction), Elasticity (the power of recovering to the original shape when an external force has been removed from the material), Plasticity (the capacity of deform permanently without rupture), Hardness (the capability of resisting penetration, scratching, abrasion or bending), Toughness (enables the material to suffer impact), Brittleness (allows the material to endure deformation), Stiffness (the resistance to elastic deformation or deflection), Ductility (the ability of being elongated into wire), malleability (makes the shape and size of the material being changed), Cohesion (resisting the material being broken into fragments), Impact strength (the ability of curbing sudden loads), Fatigue strength (the ability of enduring long effect of repeated straining) and creep strength (thwarting the deformation while under a long-term constant force) [118]. In the following section, some of the mechanical properties of Inconel alloys (718, 625 as two of the most representative Inconel alloys) will be introduced.

2.3.2.1 Hardness and tensile

A diagram of microhardness and tensile strength of the commercial Inconel 718 is listed below, as shown in the table (the data inside come from various databases on the Internet), the properties of different sized IN 718 in a room temperature are slightly different, for plate & sheet, the size ranging from 0.25 mm to 76.2 mm, for the bar is 4 mm to 254 mm and for welding wire is 0.5 mm to 2.36 mm.

Table 2.3.1. The mechanical properties of typical Inconel alloy 718 at room temperature

Mechanical properties of Inconel 718					
	Hardness (HRB)	Tensile (Mpa)	0.2% Yield (Mpa)	Young's Modulus (10 ³ Mpa)	Elongation (% in 2 in)
Sheet & Plate	-	930	482	200	15
Bar	100	930	482		12
Wire	-	1248-1448	517		12-30

Table 2.3.2. The mechanical properties of typical Inconel alloy 625 at room temperature

Mechanical properties of Inconel 625					
	Hardness (HRB)	Tensile (Mpa)	0.2% Yield (Mpa)	Young's Modulus (10 ³ Mpa)	Elongation (% in 2 in)
Sheet & Plate	145-240	827-1034	414-621	207	45
Bar	175-240	827-1103	414-758		30
Wire	-	>827	>414		>30

As shown in tables, both Inconel 718 and 625 are high-performance alloys compared with other materials, especially the tensile strength and yield strength (stainless steel 304 as a comparison, whose tensile strength usually is 72-101 ksi. and 31 ksi. for yield strength). Furthermore, the corrosion resistance of those superalloys is also at a superior level, which will be introduced in the following section.

It has been proven that the mechanical properties of Inconel can be affected by the fabrication process, welding process and working temperature. Shankar et al.[119] have studied the effect of aging onto re-resolution annealed alloy 625. They have applied a 923K aging process, and the yield strength of 625 alloys has improved with a reduction of ductility. The longer the aging time, the more significant the impact. Shankar et al. found that the principle of increment of yield strength results from the precipitation of Gamma double prime (γ'') phase, which strengthened the alloy by precipitation strengthening mechanism. Another reason is the dissolution of the Ni₂(Cr, Mo)-phase, which influences both the value of yield strength and ductility but influences more on the former. Also, a longer aging process may lead to a coarsening of the γ'' precipitates and precipitation of δ -phase, which further improves the yield strength but decreases the ductility. Another group has applied a higher temperature aging (1123K), which leads to a massive decrease in the initial 1 hour caused by the complete dissolution of both Ni₂(Cr, Mo) and γ'' phase, further aging leads to a formation of δ -phase, which improve the yield strength but decrease the ductility of the material.

Table 2.3.3. The effect of different welding methods on mechanical properties of Alloy 718 [120]

Process		Condition	UTS (MPa)	0.2% YS (MPa)	Elongation (%)	Failure region
CC-GTAW [121]	BM	980STA	1462	1315	21.6	–
	Joint	Weld + DA	1039	757	9	FZ
GTCAW [122]	BM	980ST	870	580	38	–
	Joint	As-weld	863	548	27.93	FZ
EBW [123]	BM	980STA	1500	1280	25	–
	Joint	Weld + DA	1375	1235	16	FZ
LBW [124]	BM	980STA	1475	1272	24	–
	Joint	Weld + DA	1424	1210	12	FZ

The effect of Constant current gas tungsten arc welding (CC-GTAW), Gas tungsten constricted arc welding (GTCAW), Electron beam welding (EBW) and Laser beam welding (LBW) are summarised by Sonar et al. [120]. As can be seen from the diagram, the welded joints are commonly own a lower ultimate tensile strength (UTS), yield strength (YS) and value of elongation compared to base metal (BM), that is because of the occurrence of the laves phase in the fusion zone that dwindles the cohesive strength between grain boundaries, so that the tensile strength of Inconel 718 joints [120]. Analytical research has investigated 30% deformation localised in the CC-GTAW welding process. It has shown an approximate 9% of the total gauge length of the specimen [121]. Furthermore, several researchers have also proved the detrimental of laves phase segregation. It is said that the laves phase exposes the rapid commencement and also promotes the formation of solidification cracks so that the ductility of joints can be decreased [125]. Another reason for the property decline is the strength declination between the laves phase and gamma matrix. The formation of laves phase initiates the brittle microcracks and enables the growth of a low energy fracture path that accelerates the crack growth, investigated by Sivaprasad et al. [126]. Laves phase

can also impact the material by its morphological conditions, however, a finer laves phase has less negative impact than a coarsened or network laves phase [123]. Laves phase can also depreciate the solute atoms from the matrix phase, minimising the strain fields between dislocations [127]. So that the parameters that can affect the formation of the laves phase are essential in a welding process, and also the choice of welding methods—Sivaprasad et al. [128] have reported that the EBW welding was resulting in an advanced tensile strength that from the GTAW welding, which is the result of more acceptable grain size and lower level of laves phase formation in the fusion zone. Also, Jia et al. [129] did some inspections onto a newly reformed ultra-high frequency pulsed gas tungsten arc welding (UHFP-GTAW), compared to the conventional pulsed gas tungsten arc welding (CP-GTAW) methods, the elongation performance of the material can perform 106% more and also reduction of the area with just a slight decrease on the tensile, it is also because of the control of laves phase—the amount of laves phases in UHFP-GTAW are lower than that of the CP-GTAW, and the refinement of precipitation phases morphologically and grain size in the matrix phase.

More studies are exhibited for proving the effect of welding parameters, and these parameters can either enhance or nerf the mechanical performance of the material. Ramkumar et al. [130] applied two kinds of fluxes (TiO_2 and SiO_2) into the Activated flux tungsten inert gas welding method (A-TIG) for Inconel 718 joints. It has been reported that the use of TiO_2 flux shows an 8.58% more in tensile strength but a 33.70% less in ductility than that of the SiO_2 flux. The characteristic is obtained by high arc energy density caused by the arc constriction due to the oxide fluxes that reduces the heat input and improve the cooling rate of the welding process. In addition, shielding gas is also an essential parameter in welding, Anbarasan et al. have examined the effect of different shielding gases in GTAW welding, the result shows the Argon mixed with a specific component of hydrogen (about 5%) as shielding gas behaves better than a pure Argon by refining grain size and restricting the laves phase, the study reveals the addition of hydrogen has made the thermal gradient more precipitous of the welding, which deactivated the segregation of elements (Nb, Mo etc.) that can form laves phase

in inter-dendritic areas—so the formation of laves phases are diminished in Mo-rich filler addition welds [131]. What's more, as discussed in the text, parameters like heat input are another factor that affects the material's tensile strength [127]. As revealed in Sonar et al. research, an increased heat input coarsened the grain size and thick laves phase in the fusion zone, a high heat input results in a nullification in the dendritic refinement mechanism in GTAW, to prevent a poor tensile property, the selection of optimum heat input is also significant.

Unlike tensile, the factors that affect the hardness of Inconel, rather than a pack of reasons, rely on the choice of heat input and cooling rate. It depends on the partition coefficient of solute in the solidification of fusion zone—the Nb concentration in the inter-dendritic area is the main influential factor of hardness so that the depreciation of solute from dendrite core caused by the segregation of Nb or formation of laves phase leads to a declined hardness, so, higher the component of Nb in laves phase, lower the hardness performed in the material. As Hemant Kumar et al. investigated, the improved cooling rate in A-TIG welding caused by applying tri-component flux—composed with Cr_2O_3 , FeO and MoO_3 have successfully increased the hardness of the material by 12.39% compared with typical TIG welding, which is related to the oxides entanglement that bestows strength to the alloy [132]. Ramkumar et al.'s study revealed the effect of three different types of filler wires on Inconel 718 plate in PC-TIG welding, the wire types are ERNiCu-7, ERNiCrCoMo-1 and ERNiCr-3. They have found that ERNiCrCoMo-1 performs the best hardness over the three groups related to the Cr and Mo in filler wires that strengthen the matrix by generating secondary precipitates [133]. Commonly speaking, the hardness of Inconel should be constant, and even in the bulk of the material. However, the welding process may make the mechanical property of the joint area uneven. As Cortes et al. [134] carried out, the hardness value in HAZ might drop because of the evolved brittle secondary phases in HAZ that initiate the cracks. Also, Sonar et al. [122] said that a lower microhardness might happen in FZ and HAZ because of the constitutional segregation of solute atoms, with a depreciated core area left in the welding matrix.

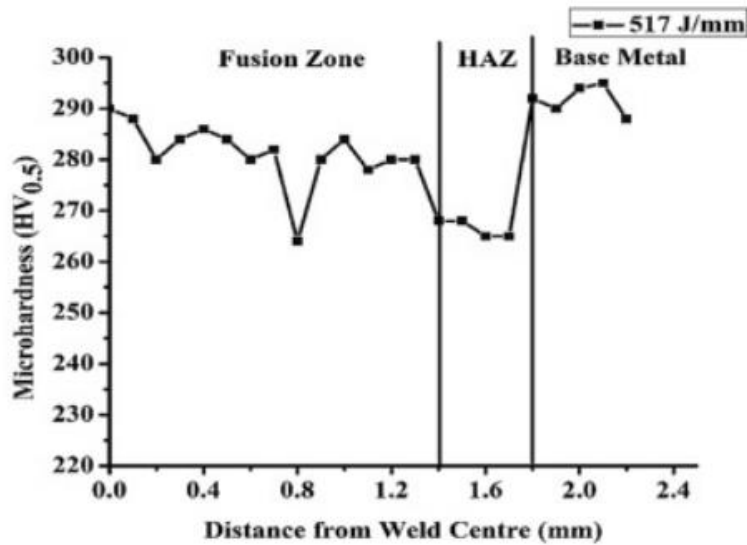


Figure 2.3.1. Distribution of microhardness of welded Inconel 718 joint

Another reason for affecting hardness is the annealing temperature and duration, which affects the formation of strengthening precipitates. As Thomas et al. [135] investigated in their study, they have used several groups of Inconel 718 samples that have been annealed from 600°C to 1000°C isothermally with different duration of annealing times (5 mins, 30 mins, 1 hour and 3 hours respectively), after the quenching process, the value of hardness will be tested for speculating the formation of precipitations. As the figure below shows, the precipitates formed differently—as recorded by the soar of the hardness. Comparing those groups, the precipitates did not seem to be developed in 1000°C and 600°C groups, and the 800°C group showed the highest hardness right after three hours’ annealing. Thomas et al.’s research also concluded that without the strengthening precipitations, the high-temperature deformation is controlled by the glide and climb of dislocation generated by the self-diffusion of nickel.

Table 2.3.4. Vickers hardness value of Inconel 718 specimens under different annealing conditions [135]

Temperature (°C) /Time (min)	5	30	60	120
1080	-	-	222	-
1000	232	226	229	230
900	233	284	275	271
800	304	379	411	414
700	249	279	288	335
600	232	235	231	237

In conclusion, the Tensile and Microhardness of Inconel alloys depends on the material's quality and welding. Selecting material and appropriate welding techniques is necessary to gain a qualified production.

2.3.2.2 High-temperature performance

As superalloys, the high heat tensile performance of Inconel series alloys should be highly concerned. The main advantage of superalloys is the remained high performance in a high temperature compared to other typical materials. Typically, the particular characteristic of Inconel 718 allows it to perform well up to 750°C, which is achieved by the secondary phase particles after aging. When the temperature is higher than 750°C, the mechanical properties will plummet because of the dissolution of strengthening precipitates and the melting of the matrix phase (the melting range of Inconel 718 alloy is 1260-1336°C).

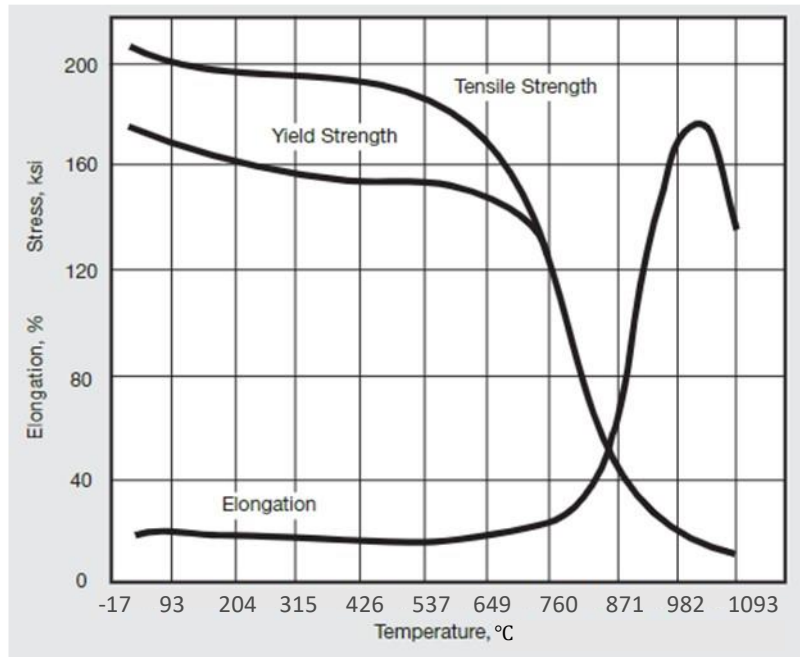


Figure 2.3.2. The high-temperature performance of Inconel 718 bar [108]

High temperature creep performance is a significant parameter of the superalloys like Inconel series materials, the principle of a high temperature affecting creep performance can be categorised into two groups. The first reason is the stability of strengthening phases is affected by the creep temperature—which is decided by the size, shape and type of their own, as revealed in Chen’s study, the Ostwald ripening in his experiment coarsened the spherical γ' precipitates, and that increases the services temperature from 650°C to 750°C, but in a surrounding temperature that higher than 850°C, the metastable γ' phases are tending to transform into η phases, causing a thermal instability [136, 137]. The second reason is the service temperature, which influences the creep formation mechanisms to a large extent. The creep deformation depends on grain boundary sliding, diffusion creep, and dislocation creep. Dislocation is always crucial in deciding creep temperature [138]. Such as in the CM 247 DS LC alloy, the dominating factors of creep deformations at 700°C are antiphase boundary and dislocation partial shearing γ' precipitates, however, the primary deformation mechanism becomes to the existence of network-shaped dislocations and their climbing at 1100°C [139].

Factors that affect high-temperature tensile performance—such as tensile, yield

strength and elongation of Inconel series alloys, to some extent, is similar to those that impact room temperature tensile and hardness of Inconel 718. At first, the component of the material itself and the chosen service temperature. As Lin et al. investigated, the tensile flow behaviour of GH4169 alloy at a temperature range of 200-700°C is acceptable. When it is over 700°C, the brittleness of the material increases so that the tensile and elongation is much lower than that of other temperatures [140].

The second reason is welding techniques—the welding process can also affect the high-temperature performances. Janaki Ram et al. [125] reported that the result of PC-GTAW welding in their experiment has shown off a better high-temperature performance than that of the conventional GTAW method—the conventional one performs an 8.50% and 75% lower tensile strength and elongation than that of the base metal. In comparison, the PC-GTAW performs a 4.3% and 31.25% lower feature than the base metal. Also, the principle behind this is the laves phase again—the PC-GTAW welding technique refined the fusion zone dendrites to lower Nb's segregation and the volume of laves phase. In addition, PC-GTAW also leads to a finer discrete of the morphological aspects of laves phases, which helps dissolve the laves phase massively in pre-weld heat treatment, which is far better than the network shaped and coarse laves phases in conventional GTAW welds. The comparison between magnetic arc oscillation TIG welding (MAO-GTAW) and current pulsing TIG welding (CP-GTAW) has been accomplished by Sivaprasad et al. [126], the tensile performance of those two groups in 650°C are dissimilar—the sample in the MAO-GTAW group is higher than that from the CP-GTAW group, it is owing to the finer and less net-shaped laves phase generated in fusing zone in direct aged condition. In contrast, in the solution treated and aged condition, the tensile feature of MAO-GTAW welded Inconel 718 is lower than that of CP-GTAW and even typical GTAW methods owing to the formation of a large amount of needle-shaped δ phases. Reddy et al. [123] research also reported their experimental groups' high-temperature performance. The Elliptical beam oscillation has a higher tensile feature than non-oscillated beam joints at room temperature or 650°C. The oscillated beam weld showed an approximately 15.83% and 66.67% higher

tensile and elongation than the non-oscillated beam joints.

Overall, the high-temperature performance of Inconel series alloys depends on the material, the working temperature, and the welding methods. Those factors should be cautiously and comprehensively concerned for a promising material for the working surrounding.

2.3.3 Corrosion and oxidation resistance of Inconel

Corrosion is a natural process that can gradually destroy the material by chemical or electrochemical reaction with the working environment (water vapour, oxygen, acid, alkali or sulphur etc.). The happening of corrosion is always slow, but this unpredictable reaction can happen anywhere, which makes the material's property severely harmed and finally may lead to a total failure of a component or even a whole project. The types of corrosion are various—uniform corrosion is the most common type. It usually happens on the surface of a large area of the material evenly. It is generally formed by the contact of substances from surroundings like oxygen and vapour. The second type is pitting corrosion, which is the most unpredictable, hard-to-measure and harmful corrosion. It is happened by the anodic or cathodic point that exists on the surface. It is always caused by the break in the oxide film or protective coating or the non-uniformities of the material itself. This pitting does not limit surface corrosion but may create deep holes or even penetrate the whole material, leading to the most dangerous consequence but with a bit of loss of material. Another kind of corrosion is crevice corrosion, it happens where the oxygen is limited, such as the area below the seal, near the nut, rivet head, and it is usually caused by the different ion concentration between two joining metals, as well as the prevention of oxygen circulation so that stagnant liquids can be accumulated inside, this unstable environment compared with the rest of materials makes the corrosion happens strictly. Other corrosion like intergranular corrosion (caused by the uneven distribution of the alloying elements at grain boundaries) stress corrosion cracking (related to the tensile stress in a high temperature), and galvanic corrosion (usually happens when two metals are physically

or electrically contacted) is also noticeable for the use of metallic materials. Oxidation of alloys is similar to corrosion, and it is the surface chemical degradation of alloys because of the chemical reaction between alloy surface and environment (usually air). Both corrosion and oxidation can lead to the degradation of metallic materials, and a poor project plan may cause not only the destruction of the economy but also loss of life. Thankfully, Inconel series alloys own a high corrosion and oxidation resistance even at a high temperature. The following text will introduce an overview of the corrosion and oxidation resistance of Inconel series alloys.

2.3.3.1 Corrosion resistance

Corrosion resistance can prevent alloys from environmental deterioration caused by chemical or electrochemical reactions. Typically, the materials not tending to be corroded may include features like low dissolution in an aggressive solution, high resistance to physical damage, high chemical stability and so on. The principle of high corrosion resistance of Inconel alloys, Inconel 625 as an example, depends on the alloying elements and their effects—the high alloy contents added such as Cr provides an oxidation film to prevent from oxidises. Al is also content that generates an alumina scale for protection. The high nickel and molybdenum content bring resistance to deoxidising environments. In addition, high nickel content avoids the chloride-ion stress corrosion cracking. Molybdenum content itself can provide a resistance to pitting and crevice corrosion. Nb content stabilises the alloy from sensitisation in the welding process, preventing the intergranular attack. That is one of the reasons why the Inconel series alloys are commonly used in aerospace and chemical industries [141]. A comparison table of austenitic alloys' corrosion resistance is listed below. As shown in the table, the Inconel 625 alloy offers higher overall resistance to corrosive surroundings than other austenitic materials.

Table 2.3.5. Comparison of corrosion rate (miles per year) between different austenitic alloys [141]

Alloy	Boiling nonoxidising acids					Boiling oxidising solutions	
	40% HOOC-COOH	10% HCl	10% H ₂ SO ₄	55% H ₃ PO ₄	85% H ₃ PO ₄	10% HNO ₃	50% H ₂ SO ₄ + 2.5% Fe ₂ (SO ₄) ₃
304	180	Dissolved	2200	400	9500	1	46
316	30	Dissolved	400	18	450	1	36
317	-	9000	360	-	-	0.5	28
200	10	8000	130	500	-	Dissolved	8000
600	10	4400	360	-	1800	-	-
825	8	1000	18	6	35	0.6	11
G-3	2	1000	24	5	24	0.8	11
625	7	620	44	10	110	1	23
C-276	3	220	16	7	18	18	260
B-2	0.4	7	2	3.5	3.5	Dissolved	-

In general, the chemical stability, arrangement, compactness, strength, coefficient of thermal and plastic expansion to the corrosion environments decide the corrosion resistance of the alloy to a large extent [142]. Zhao et al. tested the corrosion resistance of Inconel 740. In their study, two groups of Inconel 740 specimens are corroded under an ASTM G54-77 standard for 1984 and 5008 h respectively, the average metal loss of the two groups is 8.89 and 19.37 μm . Both of them exhibits an isolated internal sulphide. It proves the corrosion performance of alloys depends on corrosion time, which should also be considered a parameter that affects the material's lifespan.

Considering the submarine use of Inconel series alloys, the corrosion behaviour in an aqueous surrounding like seawater and acid solutions should be highly concerned, as a submarine material, Inconel series alloys perform better than stainless steel 316 in a temperature excess 1000°F, which is the most famous building material for submarines. Inconel also retains a better oxidation resistance than stainless steel 316. Alloy 718 is a popular material used for constructing fasteners and hardware in submarine systems. It is because of the passive NiO or Ni(OH)₂ thin film generated by

nickel content [143]. Furthermore, Cr and Al etc. provides different varieties of protection to the alloy, as introduced in the previous text. On the contrary, the existence of TCP phases significantly reduces either the corrosion resistance or the oxidation resistance of the alloy. Thus, the importance of controlling the content of elements and detrimental phases has emerged for a feasible corrosion behaviour of alloys.

Besides elements of the ontology, adding other alloying elements can highly improve the corrosion resistance of Inconel alloys to become special alloys. As Amin et al. [144] researched, the addition of a certain content of Re into Inconel 718 alloy makes the corrosion resistance of the alloy increased, they have used three groups of re-containing Inconel 718 alloy with different content of Re (2.4%, 3.5%, 6%), and commercial Inconel alloy as a controlled group, the specimens are electrochemical tested via 0M, 0.1M, 0.3M and 0.6M NaCl in 1.0 M H₂SO₄ solution, the result shows that the corrosion resistance sequence of different alloys are: 6% Re-718<Inconel 718<2.4% Re-718<3.5% Re-718, it is concluded that the addition of Re suppresses the susceptibility of Inconel 718 alloy from Cl ion pitting attack when the content up to 3.5%, however, a higher content of Re accelerates the pitting and uniform corrosion. Similar conclusions have been found by Kurzynowski et al. [145]; the addition of 14 wt% Re positively influences the corrosion resistance of Inconel 718 in a 3 wt% NaCl solution. In addition, they have also found a 28 wt% Re addition to Inconel 718 (partially dissolved Re powder) leads to a 160% higher microhardness than typical Alloy 718.

Another factor that affects corrosion resistance is the welding process, which is basically because of the consumption of strengthening elements (Nb, Mo, Ti, Al, etc.) and the formation of laves phases, making the alloy more vulnerable to attack by oxidises and rust. Hence, the mitigation of laves phases is critical, especially for aerospace and submarine applications. By using Mo-rich fillers in welding, this issue can be handled. As Ramkumar et al. [146] explored, the application of ERNiCrMo-10 and ERNiCrMo-14 fillers have improved the corrosion resistance of both the filler wires and fusion zone generating Cr₂O₃ and NiO films at a high temperature. Anbarasan

et al.'s [131] method of controlling laves phase by applying Argon+ 5% Hydrogen as a shielding gas, compared to that uses pure Argon as protection, has shown a higher corrosion resistance than typical methods because of the reduction of laves phase as mentioned in the previous section. In addition, Hernandez et al. [147] have explored that the parameter in the welding process can also influence corrosion resistance. They have used Inconel 718 as a welding material and getting tested in a 3.5% NaCl solution after welding with different heat inputs. The result shows an inverse relationship between heat input and corrosion resistance—the higher the heat input, the lower the corrosion resistance to NaCl solution. It is because of the microsegregation of Nb and Mo, which leads to a dilution of Fe into the welding pool.

Surface treatment, as an effective technique for enhancing corrosion and oxidation resistance of alloys, has been widely utilised in gas turbine components. Prevalent surface treatment techniques like aluminising, chromising and siliconised are used for Inconel alloys. As Sharvan et al. [148] discovered, the development of a uniform 280 μm thick aluminide coating brought by the aluminising process followed by ultrasonic shot peening process in Inconel 718 alloy has successfully suffered the attack of either mixed salt (75%Na₂SO₄ +15%NaCl +10%V₂O₅) or pure NaCl environment for 5 hours at 700°C, which performs better than aluminised-only alloy and bare alloy. A similar conclusion has been examined by Bai et al. [149], the effect of silicon coating aluminised coatings. Aluminised–chromised layer in IN-738-LC has been compared in a molten Na₂SO₄ at 900°C, they have summarised a ranking of different kinds of pack cementation coatings as follows: Rh–Al>simple Al>Pd–Al>Si+TiB₂>simple Si>Pd–Al–Cr>Rh–Al–Cr>simple Al–Cr coating.

To conclude, corrosion resistance of Inconel series alloy is a vital parameter that can be affected by various factors and processing techniques. It is crucial to evaluate the corrosion resistance required and balance the elemental content, processing cost and corrosion feature.

2.3.3.2 Oxidation resistance

Oxidation resistance is defined as the ability to resist oxidising of alloy in an oxidising environment. In an oxidising atmosphere, alloys are usually thermodynamically unstable, leading to severe quality issues like degradation to the alloy. A high corrosion resistance means the reaction rate alloy is low enough to work for an extended period. In the content of Inconel series alloys, the elements that provide oxidation resistance to the matrix are chromium, silicon and aluminium, which can provide compact, uniform and stable oxide films (Al_2O_3 , Cr_2O_3 and SiO_2) to protect the alloy from further oxidation at a high temperature. Also, the primary element nickel has the same function as chromium, silicon and aluminium—it generates oxide and protects the material. The growing oxide film governed the further oxidation to control the oxidating rate [150].

The oxidation resistance of a specific material depends on several working factors, such as operating temperature and working environment. Greene & Finrock [151] have tested the oxidation rate of Inconel 718 alloy at different temperatures. The Inconel 718 rods are oxidised in air at three temperature ranges (973-1223K, 1173-1573K, 1473-1614K), the low-temperature group behaves an early passivated performance against oxidation in a short period, the intermediate group shows a parabolic-rate dependence in oxidation rate owing to the controlled diffusion rate that makes the material keeps steady for a long time up to several weeks, the high-temperature specimen exhibits a severe deformation and damage caused by high oxidation rate.

To improve the oxidation resistance of the material, besides changing the metal's composition, further processing should be applied to the raw materials. Ion irradiation can improve corrosion resistance by facilitating the formation of the oxide layer. As Wan et al. [152] examined, the effect of the application of helium ion irradiation on Inconel 718 high-temperature oxidation resistance has been affirmed, they have used 0.4, 4, 40 dpa doses of 50 keV helium ion to irradiate Inconel 718 specimens and commercial Inconel 718 without irradiation as the control group, the comparison

between irradiated and unirradiated samples reveals that the higher the dose of ion irradiation, the lower the corrosion rate. The research investigated that irradiation facilitates the nucleation of oxide particles by increasing the surface layer's energy of the material. Furthermore, the irradiation induces defects onto the surface, which also accelerates the formation of the outer Cr₂O₃ oxide layer and so the further penetration of oxygen atom can be restricted. Post-processing treatments, in addition, can be used for enhancing the oxidation behaviour of as-built materials. Kang et al. studied the effect of hot isostatic pressing on the high-temperature oxidation resistance of additively manufactured (Selective laser melting) Inconel 718 alloy, the comparison between two groups of specimens (hot isostatic pressing treatment+ aging (HIP), solution treatment+ aging (SA)) reveals that the HIP treated sample behaves a better oxidation resistance than another group—the HIP treated group formed a thin, single and dense passive Cr₂O₃ oxide layer on the surface nucleated by NiC phase (which precipitated along the grain boundary so that the inner diffusion of oxygen can be suppressed), however, SA treated group formed a mixed oxide layer (Ni-, Fe-, and Nb-based) on the top of the passive Cr₂O₃ oxide layer, and dramatic oxidation has been found along grain boundaries. The HIP treatment enhances the oxidation behaviour of Inconel 718 alloy.

In conclusion, the oxidation resistance depends on the properties of the outer passive oxide layer. It usually comprises Al₂O₃, Cr₂O₃ and SiO₂ and can be enhanced by different processing procedures.

2.4 Stainless Steel

2.4.1 Introduction

As late as the early 20th century, iron and steel's rust and corrosion issue have not been solved. However, several materials can be used in corrosive environments—they are mainly nonferrous metals, including nickel, nickel-silver (nickel-copper-Tin), copper, Brass, Al, Monel (nickel-copper) etc. However, the nonferrous material works

effectively, the higher cost and a lower strength compared with steel have limited their application, as an article in the British Journal said: “The tendency to rust is a characteristic inherent in the element known as iron, and will, in all probability, never be overcome.”

However, just in the 19th century, a bunch of scientists have noticed that the addition of chromium in alloys of iron makes the material more resistant to corrosive environments compared to carbon steel, but none of them has studied the alloy containing both carbon and chromium at the same time, which might be known as stainless steels. Robert A. Hadfield has somewhat touched the edge of stainless steel. He has created chromium-containing samples also with carbon content; however, he dissolved all his samples in the sulfuric acid and concluded the addition of chromium reduces the corrosion resistance of alloy and discontinues his chromium-based study.

From 1905 to 1912, seven scientists from four different countries have accidentally created an alloy that we call stainless steel now, which is suspected this kind of high corrosion resisting alloy must be helpful in some places. However, due to its high cost and different manufacturing processes with regular steel. Initially, stainless steel was used as knife blade material before WW1, developed by Harry Brearley as the knife blade material of cutlery industries. A short announcement has been set in New York Times. Royal Air Force developed the soar of commercial stainless steel. They have found the cutlery material fits the demands of “aeroplane” very well. Thus, the materials are shipped to aircraft engine factories and sold by Firth with the name of “Firth’s Airplane steel”. Therefore, stainless steel is gradually known by the public [153].

2.4.2 Categories of stainless steel

stainless steel, as one in the ferrous group alloys that contain a chromium content higher than 11% [154], that added element provides the high material level of heat resistance and rust resistance. The categories of stainless steel are various, depending on the specific element content of stainless steel. The particular types of stainless steels are named by the American Iron and Steel Institute (AISI) with a three-digit number,

such as stainless steel 201, 316, 405 etc. [155] There are five main classes of stainless-steel classified by the microstructure of them: austenitic, ferritic, martensitic, duplex, and precipitation hardening stainless steel.

Austenitic steels are the largest group (about two-thirds of the whole stainless-steel family) of stainless steels. They own a Face-Centred-Cubic (FCC) microstructure (same as nickel) achieved by adding nickel, magnesium, and nitrogen. Dislike iron and steel. The austenitic steel is non-magnetic and can be cold hardened but cannot be heat-hardened due to its austenitic structure. There are two subgroups of austenitic stainless steels: 200 series and 300 series, the difference of them is based on the formation of austenite with different elemental contents—300 series is mainly based on the nickel content, and 200 series is achieved by nitrogen and magnesium, which are added for partially substituting nickel. Due to the excellent corrosion behaviour, formability, and high strength caused by cold work, austenitic steels are usually applied as corrosion resistance material. The most common austenitic steel is SS 304, also called 18-8 (18% of chromium, 8% of nickel) [156]. It is an excellent choice as the building material of cookware, cutlery, and kitchen devices, so it is also the most known stainless steel by the public [157]. Another representative austenitic steel is 316 alloy for severe environment applications because it contains molybdenum content, so corrosion resistance has increased. Also, Alloy 20 (C-20) can be used in corrosive environments. It owns a better corrosion feature than 304, 304L and even 316, always being used as a material that involves sulfuric acid because of the protection of copper content in the material [158]. Despite corrosion resisting alloys, heat-resisting austenitic steels like stainless steel 309, 310 and 314 are usually used in an environment higher than 600°C, the heat resistance is traditionally contributed by added chromium, supplied by Al and Si, as same as superalloys—a thin and passive oxide film provides the high-temperature feature to the material.

Ferritic stainless steels contain a chromium content from 11.5% to 18%, with a low component of carbon (<0.2%) usually and sometimes nickel added. Due to its low carbon composition, the ferritic steels cannot be heat hardened and can only be slightly

hardened by a cold working similar to austenitic steels [156]. In addition, its corrosion resistance is also comparable to austenitic steels to some extent. However, unlike austenitic steels, ferritic steels are magnetic and become brittle in a sub-zero temperature—just like carbon steels, which sank the Titanic because of the increased brittleness in ice water [157]. Typical ferritic steels are part of the commercial 400 series alloys, one of the representative examples is Type 430, the applications they are particularly specified, such as Type 409 mainly used for car exhaust, Type 444 used for instant hot water units and Type 446, have a series of high-temperature applications [159].

As revealed by its name, Martensitic stainless steels are based on martensitic iron as matrix phase, containing 12%-17% chromium and 0.1%-1.2% carbon. The application is based on their difference in components. For 0.4% carbon or less steel, the use of them is mainly depending on the high mechanical properties such as pumps, valves and shafts, for that with 0.4 % and higher carbon component, wear resistance is the prior property that is concerned for an application like cutlery surgical blades and nozzles [156]. Martensitic stainless steels can be hardened by heat treatment. Their application is based on its advanced mechanical properties enhanced by heat treatment like aging, quenching and annealing. Typical martensitic steels are another part of 400 series sheets of steel, some of the outstanding examples of them are Type 410—general-purpose martensitic steel typically used at fasteners, pins, cutlery, gun clips and so on, Type 420—specific applications like surgical tools and firearms due to its versatile hardness range, Type 440—higher hardening capability than the former two kinds and higher hardness that are used at cutlery, surgical instruments and bearing [160].

Duplex stainless steels are named by their mixed metallurgical phases. They usually contain two kinds of phases—austenitic (FCC structure) and ferritic (face-centred-cubic structure). The ratio of them is ordinarily equal. However, the ratio can be affected by heat treatment, and the lesser phase should occupy at least 30% of the material by volume [156]. For balancing those two phases, the stabilising elements for the austenite phase (Ni, Mn, N etc.) and the ferritic phase (chromium, Mo, S etc.) should

be balanced [161]. They have a better corrosion resistance (especially for chloride stress corrosion cracking, pitting and crevice corrosion) and higher strength (about twice as typical grades) than ordinary austenitic steels such as 316 or 304, which was the initial motivation of designing this kind of alloy. The duplex steels can be categorised by their pitting corrosion resistance, characterised by a specific number called pitting resistance equivalence number (PREN), calculated by equation $PREN = \%Cr + 3.3 \%Mo + 16 \%N$, the first kind is lean duplex (PREN 22–27), which is designed for several specific applications such as building construction, another category is standard duplex (PREN 28–38), one of the typical alloys is Alloy 2205, which is the most commonly used duplex steel due to its moderate properties, the third kind of duplex steels is Super-duplex (PREN 38-45), also with hyper duplex grades (>45) are developed later than the former two kinds, it is also a specific class that provides ultra-high corrosion resistance for reaching the demand of chemistry industries for containing or transporting oil and gases [162].

Precipitation hardening (PH) stainless steels, as high corrosion resisting steel comparable to austenitic steels, can be precipitation hardened to gain three- or four-times higher yield strength than austenitic steels, even higher than other martensitic steels. Based on their microstructure, precipitation hardening steels can be divided into three classes: low-carbon martensitic, semi-austenitic and austenitic PH steels [163]. Low-carbon martensitic PH steels usually contain a high chromium content that provides a superior oxidation resistance and exhibits high strength and other beneficial properties like dimensional stability in an elevated temperature environment. One of the typical martensitic PH steels is 17-4 PH, which contains 17% Cr and 4% Ni inside, it is a popular material in petroleum, chemical industries, and aircraft. Austenitic PH steels own a moderate corrosion resistance but high strength and good fabricability. The A286 stainless steel is the most well-known alloy in the austenitic PH group, it contains 15% Cr, 25% Ni and remains austenitic structure at all temperatures, A286 alloy owns good mechanical properties and creep resistance even at a high temperature, so it is usually considered as Fe-based superalloy [163]. Semi-austenitic PH steels possess a

more complex metallurgically than others. They are austenitic structures in annealing while becoming martensite at the same time of age hardening. An outstanding example is 17-7 Alloy, which contains 17% Cr 7.2% Ni, and it is the most formable alloy over all the PH steels. 17-7 Alloy is usually called “Workhorse Alloy” because of its good corrosion resistance, high strength and high formability, making it apply from knife blades to aerospace [164].

2.4.3 Characteristics & Properties of austenitic stainless steel

Although it has a history of more than 100 years, austenitic steel is still the most significant stainless steel. One of the fastest-growing materials, as the most frequently used stainless steel, austenitic steels are well known for their high performance in high/low-temperature environments, high stability, excellent corrosion resistance, high toughness, weldability and formability. Also, the long lifespan of austenitic steels has been proven, which leads to a low maintenance cost than other highly alloyed materials in a machine [165]. However, it is hard to conclude all the austenitic steels in one paragraph because their features are differed by different contents. The following text will explore some of the austenitic stainless steel's general characteristics and properties for further investigation.

The alloying elements of austenitic steels are versatile because the addition of elements can enhance their properties. For example, the nickel content provides strength, ductility, and toughness to the material, which also generates oxides that protect the material from corrosion. The addition of chromium content leads to an improved oxidation and corrosion resistance and develops the stability of austenitic structure because those nickel equivalents balance the content. The addition of Mo, another nickel equivalent, also leads to an increase in corrosion resistance. If nitrogen, the stabiliser of austenitic structure, is added for balancing Cr and Mo content, the corrosion resistance can also be increased. Other elements can also be added to content for some specific applications. Si is added to promote corrosion and oxidation resistance and is also used as a deoxidiser. Cu was added for contrasting sulfuric acid

and improving the machinability. Nb was added to prevent the formation of chromium carbides along grain boundaries, improving the creep resistance and intergranular corrosion resistance. Ti is used for high carbon austenitic steels to prevent chromium carbides [166, 167].

Besides the primary phase, some carbides or nitrides can exist in austenitic steels. Carbon is customarily considered as impurities; however, it stabilises an austenitic structure and has a solid thermodynamic affinity for chromium. Therefore, the formation of chromium carbides occurs whenever the carbon is supersaturated in an austenitic structure owing to that affinity. Nitrogen, which has a higher solubility than carbon in austenitic steels, is usually not considered a threat in austenitic steels but may occur in those with high solubility like ferritic steels. While the corrosion resistance of the material depends on the chromium content, it may be affected by the consumption of chromium—caused by the chromium carbides penetration. If the chromium content level is low enough, the material feature may not even reach “stainless” [168].

As discussed in previous texts, the performances of austenitic steels are mainly achieved by the austenitic microstructure, which remains an FCC structure at any temperature (from room temp to its melting point). Generally, the austenitic steel should hold a single-phase austenitic microstructure; however it can also be affected by the manufacturing processes—it has been reported that the additive manufacturing (AM) process may vary the single-phase material to multi-phases, including austenite, ferrite, σ -phase and alloying elemental segregations because of the complexity of thermal history and nonequilibrium crystallisation in AM process [169]. For some reason, the metastable austenitic phase can transform into martensite phases, the martensite is harder than austenite, and that is one of the hardening principles of austenitic steels. The phase transformation obeys the sequence of $\gamma \rightarrow \varepsilon \rightarrow \alpha'$ (may happen reversely if being heated to 500°C and 700°C), γ phase is the matrix—austenite, ε is ε martensite (hexagonal closed packed structure) and α' for α' martensite phase (body-centred tetragonal lattice structure), transformation process may take place through $\gamma \rightarrow \varepsilon \rightarrow \alpha'$ or $\gamma \rightarrow \alpha'$ directly. On the one hand, the phase transformation can thermodynamically occur

at room temperature; on the other hand, the transformation process mainly depends on the stacking fault energy (SFE) of the material, which is defined as the interruption of atomic planes typical stacking sequence in a closed-packed structure, a low SFE promotes the phase transformation of austenitic steels, which is achieved by the formation of ϵ phases—as a pioneer of the α' phases it has been investigated that with the increasing of SFE, the formation of ϵ martensite is hindered and tend to deformation twinning and slip [170]. In addition, hydrogen absorption can also lead to a phase transformation in metastable alloys [166].

Despite phase transformation, another strengthening mechanism is a precipitation hardening, which transforms austenitic steel into precipitation hardening steels—the PH steels are mainly unstable austenitic structured except A-286 iron-based superalloy.

The tensile property of austenitic steel is strongly related to the compositions, as summarized by researchers, the equations of calculating yield strength and tensile strength are listed below:

$$\text{YS(MPa)} = 15.4[4.4 + 23(\%C) + 32(\%N) + 0.24(\%Cr) + 0.94(\%Mo) + 1.3(\%Si) + 1.2(\%V) + 0.29(\%W) + 2.6(\%Nb) + 1.7(\%Ti) + 0.82(\%Al) + 0.16(\%Ferrite) + 0.46(d^{-1/2})]$$

$$\text{TS (MPa)} = 15.4[29 + 35(\%C) + 55(\%N) + 2.4(\%Si) + 0.11(\%Ni) + 1.2(\%Mo) + 5.0(\%Nb) + 3.0(\%Ti) + 1.2(\%Al) + 0.14(\%Ferrite) + 0.82(d^{-1/2})]$$

Where d is the grain diameter (mm)

Also, these two equations can be used in duplex steels.

Austenitic steels have no clear yield point; however, they may deform from 40% yield strength of them. It is considered that austenitic stainless steels are quasi-elastic materials according to the rule of thumb, which leads to a bunch of active slip systems in the face-centred-cubic crystal structure [168]. Also, the tensile properties of austenitic steels are indeterminate as well; it is because of the testing temperature—adiabatic heating enhances the stability of austenite. In contrast, a constant temperature produces lower strength. However, several reported tensile strengths should not be

considered absolute values because testing conditions can easily affect them even by an accepted standard [168]. Another unique characteristic of austenitic steels is there is no ductile to brittle transition temperature for them, which is different from martensitic or ferritic steels because of the 12 slip systems of FCC structure—4 {111} planes and 3 $\langle 110 \rangle$ directions, and they do not need thermal activation even in a low temperature, which means the moving force of dislocations is not strongly relating to the temperature. In contrast, although the BCC crystal structure also owns a 12-slip system (6 {110} planes and 2 $\langle 111 \rangle$ directions), the movement of dislocations in a low temperature is too high to achieve because of the screw dislocations lock [170].

Austenitic steels own a high mechanical property; highly cold-worked austenitic steels are widely used for their sturdy performances that other materials cannot achieve. For example, cold-worked 301 alloy's yield strength can achieve 200Mpa because of the phase transformation effect. Austenitic steels also own an outstanding toughness, impact strength and elongation, owing to the diversity of the slip systems in the FCC structure and the low activation temperature they require. Thus, the austenitic steels surpass other steels in cost, toughness, and corrosion resistance.

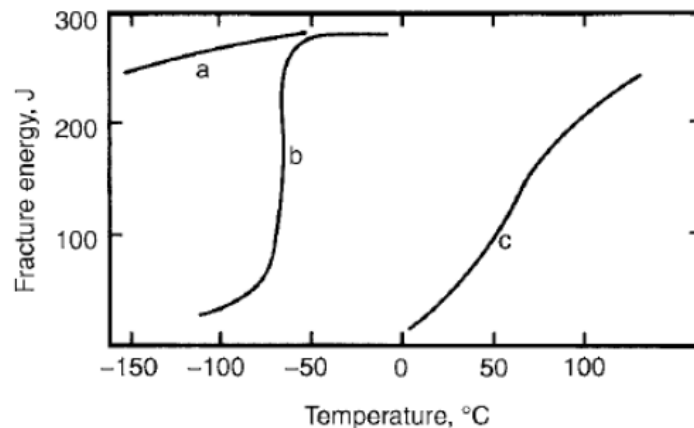


Figure 2.4.1. Comparison of impact strength in temperature between (a) austenitic steel, (b) duplex steel and (c) ferritic steel.

According to the element composition and applications, austenitic steels can be categorised into three groups: lean alloys (with high strength and weldability such as 304 & 201), oxidation resisting alloys (Cr-Ni alloys such as 309 & 310), and corrosion

resisting alloys (Cr-Mo-Ni-N alloys such as 316L & 904L), those classes behave different features from each other, the following text will introduce some unique properties of them separately.

2.4.3.1 Lean alloys

Lean alloys occupy the most considerable portion of produced austenitic stainless steels because stainless steel 304 is located in this category owing to an elemental content of nickel <14% and chromium <20% due to their moderate corrosion resistance, good weldability, formability and high flexibility in surface finishing. The lean alloy is to some extent a good countermeasure against the rising alloying elements price—a direct advantage of lean alloys is lower cost than other highly alloyed materials; however, the requirement of corrosion resistance has limited the application of lean alloys only as a material for daily life or in favourable working environments—a lean alloy can be used in any environments in our daily life except coastal.

In general, lean alloys, as the most typical austenitic steel, has followed almost all of the rules of austenitic steel except the tensile equation. As mentioned before, there are two equations to calculate the strength of austenitic alloys. However, those two formulas do not work in lean alloys, especially for leaner alloys like 310, which owns a low alloying element content—which lowers the effect of phase transformation and produces an enormous tensile strength [168].

2.4.3.2 High-temperature alloys

The high-temperature alloys have high strength and corrosion resistance even at a temperature above 500°C. They are always required to resist severe corrosive substances like oxygen, sulphur, carburising, nitriding, halogens, and molten salts. In addition, the alloying with elements like C, N and Nb significantly improves the material's high-temperature strength, so the high-temperature steels are used in the heat exchanger, fossil tubes, and aerospace and aircraft.

The oxidation resistance of High-temperature alloys depends on the protective

Cr₂O₃ scale, and the formation of this protective scale will be continuous when the chromium content is above 18%. It acts as a shield that slows oxygen penetration and prevents further metal oxidation below. For those with a chromium composition of less than 18%, the protective film will also contain spinel Fe₃O₄, which is less protective than the Cr₂O₃ scale. The generation of oxide scale obeys a parabolic equation, pressed as:

$$R = \sqrt{kt}$$

The oxide growth rate is, however, increases exponentially with temperature when diffusion governs this process and drops massively when the concentration of chromium is high enough to generate an oxide layer.

Other elements can generate oxide layers even more protective than the Cr₂O₃ scale despite chromium. The addition of aluminium and silicon is the most common one—Al causes Al₂O₃ that is more prohibitive to the diffusion of oxygen, and Si provides SiO₂, which is similar to the former. Alloy 302B, 153MA and 253MA are three successful examples that used an elevated Silicon level [168].

The most familiar environment followed by high temperature is humid surroundings with water vapour inside stainless steel. It is noticeable that the water vapour will accelerate the oxidation progress—10% of water vapour will increase the oxidation extent ten times by expanding the scale porosity promoting or forming unstable CrO₂(OH)₂ on the surface. Thus, the working temperature of high-temperature alloys in a steam presence is limited at 50-100°C [171]. Also, halogens are best prevented because of the degradation caused by the attack on the oxide layer. Other environments like carburising and nitriding surroundings can be controlled by increased Cr and Si content [168].

Considering high-temperature applications, the mechanical properties of high-temperature steels should be the top priority. When the temperature is above 500°C, the creep strength is far more critical than any other features for austenitic steels, which can be measured by creep strength. Compared with other stainless steels, the rupture

strength of high-temperature steels is excellent at an elevated temperature, as shown in the figure below (353, 253 & 153 are typically high-temperature steels) [168].

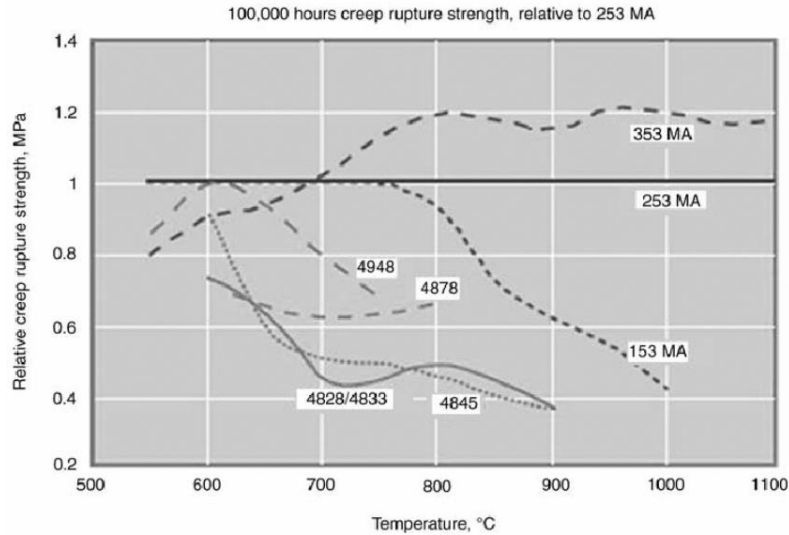


Figure 2.4.2. Relative creep rupture strength (100,000 hrs.) comparison between a series of stainless steels [172].

Typically, processes like cold-working and precipitation can increase the creep strength of the material. However, they do not act as effective strengtheners in a high temperature that lead to solution annealing and over-aging. The most effective method is solid solution strengthening by interstitial strengtheners like carbon and nitrogen—mainly nitrogen, which can also hinder the formation of intermetallic phase precipitation [168].

2.4.3.3 Corrosion-resistant steels

The property of “stainless” is achieved by adding over 10.5% of chromium that makes steel does not rust under normal atmospheric conditions. However, for high-temperature applications, austenitic stainless steels require more chromium content than 10.5% to stabilise their microstructure at room temperature. Thus, the corrosion resistance of austenitic steels is ordinarily superior. In addition, one of the advantages of austenitic steels is the availability of nitrogen, which is a powerful and highly low-priced alloying element.

As an ordinary ion in our daily life, chloride ions are the main issue that a corrosion resistive material should deal with. Those ions can destabilise the passive film and penetrate the material while localised and lead to pitting corrosion that may grow unlimitedly. For austenitic stainless steels, resisting Chloride corrosion is seemed as specially designed for them because of the universality of the existence of Cl ions [168].

The resistance of Cl ions is achieved by the synergy of Cr, Mo, and N, from which a homogenous passive film is generated—thinner and more effective than oxide layers. Especially the effect of Nitrogen, despite the formation of the passive film, Nitrogen can also decrease the required temperature to generate carbides. As reported, the corrosion-resistant steels ranging from commercial 316 to 4565 alloy both contain a certain content of Mo and N. Furthermore, as investigated by Speidel [173], a generous nitrogen carbon ratio might further help to reduce the content of nickel and even totally replace it for a more affordable producing cost.

In conclusion, austenitic stainless steels are a kind of high strength, weldability, toughness, and ordinarily high corrosion resistant alloy. It is common in daily life, industries and even aerospace wherever a “strong” material is needed. Also, the difference in elemental contents affects the performance of alloy, which enables the specialisation of austenitic steels by adjusting the ratio between different elements.

2.5 Wire Arc Additive Manufacturing

2.5.1 AM and AM for Metals

Additive Manufacturing (AM), also called 3D printing for some cases, has become a popular topic in material science. The history of AM can be traced back to the 1980s [174], a computer-aided design (CAD) based method called Rapid Prototyping, the first kind of 3D printing all over history, has been invented. However, the technology in that year is not mature enough for industrial yielding. It is expensive and time-wasting—without the supplies of reliable technologies. In recent years, with more evolved technologies taking parts such as multiple printing heads or high-speed laser cutters,

the AM process has become more advanced and is gradually being concerned by industries [174]. It is proved that the 3D printing technology can produce a whole part rather than models, and the entire process can be controlled by a computer, which means less cost less time. Also, less human resources, so timesaving is one of the advantages of AM. In addition, AM technology allows customers to print their products by only using specific software, which makes personalised production (such as rapid repair or unique items) possible, almost all kinds of materials, including metallic, ceramics, polymers and other non-conventional materials (paper, carbon fibre, etc.) [175] can be used in AM, which means AM is far more flexible than conventional methods. Due to its flexibility and timesaving, AM will occupy the most significant role in processing fine products in the future. Wohlers et al. predicted that the AM industries would continue to breed in the next few years; the sale of AM products may be over AU\$22.9 (US\$15.8) billion worldwide [176].

AM of metallic materials is one of the most promising processes of producing metallic parts [177]. However, it is not been that concerned by industries for several years owing to the low efficiency and high cost, thanks to those advanced technologies and research, making the AM a profitable and valuable technique for metallic materials [178]. Compared to the conventional subtractive process, AM is more material-saving and easier to manufacture sophisticated metallic parts. There are seven categories of metallic AM technologies in the market, defined by the American Society for Testing and Materials (ASTM). Five of them are commonly used: Material Extrusion (ME) (10% of the AM market), Powder Bed Fusion (PBF) (54%), Directed Energy Deposition (DED) (16%), Material Jetting (MJ) and Binder Jetting (BJ) (16% overall) as shown in the figure below [176]. Representative techniques from each group are also listed below: for Powder bed fusion systems, Direct metal laser sintering (DMLS), Electron beam melting (EBM), Selective laser sintering (SLS) and selective laser melting (SLM) are some of the unique techniques. For the DED system, Electron beam freeform fabrication (EBF³), Wire and arc additive manufacturing (WAAM) and Laser consolidation (LC) are examples. Composite Extrusion Modelling (CEM) as one of the

archetypes of Metal extrusion group, and Powder bed and inkjet 3D printing (3DP), Ultrasonic consolidation (UC) represents Binder jetting and Lamination group respectively [179, 180].

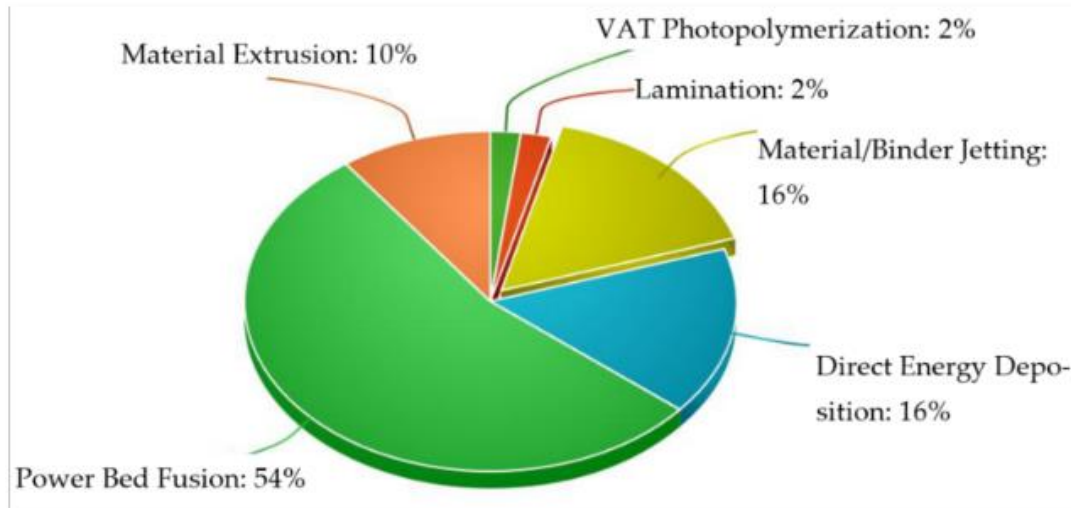


Figure 2.5.1. Categories of main AM process for metal and the proportion in the market (2020)

2.5.2 WAAM

Wire arc additive manufacturing, as one of the subcategories of Direct Energy Deposition (DED), has recently drawn attention from industries in a few decades due to its high deposition rate that makes the fabrication process faster (reduces 40-60% processing time compared with the conventional method), low equipment cost (and able to conduct at any environment) and high material utilisation rate (up to 90% to 100%) that reduces the expense [181].

Compared with the dominant metal AM method: powder-bed based systems, WAAM processes a series of advantages. It has a shorter processing time owing to the higher deposition rate. As summarised by Raut & Taiwade [182], the deposition rate for Ti_6Al_4V alloy with laser powder bed fusion method is around 0.1-0.18 Kg/h, with electron beam powder bed fusion, it is 0.26-0.36 kg/h. However, with WAAM, the rate can reach 0.5-4 kg/h. In addition, WAAM produces a more qualified as-built material than a powder-based system caused by the difference of feedstock materials—powder-

based methods are more prone to generate defects like pore and hollow that affect the integrity of the material. In addition, WAAM is wire-based, which is less likely to create large-sized defects [183]. WAAM also provides a higher material utilisation rate compared to other AM processes—as reported by Ding et al. [179], the efficiency of material utilisation of WAAM reaches up to 90%-100% although probable further surface finishing is counted, while the efficiency of powder-bed systems is around 50% overall the whole process [184].

The WAAM system is based on atomised welding techniques like GMAW, GTAW and Plasma arc welding (PAW). GMAW is the most common technique in the WAAM process, which is achieved by the arc generated by the voltage between a consumable wire (as an electrode) and the workpiece under the protection of inert gas (for Metal inert gas-MIG) or active gas (for Metal active gas-MAG) the protects both welding pool and welding material [185]. GTAW and PAW process are two similar welding processes in some cases—they both use non-consumable tungsten electrodes rather than metallic wire, and both of them are protected by inert gases, the wire is melted by the arc (non-constricted arc and constricted plasma arc, respectively) and solidified onto the workpiece. The main difference between GTAW and PAW processes is the position of the electrode. In PAW, the electrode is in the welding torch so that the plasma flow can separate from the shielding gas flow, while the electrode of GTAW is outside of the welding torch. Another difference between the two methods is the material in the PAW process are fused via plasma arc rather than an electrical arc in GTAW, which leads to a higher temperature (as high as 20000°C) and higher energy density compared with the GTAW process, it also owns a more concentrated arc, a higher thermal efficiency and a higher forming precision, so PAW is primarily used for large-sized and complex parts. However, although PAW is a newly generated and more advanced method, its high system complexity, high cost and requirement of the highly skilled operator makes it a less flexible choice for WAAM [186]. GTAW is a welding process with high stability, good user-friendly, and excellent precision with nearly defect-free results. It is also the first welding technique widely used once investigated [183].

To increase the stability of the process, several variant WAAM methods are adapted in the WAAM process [183]. One of the famous examples is Cold metal transfer (CMT), which belongs to the GMAW based AM process, developed by FRONIUS in 2004. High-speed digital control, inverters achieve it, a processor and the transfer progress is achieved by short circuit's initiation and duration with the support of mechanical methods, which is different from the typical transferring process—such as dip transfer, which is achieved by digital control [187]. In addition, the metal transferring to the molten pool in CMT is done by the support of electromagnetic and retraction forces of the molten pool. In contrast, the dip transfer is based on the contact (dipping into) between the wire and molten pool. Those characteristic makes CMT an excellent technique for low heat input material deposition by an inventive wire feed system and high-speed, high precision digital control [188]. Another GMAW variant is tandem GMAW, also called “twin wire GMAW”. In the tandem GMAW process, two wires are simultaneously fed via one welding torch and melted in a single molten pool so that the deposition rate can be significantly improved. In addition, two wires are controlled via two separate feeding systems and heat resources, which means two systems can work both simultaneously and separately, for example, the welding parameters, operating models, and even type of wire can be different, which essentially increases the flexibility of manufacturing process [185].

The final quality of wire-based arc additive manufactured parts depends on their parameters, such as current intensity, voltage, shielding gas and its flow rate, working distance, wire feeding rate, travelling speed, torch angle and colling rate of as-built material etc. [183]. Thus, it is vital to select the suitable parameters for a qualified result; an inappropriate parameter combination may change the transfer mode of AM process, which can lead to slow deposition rate, long processing time or even severe defects and deposition failure.

Recently, WAAM has been chiefly used in manufacturing titanium, aluminium, nickel alloys and steel. Titanium alloys are excellent aerospace materials with high strength-to-weight ratios and corrosion and oxidation resistance. However, owing to its

high material cost, a higher efficiency manufacturing method should be applied rather than conventionally subtractive manufacturing. It is WAAM that owns a high utilisation rate and can reach the flexibility of aerospace parts. Thus, WAAM has a considerable market in manufacturing titanium alloys, especially for large-sized and complex parts [181, 184]. A few studies based on Ti alloy (normally Ti_6Al_4V) fabricated by the WAAM process has proven that the tensile properties of as-built Ti_6Al_4V alloy by WAAM is close to wrought alloy and higher than cast Ti_6Al_4V alloy [181]. Apart from Ti-based alloys, nickel-based alloys are another essential material for WAAM. As introduced before, nickel alloys are commonly used in aerospace, submarines, chemical and petrochemical industries. The main challenge for manufacturing nickel alloys is its high strength even at an elevated temperature, which is a double-sided-blade for industries—it enables the application in a severe environment. It makes the fabrication process in a conventional way harder also improves the financial requirements. By applying the WAAM process, the difficulty of fabrication is solved via directly melting the material and resolidifying it into the parts wanted [189]. As reported by Wu et al. [181], the mechanical property values of WAAM processed Inconel 718 lie on the minimum standard values specified by ASTM, and that of as-built Inconel 625 is higher than cast materials but marginally lower than wrought alloys.

2.5.3 Joining dissimilar metals by WAAM

Joining dissimilar materials is commonplace in manufacturing; a few benefits can be achieved by joining them, such as reduced weight, lower cost, higher toughness and so on [182]. The material with a gradually changed component and structure over volume is called functionally graded material (FGM). For a natural example, teeth or bones are considered FGMs due to their changing features over a changing dimension. For industries, producing FGM components is an excellent way of achieving all the required properties [190], extensive applications of FGMs are already by aerospace industries that need an ability that can withstand a high thermal gradient [191], medicine area that requires a replacing material for living tissues [192], defence

application that needs inhibition to crack propagation [193], energy devices that demand thermal barriers [194], and optoelectronics as graded refractive index materials [195].

The joining of dissimilar materials, or FGM manufacturing, can be achieved via many techniques; conventionally, it can be accomplished via standard fusion welding. However, although a few fabrication methods can fabricate bimetallic joints such as casting, rolling, diffusion bonding, powder metallurgy and so on, both own a few restraints such as high cost, limited shape and long processing periods [182]. In addition, typically, joining them via conventional fusion welding is also followed by many challenges such as the formation of intermetallic cracks or porosities or a decreased mechanical property in the heat-affected zone (HAZ) [196]. WAAM, as an additive manufacturing technique, is capable of fabricating bimetallic materials either in a sequential or simultaneous order making it a flexible manufacturing method for FGM. Ahsan et al. [197] have investigated the fabrication process of low carbon steel (LCS) to stainless steel 316L via the GMAW technique. The joining of those two materials succeeds without defects, but the failed strength property was shown on the LCS site. A steel (ER70S-6) to nickel (ERNi-1) research has been examined by Bintao Wu et al. [198]; in this research, an interweaving fabricating strategy has been applied on GTAW welding, the result shows an increased average tensile strength than any of the feedstock materials, which is owing to the interweaving building strategy—creates an interlocking microstructure of nickel and steel in bimetallic section and improves solid solution strengthening effect of the material. Liming Liu et al. [199] has examined the feasibility of joining Fe (ER70S-6) and bronze (SG-CuSi₃) via GMAW. The interface layer of the final part shows an outstanding mechanical property and is free of defects, which has confirmed the high capability of WAAM of joining dissimilar materials. Defect-free works are also designed by other researchers, A. Rajesh Kannan et al. [200] has explored the joining of stainless steel 904L and Hastelloy C-276, which has been observed that a sudden increase of microhardness in the bimetallic area owing to the diluted alloying elements. While Yinbao Tian et al. [201] has probed the

formation of bimetallic components and tensile properties are depending on the sequence of material deposition, the research is based on CMT welding Ti6Al4V, and Al-6.25Cu as joining materials, different bimetallic components and tensile strength are observed in the fusion joint according to different deposition sequences. A hybrid nickel aluminium bronze (NAB)-stainless steel 316L part was designed by Dharmendra et al. [203]. The material in this study is also defect-free, and a series of Fe₃Al intermetallic compounds are formed. However, occasional liquation cracking is also found in HAZ. Md. R.U. Ahsan et al. [202] have studied joined bimetallic austenitic stainless steel 316L. Inconel 625 part fabricated via GMAW by an overlapping building strategy. The result shows a homogenous hardness distribution except for the first & last layers. Still, it also offers a large amount of detrimental laves phase in the Inconel 625 part, which is suggested to be eliminated by heat treatment.

In summary, for several specific applications, joining dissimilar materials is required, and it can be achieved by fabricating FGM products, compared with traditional welding techniques that with many inappropriate, WAAM is an excellent choice for manufacturing FGM due to its flexibility and high material utilisation rate and minor defect compared with conventional welding methods.

2.5.4 Common defects in WAAM parts and improvement

Although WAAM has a range of advantages, several disadvantages affect the final quality of as-built products. Severe defects like cracks, porosity, and high residual stress must be eliminated for crucial applications, which may cause a disaster for the industry or even endanger the personal safety of the public. There are generally many reasons that cause defects in the WAAM process. Besides feedstocks' quality, programming strategy, and parameter setup, heat accumulation during welding, environmental conditions, or even accidental equipment failure can significantly impact the overall quality of manufactured parts. In addition, different materials have different trends of defect generation, such as severe oxidation usually happens in Ti-based alloys, porosity for aluminium, rough surface for steel and severe deformation or thermal cracks prone

to occur in bimetallic parts [181]. The following text will introduce a few defects that are common in WAAM and ways to prevent them.

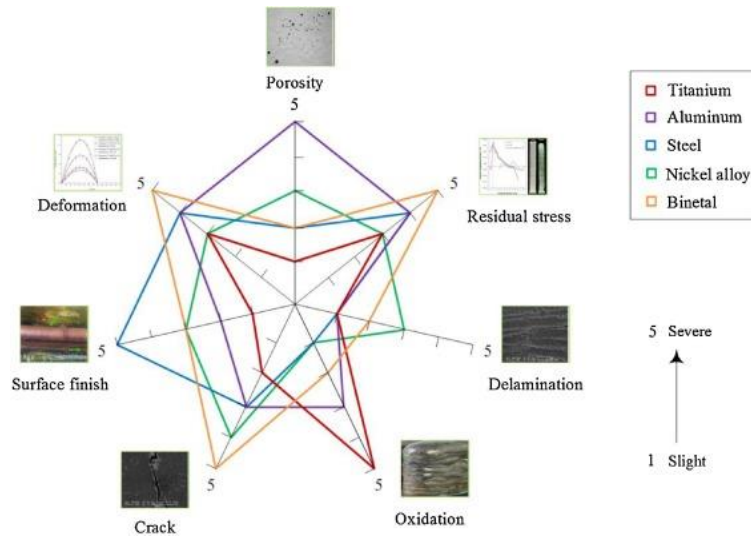


Figure 2.5.2. Interrelationships between materials and defect tendency in WAAM [181]

2.5.4.1 Deformation and residual stress

Like distortions in standard welding techniques, deformation is a typical defect in the WAAM process. It so does residual stress, which is one of the reasons that form deformations in WAAM parts and can also result in low geometric tolerance, layer delamination and so on. Thus, it is necessary to get them controlled and minimised for gaining a qualified as-built part.

Deformations can be categorised into several conventional welding techniques; some like longitudinal and transverse shrinkage, angular, rotational and bending distortion may exist at WAAM parts. These deficiencies principally rely on the thermal shrinkage and expansion caused by the heating-cooling-reheating cycle, which is fair common in the WAAM fabrication process [203].

Residual stress is the stress that remains in the material when all external loads are removed, it is beneficial for brittle materials (such as glass and concrete) to improve

their toughness, but for AM materials, warping or plastic deformation may be caused by residual stress that exceeds the material's local yield stress. In contrast, residual stress exceeds the local ultimate tensile strength. Severe consequences like cracks may occur. When the residual stress in the material is sufficient, the mechanical properties may be enhanced [204].

In the AM process, welding materials are also a key role in generating deformations or residual stress, such as the bimetal parts are more prone to exhibit high residual stress and deformations due to the different thermal expansion between two feedstocks. Thus, the interlayer temperature should get controlled properly for preventing defects. Soft materials like aluminium are more likely to deform due to their high thermal expansion [181].

Deformation and residual stress in the welding process are fundamentally relying on welding factors like transient temperature field, deposition design, and cooling rate, which can be adjusted by using appropriate welding parameters like welding current, gas flow rate, feeding speed etc., a proper selection of welding parameters is essential for avoiding those defects. Furthermore, post-welding treatments can also eliminate the effect of those defects. As introduced in the heat treatment section before, stress-relieving and stress equalising are two annihilating methods for residual stress. Other post-process treatments like interlayer cold rolling, interlayer cooling, peening and ultrasonic impact treatment summarised by Binta et al. [181] are also practical techniques for removing or mitigating those imperfections.

2.5.4.2 Porosity

Porosity is another common defect in the WAAM process, it behaves as a gas pocket or void that is free of material, and it is considered as the initiation of cracks when the diameter is larger than 50–100 μm [205], Kobayashi et al. [206] have found that porosity can cause a detrimental effect on the strength of aluminium alloys, which is because of the low tensile load-bearing capacity around the porous area and that leads to a strain concentration so that the material may fracture precociously. The Al alloys

should be most concerned about preventing porosity because of the severe restriction caused by porosity to mechanical properties. Thus, the mitigation and elimination of porosity is also a grim task for the WAAM process.

The formation of porosity in WAAM parts can be attributed to two factors: raw material or fabricating process. One of the common reasons for generating porosity is the remained contaminants such as oil, moist or gaseous molecules from the feedstock material, shielding gas or substrate surface, which are hard to prevent, those impurities follow the welding process, absorbed by the welding pool, and generates spherical porosity after solidification [181]. One of the outstanding examples is the porosity in AM built aluminium alloys—which is caused by the absorption of hydrogen for liquid material (0.65 ml/g for pure Al) in the melting process and rejection of supersaturated hydrogen from solid material (0.035 ml/g for pure Al) to surrounded liquid phases [207]. Due to Al alloys' high thermal conductivity, the fast solidification traps bubbles into solidified materials; thus, porosity is generated [208]. Similar porosity can also be found in Ti-based and other materials. As Wang et al. described, the metallic wall fabricated by contaminated wire shows a series of visible porosity, while the wall built by standard clean wire is free of porosity [209]. Thus, the cleanness of the feedstock material, substrate and shielding gas should pay attention to.

Another kind of porosity is caused by process matters, which include mishandling and inappropriate welding parameter, those porosities are non-spherical and can be easily determined by their irregular shape and size. As Cong et al. [210] discovered, different arc modes for Al-6.3% Cu alloy results in a dramatic difference in size and quantity of porosity. It is disclosed that using a conventional CMT method for Al-6.3% Cu alloy results in approximately 150 micro-pores with diameters of 50–100 μm , while the CMT pulse advanced (CMT-PADV) arc mode leads to a far fewer porosity than the former one and with a smaller size ($d=10\text{--}15\ \mu\text{m}$) as well, which is because of the low heat input and effective oxide cleaning of CMT-PADV arc mode.

2.5.4.3 Cracks

In welding, cracking is a common defect that occurs in the working part. Commonly, cracks are caused by the propagation energy generated from material's properties like brittleness, residual stress or environmental factors like thermal effect, mechanical effect, or the synergistic effect of both, which may significantly impact the mechanical property of the material or even cause a fracture and normally without any warning that severely threatens the life safety of the public [211]. Common cracks existing in metallic materials include cooling, hot, solidification, liquidation (hot tearing), plating, pickling, centreline, creep, crater, grinding, stress corrosion, heat treatment (quenching), machining tears, fatigue and hydrogen cracks [212].

Based on the formation principle, cracking in welding can be categorised into two main categories—cold cracking and hot cracking. Cold cracking is also called delayed crack. It generates after the solidification of the material, as a result of residual stress and structural transformations with time, cold cracks generate between grains or through grains, along the weld and fusion line [213, 214]. One of the outstanding examples of cold cracking is hydrogen crack, which results from a certain amount of diffusible hydrogen, a susceptible microstructure, tensile stress, and room temperature [215]. Hot cracking is a group of cracking that initiates at high temperatures. According to standard EN ISO 17641-1, hot cracking segregate materials at a high temperature occurring along grain boundary when the strain level and strain rate are over a specific level [216]. Two representative examples are solidification cracking and liquation cracking, they are often mentioned together because both happen intergranular, but the principle behind them is different. Solidification cracks are formed in the final step of the solidification stage, that is, when the material is weak—the dendrites are growing into grains and separated only by a small amount of grain-boundary liquid films, a generalised theory believes that when the localised stress that exceeds the resistance of cracking is applied, cracking may happen in the grain-boundary fluid movies or the grain-grain bridges, and that is why solidification cracking often occur along the grain

boundaries [217, 218]. Liquation cracking happens in the HAZ, where the solidified material can be affected by the welding technique because of the temperature over the eutectic temperature of the partially melted zone (or solidus temperature for totally solidified material). The material in HAZ is weakened because of the melted grain boundary. Hence, the strain induced by the welding process makes the HAZ prone to crack [217, 219].

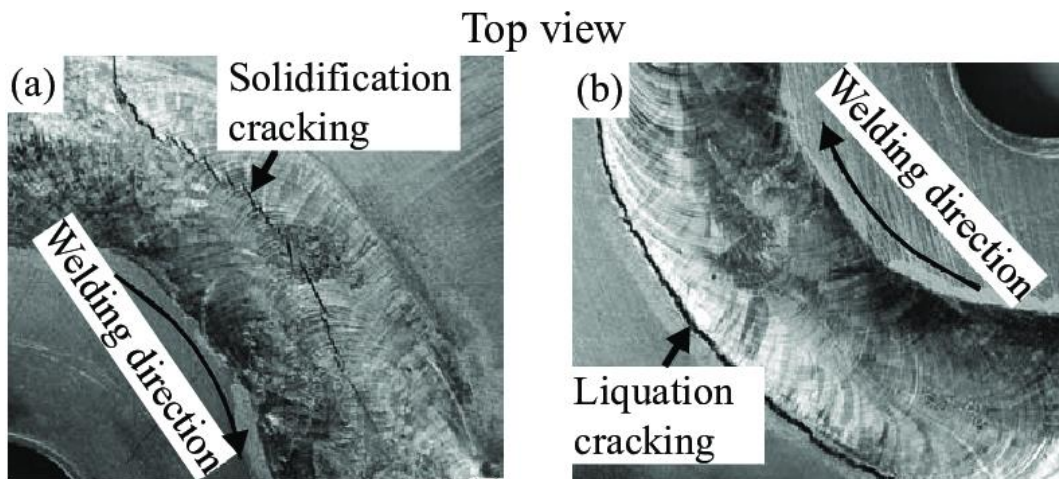


Figure 2.5.3. The typical image of (a) Solidification cracking and (b) liquation cracking [220]

For eliminating or mitigating cracks, a few methods are investigated by researchers. Thavamani et al. [221] have examined the effect of ultrasonic vibration on cracks. It was discovered that the application of ultrasonic vibration had decreased the sensitivity of cracks in Inconel 718 from 47.5% to 13.3%, and they also observed the welding current is hard to influence the generation of hot cracking. By adjusting the metallic component, cracking can be in the alloys [217]. Applied electromagnetic stirring significantly reduces the likelihood of cracking avoided in aluminium alloys, discovered by MG Mousavi [222]. In addition, adjusting welding parameters like lower heat input, interlayer temperature etc., are also proved as cracks preventing methods [223, 224].

Chapter 3 Research Approach and Methodology

Several research equipment and methodology are used in the thesis to achieve the research goal. The following text will briefly introduce some of the details of them.

3.1 Materials

The materials used in this study are commercial Inconel alloys, Monel alloy, stainless steel and Mild steel. Part of the composition of those materials are listed below.

Table 3.1.1. Elemental components of materials used in this study

Chemical composition of selected alloys										
Composition (at %)	Ni	Fe	Cr	Nb	Mo	Ti	Al	Cu	C	Co
Inconel 718	50-55	Balance	17- 22	4.75- 5.5	2.8- 3.3	0.65- 1.15	0.2- 0.8	<0.3	<0.08	<1
Inconel 625	>58	<5	20- 23	3.15- 4.15	8.0- 10.0	<0.4	<0.4	-	<0.1	<1
Monel 400	>63	<2.5	-	-	-	-	-	28- 34	<0.3	-
Stainless Steel 316	10.0- 14.0	Balance	16- 18	-	2.0- 3.0	-	-	-	<0.08	-
Mild steel (AWS ER70S-6)	<0.15	Balance	<0.15	-	<0.15	-	-	<0.5	0.06- 0.15	-

3.2 Experimental Equipment

Installations used in this study include two welding systems, GTAW and GMAW; both contain a power source, two-wire feeders, two welding nozzles, and the welding are protected by shielding gas (pure Argon). While GMAW additionally includes a robot for welding, computer and robot controller for weld controlling and path planning, and GTAW system contain an extra lathe for welding control.

Research Approach and Methodology

Since the final object is a tubular component where the inside is nickel, and the outside is steel. Thus, a twin-torch is considered, which supplies steel and nickel wires synchronously, avoiding the time-wasting wire exchanging. Figure _ shows the whole twin wires WAAM system for the study, including a control PC (Figure 3.2.1 (1)), robotic controller (Figure 3.2.1 (2)), two Fronius TPS 4000 welders (Figure 3.2.1 (3)), shielding gas system (Figure 3.2.1 (4)), and ABB robot (Figure 3.2.1 (5)).

The tandem weld work is illustrated in Figure 3.2.2. The twin torch supplies the steel and nickel wire separately, avoiding the redundant work of wire roll exchanging. Figure 3.2.2 (b) explains the principle of welding. The distance between two weld beads influences the shape of the dual weld bead surface. Thus, getting an accurate overlapping distance and robot tool data for both wires is necessary.

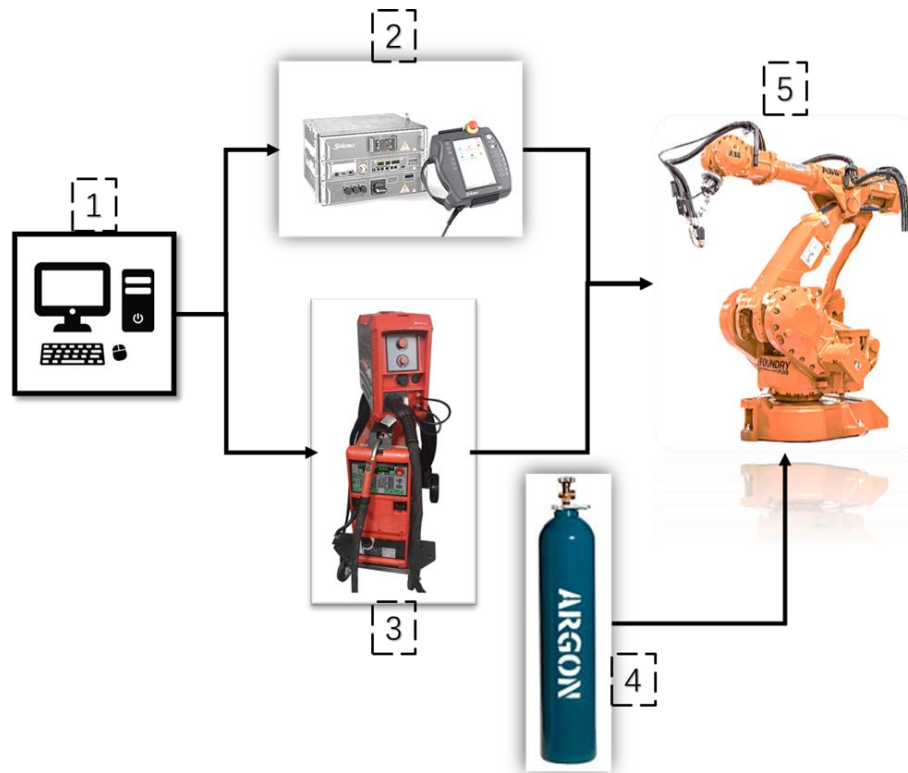


Figure 3.2.1. Illustration of GMAW welding system in this study.

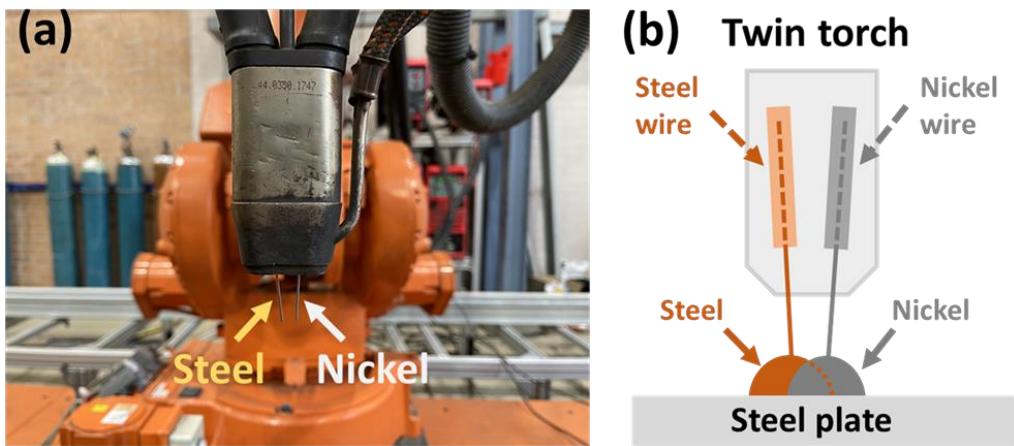


Figure 3.2.2. Illustration of (a) double welding torch and (b) the principle of the twin welding torch.

3.3 Metallography

After the wire EDM cutting process and preparation, the microstructure of cross-sections of the metallic samples are examined via Optical microscope and scanning electron microscope, the elemental distribution and chemical composition of dissimilar materials' interface and cracks are analysed via Electrical dispersive spectroscopy (EDS).

3.3.1 Preparation

The 2mm cross-section samples for Metallography observation were cut by wire EDM cutting machine and then polished by Struers automatic polisher Tegrapol 21 (as shown in figure 3.3.1) with a metallographic polishing way (as shown in table 3.3.1). The generated cracks of the specimen can be observed clearly after polishing. After that, a 5-gm. Oxalic acid mixed with 95 ml HCl (reagent grade) etching solution with an Electrolytic etch - approx. 3.5 volts DC for 2-3 secs etching method are applied to all the samples for further detailed observation.

For measuring the mechanical properties of the intermetallic interface of selected groups, the preparation for a small punch test is required: four samples from the intermetallic interface area each group with a diameter of 8 mm and thickness of 0.8

Research Approach and Methodology

mm are cut by electrical discharge machining, then the samples are grounded using 800 and 1200 grit silicon carbide paper and polished using a 2400 grit abrasive suspension down to a final thickness of $500 (\pm 5) \mu\text{m}$ (the process is shown in figure 3.3.2)



Figure 3.3.1. Struers automatic polisher Tegrapol 21

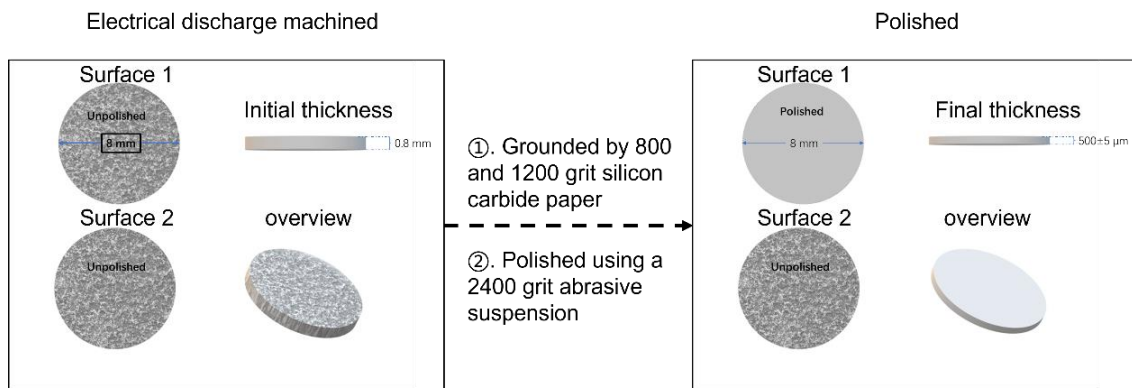


Figure 3.3.2. The preparation of small punch test samples

Table 3.3.1. Metallography polishing process of as-fabricated samples

Step num.	Surface	Suspension	Lubricant	Time
1	Piano 220	-	Water	1min 10s
2	Largo	DP-P 9 μm	Blue	6min
3	Dac	DP-P 3 μm	Green	5min
4	Chem	OP-S	-	3min

3.3.2 Optical microscope (OM)

For obtaining the magnified images of as-built specimens, Leica DMR optical

microscopy (figure 3.3.3) is used to observe metallographic structure, the numerical information and part of the structural details of cracks.



Figure 3.3.3. Leica DMR optical microscope

3.3.3 Scanning electron microscope (SEM)

In this study, a JEOL 6000 operating Scanning Electron Microscope (SEM) equipped with an energy dispersive X-ray spectrometer (EDS) are used for the observation of a higher magnification than OM to acquire more detailed microstructures of interface and cracks.



Figure 3.3.4. JEOL 6000 operating Scanning Electron Microscope

3.3.4 Electrical dispersive spectroscopy (EDS)

The elemental distribution and atomic concentrations of the cracks and interface at cross-sections are analysed by Electrical dispersive spectroscopy installed with a Scanning electron microscope.

3.4 Mechanical Properties

The mechanical properties of specimens are tested in different directions for comparing different welding materials and welding parameters.

3.4.1 Vickers hardness testing

Vickers hardness testing of specimens in this study is achieved by MATSUZAWA Vickers automatic hardness tester (Figure 3.4.1) with a load of 1.96 N and a dwell time of 10s. The results are presented graphically.



Figure 3.4.1. MATSUZAWA Vickers automatic hardness tester

3.4.2 Small punch test (SPT)

The Small punch technique is supported by the Australian Nuclear Science and Technology Organization (ANSTO).

Small punch test, also called “disk bend test”, is a newly existing testing method that was initially raised by Kurtz et al. for characterising the mechanical properties of Ultra-high molecular polyethylene [225]. In the 1980s, the nuclear industry developed

Research Approach and Methodology

and widely used SPT as a testing method for irradiated metals [226]. Nowadays, besides the initial application for ultra-high molecular polymers, SPT has a widespread application in analysing the properties of metallic materials. The significant advantage is that it enables the testing of mechanical properties even with a small volume of material without any destruction [229], which can be extracted from a large piece of a workpiece without hindering its usual service. In addition, SPT is also an excellent testing method for irradiated metals in nuclear industries and small-sized structural components that are impossible to go through standard testing techniques, such as the small area of heat-affected zones in welding joints or thin coatings [227].

After the preparation process, the samples are sent to ANSTO for small punch tests that measure a series of mechanical properties such as tensile properties, fracture toughness, and ductile-to-brittle transition temperature.

Chapter 4 Material Selection

4.1 Introduction

For gaining a defect-free bimetallic part, the selection of materials is a critical factor that affects the final WAAM built result. Due to the different elemental components and solidified microstructure of other materials, the choice between nickel superalloys and stainless steel can vary. In this experiment, the feasibility of joining with stainless steel 316 of Inconel 625 and Inconel 718 has been compared, and the joining of Monel 400-Mild steel via the same welding procedures as previous groups as the control group. This study is a preliminary experiment, which supports the following experiments by selecting the most appropriate welding materials.

4.2 Experimental Procedures

As illustrated in the previous text, the WAAM welding process is achieved via a Tandem GMAW welding system that consists of a central computer, shielding gas unit, robot controller, two-wire feeders, and an industrial welding robot. Feedstock materials are Inconel 718 1.2mm commercial wire, Inconel 625 1.2mm commercial wire, stainless steel 1.0mm commercial wire, Monel 400 1.0mm commercial wire, and mild steel (AWS ER70S-6) commercial wire with a diameter of 1.0mm, respectively. The thin metallic walls are manufactured onto mild steel substrate with planned height, length and overlapping distance (width depends on the heat input). The welding parameters are shown in the table below. High purity Argon gas protects the weld pool from severe oxidation while welding. The welding process follows a layer-by-layer building strategy, oxides and other contaminants are removed from each layer by iron wire brush for preventing porosity and other defects after every layer was welded, and additional pressured air is used for rapid cooling—the inter pass temperature between layers is controlled at about 150°C, which is monitored via thermal camera.

Table 4.2.1. Welding parameters of fabricated bimetallic walls

Sample Composition	Length (mm)	Width (mm)	Height (mm)	Wire-speed (m/min)	Travel Speed (m/min)	Dist. (mm)
IN625-SS316	121	17	49	6.5	0.35	6.4
IN718-SS316	125	15	49.7	6.5	0.4	6.7
M400-Mild	128	17.2	51	6.5	Mild: 0.3	6.5
					Monel: 0.35	

4.3 Results and Discussion

4.3.1 Macrostructure

Both Inconel 718 and Inconel 625 have excellent anti-corrosion properties, while 316 steel has high strength. For comparison, a wall was also built with mild steel and Monel 400, As shown in Figure 4.3.1.



Figure 4.3.1. Three thin wall samples (a) Inconel 718 (IN718)-stainless steel 316 (SS316), (b) Inconel 625 (IN625)-stainless steel 316 (SS316), (c) Monel 400 (M400)-Mild steel (LCS)

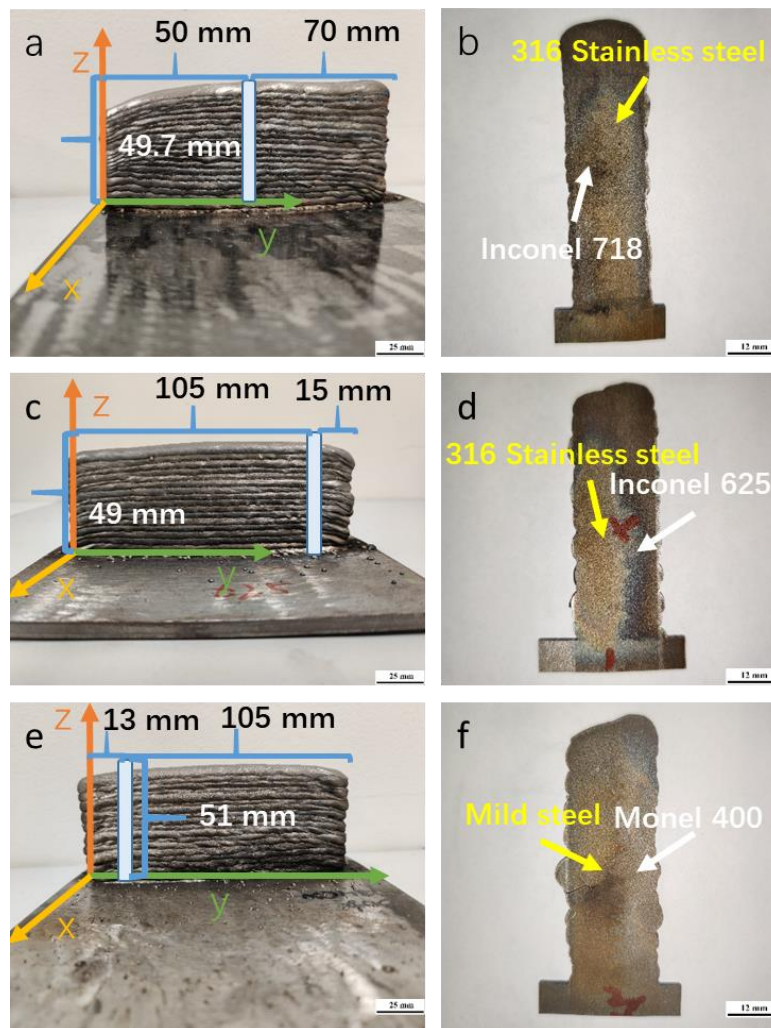


Figure 4.3.2. The image of three samples and their cross-section cuts

Figure 4.3.2. (ae) show three samples and their sizes produced using the WAAM process. Figure 4.32. (bf) show the cross-sections of (a – e). It can be seen that the surfaces of all three walls are smooth, with the height of the IN178-SS316 (a) metallic wall is relatively uneven, the left two groups are uniform. As for cross-section cuts, the cracks in IN718-SS316 (b) and Monel400-Mild steel (f) are visible, but the cross-section of IN625-SS316 (d) is crack-free and neat. In addition, the different extent of deformations has happened in the area between lower layers and substrate. The successfully fabricated metallic walls prove that the parameters in the WAAM process are acceptable.

4.3.2 Microstructure of specimens

Three different material combinations (SS316/IN718, SS316/IN625, LCS/M400) were selected to fabricate Batch 1 samples, including three thin-wall steel-nickel structures. The initial metallographic examination was conducted on each sample's polished surface. Lack of fusion and a large number of cracks were observed in all three walls. Figures 4.3.3 (1-3) in this section show the microstructure in the cross-section of the three walls after etching. The stainless steel and nickel-based alloys presented a typical dendritic structure, while the low carbon steel was easily over etched with a ferritic structure. It should be noted that acicular ferrite and large bainite are common microstructural features with a typical texture in additively manufactured mild steel samples [228, 229]. The hardness results will further confirm the presence of bainite.

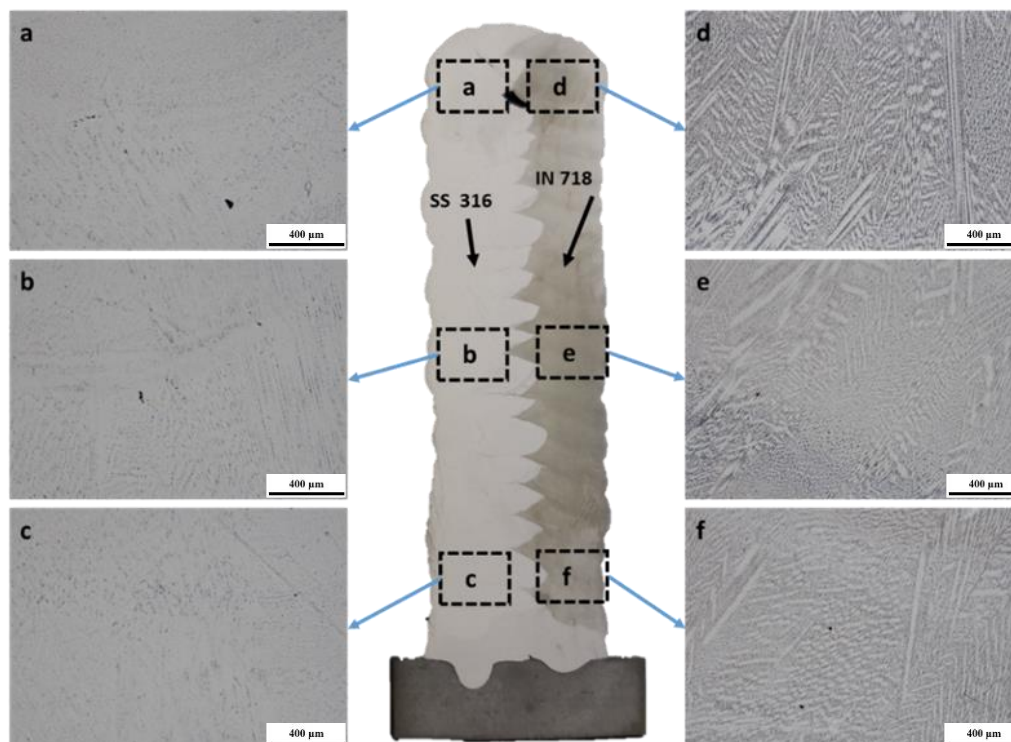


Figure 4.3.3 (1). The representative microstructure in both SS316 and IN718 sides of Wall 1

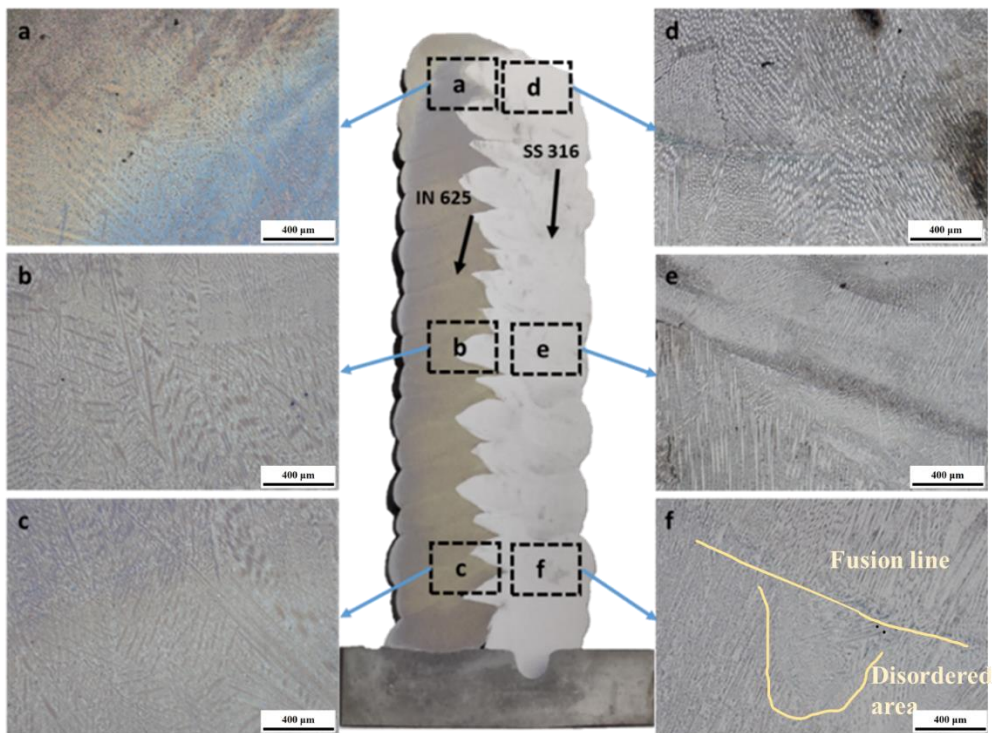


Figure 4.3.3 (2). The representative microstructure in both IN625 and SS316 sides of Wall 2



Figure 4.3.3 (3). The representative microstructure in both LCS and M400 sides of Wall 3

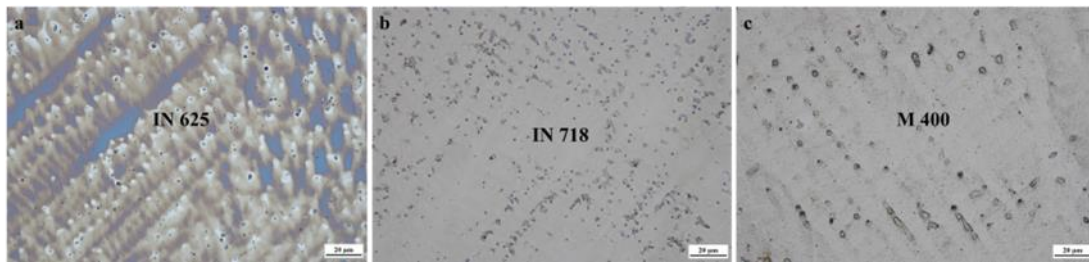


Figure 4.3.3 (4). Microstructure of nickel alloys sites in as-built walls under 50*10 magnification

As shown in these images, all the dendritic structures from the top to the bottom regions are at the similar inclination angle. The dendrites on the top of the as-built part are coarsened than that from the middle and bottom areas, owing to a slower cooling rate due to the thermal accumulation and the low thermal conductivity of Inconel alloys [230]. The layer boundaries (fusion lines) can be easily observed via OM. The dendritic structure on both sides of the layer boundaries is different—the grains on the downside are coarser than the upper sites. The grain size becomes finer while a certain distance has looked down. It might be because of the reheating of the already solidified materials in the heat-affected zone, which is prone to generate liquation cracking to some extent, as mentioned in the literature. In addition, a certain number of disordered dendritic structure (exampled as Figure 4.3.3 (2). f) are found in HAZ near the fusion line, which is concluded by the uni-directional crystal growth orientation caused by the pressured air cooling that is uneven and relatively low effect compared to other cooling techniques like water cooling [231]. The image of Monel 400-Mild steel Wall (4.3.3 (3)) shows a typical consequence of over-etching of the materials, leading to an ambiguous picture of microstructure. It is considered that the etching solution for Inconel-stainless steel is far stronger than the requirement of Monel-Mild samples, although a slighter etching condition is needed. However, no further re-etching is applied because the mission of this sample as a control group for an elementary crack observation is accomplished.

While comparing with these different groups (Figure 4.3.3 (4)), no significant difference between IN718 and IN625 at the microscopic crystallographic point of view even at a much higher magnification of optical microscope (Figure 4.3.3 (4). a, b),

which is similar to other literatures' discovery—because of their similar composition. However, that of the Monel400 (Figure 4.3.3 (4). c) for the third group are not as same structure as formers—which is not surprising because its composition is dramatically different from previous two materials.

4.3.3 Observation of cracks

Microcracks were found in the cross-section sample from as-etched metallic samples, as shown in Figure 4.3.4.

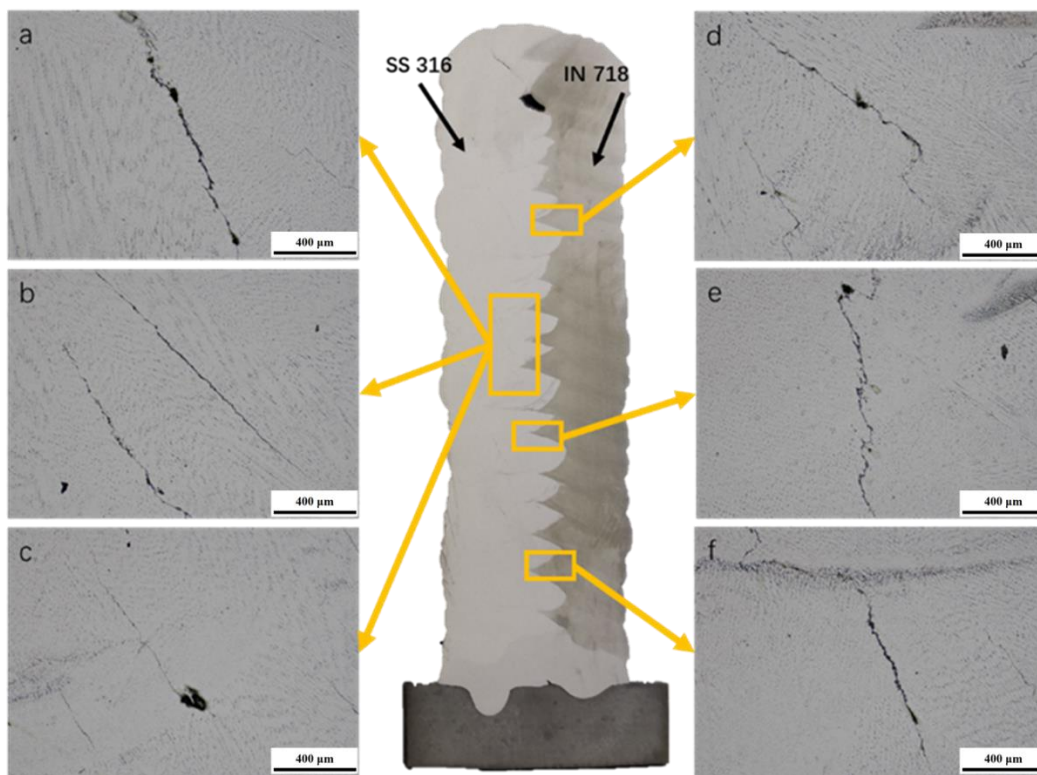


Figure 4.3.4 (1). Image of cracks in Inconel 718-stainless steel 316 wall observed via Optical Microscope (etched)

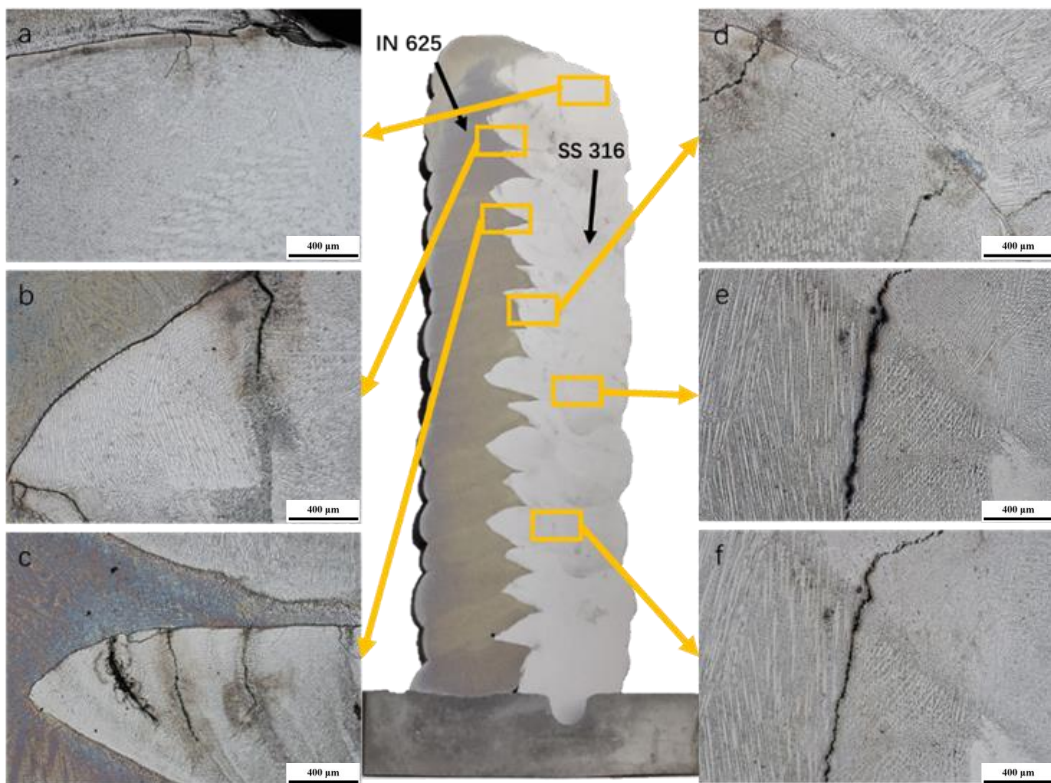


Figure 4.3.4 (2). Image of cracks in Inconel 625-stainless steel 316 wall observed via Optical Microscope (etched)

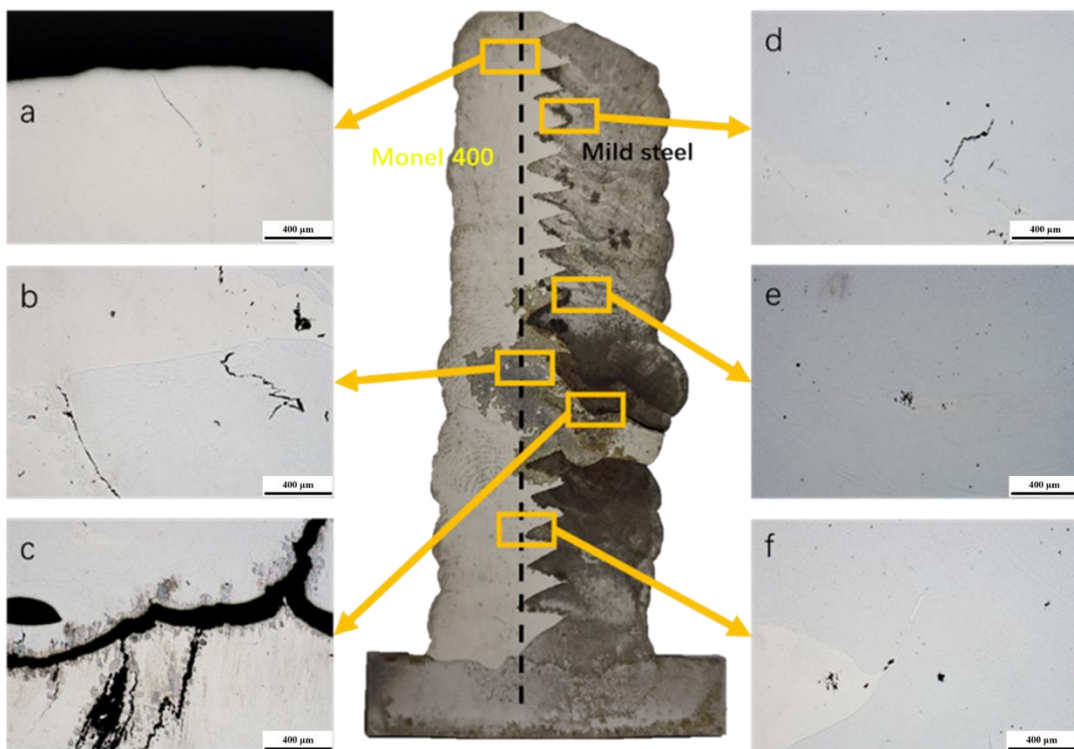


Figure 4.3.4 (3). Image of cracks in Monel 400-Mild steel wall observed via Optical Microscope (unetched)

It is interesting that cracking only occurred in the SS316 side with a series of cracks close to the interface. However, none of those cracks exists in the nickel side. It is well known that weld metal and HAZ cracking can occur due to impurities. These harmful impurities can form low melting point segregates and inter-dendritic cracks during the welding process. As revealed by images, the cracks that parallel or perpendicular and near to the interfaces and layer boundaries are considered as liquation cracking, the main characterisation of liquation cracking is they always exist in HAZ, where is because of the included heat brought by the upper layers, while those irregular shaped cracks or those who happen along the grain boundaries are defined as solidification cracking, which is caused by the solidification process of material as per introduced in 2.5.4 section. Image 4.3.4 (3) shows a few cracks in the Monel400-Mild steel Wall; however, those cracks no longer exist after the etching process (except the large-sized defect), suspected as impurities or microcracks—which is acceptable in material science.

There are also large-sized defects like the porosity shown in the top middle position of the Inconel718-SS316 sample and the big crack-like defect that existed at the Mild steel part of the Monel-Mild sample. They cannot be determined as cracks caused by metallographic reasons but the effect of welding parameters or misuse such as inappropriate wire feeding rate or travel speed, water vapour brought by the misoperation or uncleaned oxides, which are noted and analysed by our research groups and are avoided in the following experiments.

Although austenitic stainless steel is readily welded, weld metal solidification cracking is more likely in fully austenitic structures [232]. Overall, the cracking inspection for the three Walls has concluded that the Inconel 718 is more feasible than Inconel 625 alloy for joining stainless steel 316 in WAAM. This is basically because of the smaller number and lower density of cracks. Therefore, it is necessary to optimise the welding procedures and welding parameters for Wall 1 (SS316/IN718) to produce crack-free samples in future studies.

4.3.4 Microhardness

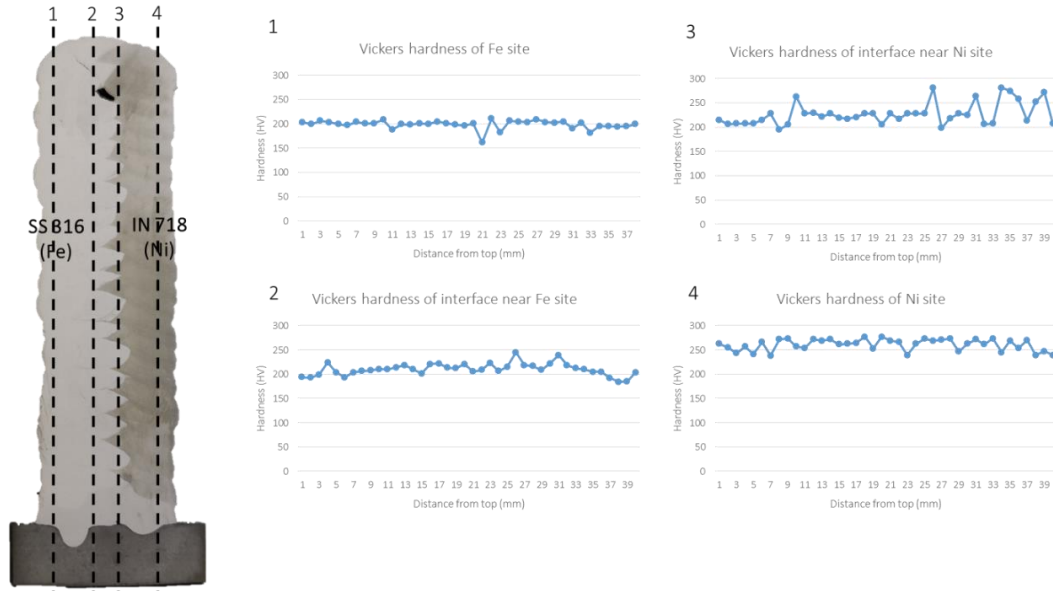


Figure 4.3.5 (1). Hardness distribution from the bottom to the top in the cross-section of Wall 1 (SS316/IN718)

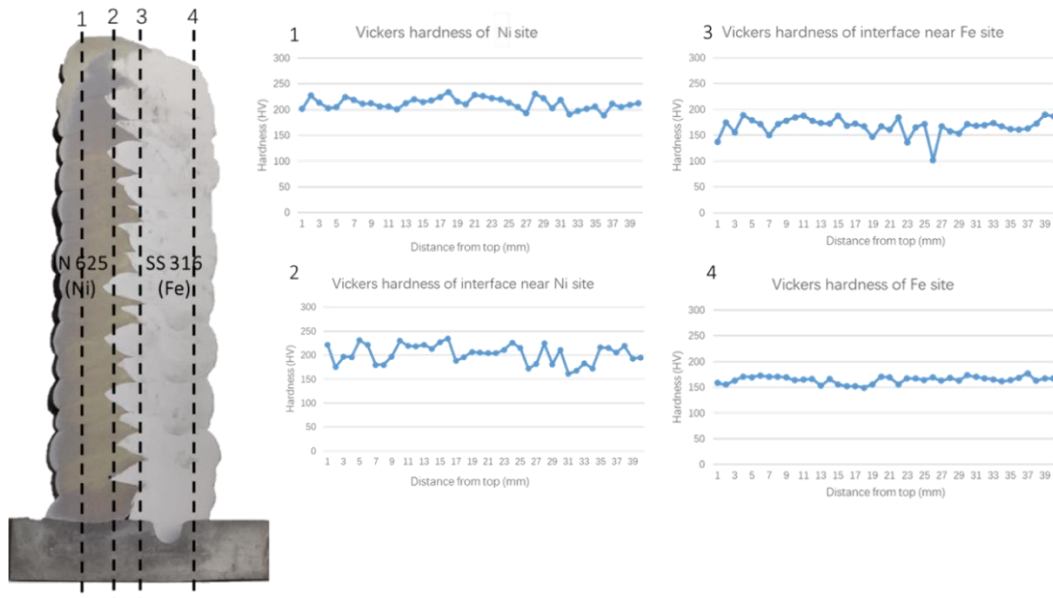


Figure 4.3.5 (2). Hardness distribution from the bottom to the top in the cross-section of Wall 2 (SS316/IN625)



Figure 4.3.5 (3). Hardness distribution from the bottom to the top in the cross-section of Wall 3 (LCS/M400)

The hardness values for the steel side, nickel side and interface of each wall are shown in Figures 4.3.5 (1,2,3). All three walls presented similar hardness variation along the build-up direction. The evenly distributed hardness of the SS316 side exhibited an average value of 200HV for Wall 1 and 170HV for Wall 2, which is similar to the typical hardness values of additively manufactured samples [233]. The low carbon steel in Wall 3 (average 380HV) was significantly harder than the general mild steel sample (average 160HV [234]). This should be attributed to the hard bainitic structure generated during welding, which is well known to be brittle and can easily lead to a severe cracking problem. The nickel side in all three walls revealed a uniform hardness distribution from the bottom to the top, with an average of 250HV, 210HV and 130HV for IN718, IN625 and Monel, respectively. There was no apparent difference in hardness values between interface and both single metal sides, although hardness at interface fluctuated significantly due to the interlocking microstructure.

Comparing the hardness difference between as-built samples, the IN718-SS316 material combo is the best throughout the three combinations because of the high consistency of hardness of both sites—a significant gap in the hardness value of different locations may lead to a limited application or even material failure while

using.

4.4 Conclusion

In conclusion, applying GMAW into the fabrication of a bimetallic Ni-based and Fe based metallic wall is feasible. Nevertheless, welding parameters should be modified to prevent cracking in future studies. In the current research, the WAAM built nickel alloy-Fe alloy metallic walls' microstructure, and hardness is observed and examined to select the most suitable material combination for creating a bimetallic part. The result of this preliminary study is concluded as:

- 1) Three groups of bimetallic walls were successfully fabricated via WAAM, with the components of Inconel 718-stainless steel 316, Inconel 625-stainless steel 316, Monel 400-Mild steel, respectively. No macroscale failure was observed throughout all the specimens.
- 2) Microstructure observation has revealed a typical, even dendritic microstructure similar to the other AM-built samples.
- 3) Cracking is common in as-built Inconel-stainless steel walls, which always appear in the steel part or near the bimetallic interface but rarely happen in the nickel part.
- 4) The top-to-bottom Vickers hardness values of every metallic wall are similar, while the fluctuation caused by microscale defects or interlocking structures commonly exist.
- 5) Throughout all three groups, the IN718-SS316 owns the best cracking behaviour and the most reliable mechanical properties, so the fabrication for the IN718-SS316 material combination is nominated for defect-free work part future studies.

Chapter 5 Hot Crack Investigation

5.1 Introduction

As concluded in the previous study, the IN718 is considered the most suitable material for combining with SS316 for manufacturing the final part. In this study, further investigation for avoiding hot cracking generated in the IN718-SS316 metallic wall was done by adjusting working parameters in welding. Six groups of IN718-SS316 samples are fabricated with different working parameters such as welding sequence, torch angle, interpass temperature, and heat input, as informed in the experimental procedure below.

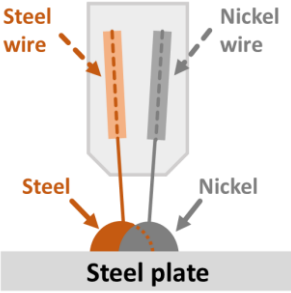
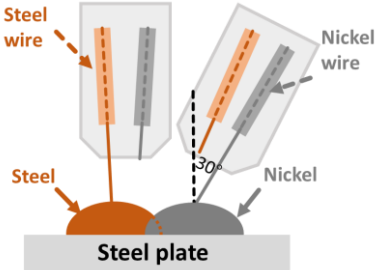
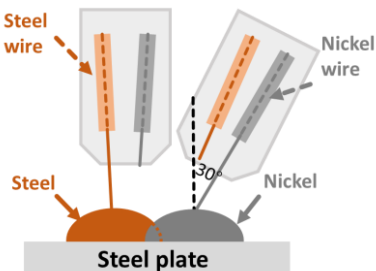
5.2 Experimental Procedure

The WAAM welding process is achieved via a Tandem GMAW welding system that consists central computer, shielding gas unit, robot controller, two-wire feeders, and an industrial welding robot, the same as illustrated in the previous study. Feedstock materials are Inconel 718 1.2mm commercial wire and Inconel 625 1.2mm commercial wire, respectively. The thin metallic walls are manufactured onto mild steel substrate with a planned height, length and overlapping distance. The width depends on the parameters like heat input in welding, as shown below. Like the previous study, High purity Argon gas is also applied for protection, and the welding process follows a layer-by-layer building strategy. Oxides and other contaminants are removed from each layer by an iron wire brush to prevent porosity and other impurity-caused defects after every layer are welded. The additional pressured air is used for rapid cooling—while some of the groups in this study does not apply the pressured air or interpass temperature control due to the controlled trial conditions, the modified welding conditions and parameters are shown in the table below. According to literature, some of the welding parameters may influences the generation of other materials' cracking generation, such as interpass temperature, cooling rate and heat input [181, 235, 236]. The condition difference

Hot Crack Investigation

between Wall 1 and Wall 2 is the welding sequence—Ni was welded first in Wall 1 while Fe was firstly welded in Wall 2. Walls 3 & 4 own different torch angles than Walls 1 & 2. The interlayer temperatures are also different—controlled interpass temperature is monitored via thermal camera during experiment for other walls while a rough interlayer temperature estimation for Wall 3. Walls 5 & 6 shows a different heat input between them when comparing Walls 3 & 4, pressured air cooling has been applied in the welding process of this group of bimetallic walls, and a lower travelling speed and wire feeding rate has been used to Wall 6 to investigate the influence of them.

Table 5.2.1. Comparative experiments plan with modified working parameters

Wall NO	Welding sequence	Torch angle	Cooling methods	Interpass temperature
1	Ni 718 → steel 316		Natural cooling	<150 °C
2	steel 316 → Ni 718		Natural cooling	<150 °C
3	steel 316 → Ni 718		Natural cooling	~150 °C ~ 200 °C (No temp controlled purposely)
4	steel 316 → Ni 718		Natural cooling	<150 °C
5	steel 316 → Ni 718		Pressured air cooling	<150 °C
6	steel 316 → Ni 718 Reduced WFS & TS		Pressured air cooling	<150 °C

In this experiment, the Travel speed and Wire-speed of Wall 1~5 are 6.5 (m/min), and 0.3 (m/min), that of the Wall 6 is 5 (m/min) and 0.25 (m/min), respectively, the calculated heat inputs between different walls are listed in the table below.

Table 5.2.2. Welding parameters and heat inputs of as-fabricated walls

	Current (A) (Ni/Fe)	Voltage (V) (Ni/Fe)	Travel speed (m/min)	Wire-speed (m/min)	Heat input for Ni	Heat input for Fe	Average heat input
Wall 1-5	191/158	21.6/22.8	0.3	6.5	660.10	576.38	618.24
Wall 6	152/120	20.2/22.3	0.25	5	589.52	513.79	551.65

5.3 Results and Discussion

5.3.1 Macrostructure

All the samples built in this experiment exhibited no material failure while welding, and no obvious large cracks exist in the final bimetallic wall. The macrostructure of as-built samples is shown in the image below.

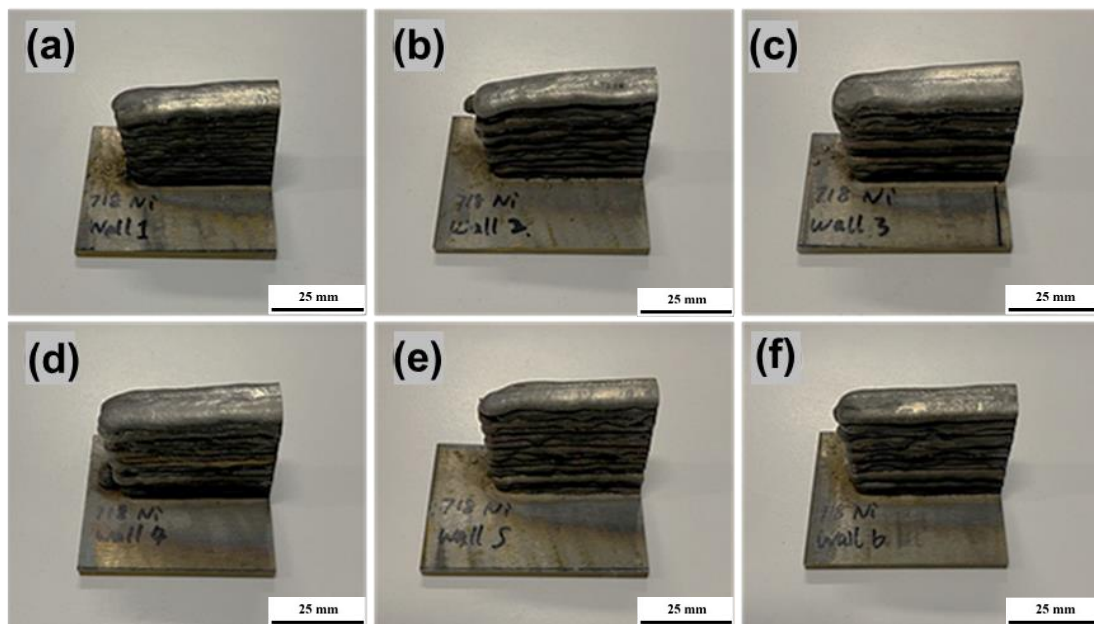


Figure 5.3.1. Six walls under different welding parameters and conditions.

As shown in the image, the macrostructures of as-built walls are similar, both of them showed a uniform profile, and without any collapse, a slight deformation happened in the substrate and the edge of all the bimetallic walls, which is because of the thermal accumulation caused by welding and inconsistent cooling rate between the edge and middle area.

Those walls are cut by a waterjet. Although no apparent cracks are found, a series of small-sized cracks are revealed on the surface after being roughly polished via abrasive paper. A further investigation of microcracks is demonstrated in the following section.

5.3.2 Microstructure

An optical microscope investigated the microstructure of the as-built thin walls via different fabricating strategies. All six thin walls presented similar microstructure in the SS316 side, interface, and IN718 side. The grain morphology at various locations (top, middle and bottom) was also identified in the corresponding area of all six samples. The following figure has shown the microstructure of Wall 6 as a representative of all six as-fabricated walls.

The representative microstructure is shown in Figure 5.3.2. It can be seen that the microstructure in both SS316 and IN718 sides was composed of a combination of dendritic and coarse-columnar grain structure. Similar microstructural characteristics have been reported in wire and arc additively manufactured single material with SS316 [237] and IN 718 [238], respectively, as shown in Figure 5.3.3. Overall, the dendritic microstructure of the SS316-IN718 bimetallic wall does not offer any dramatic difference compared with the preliminary (Section 4).

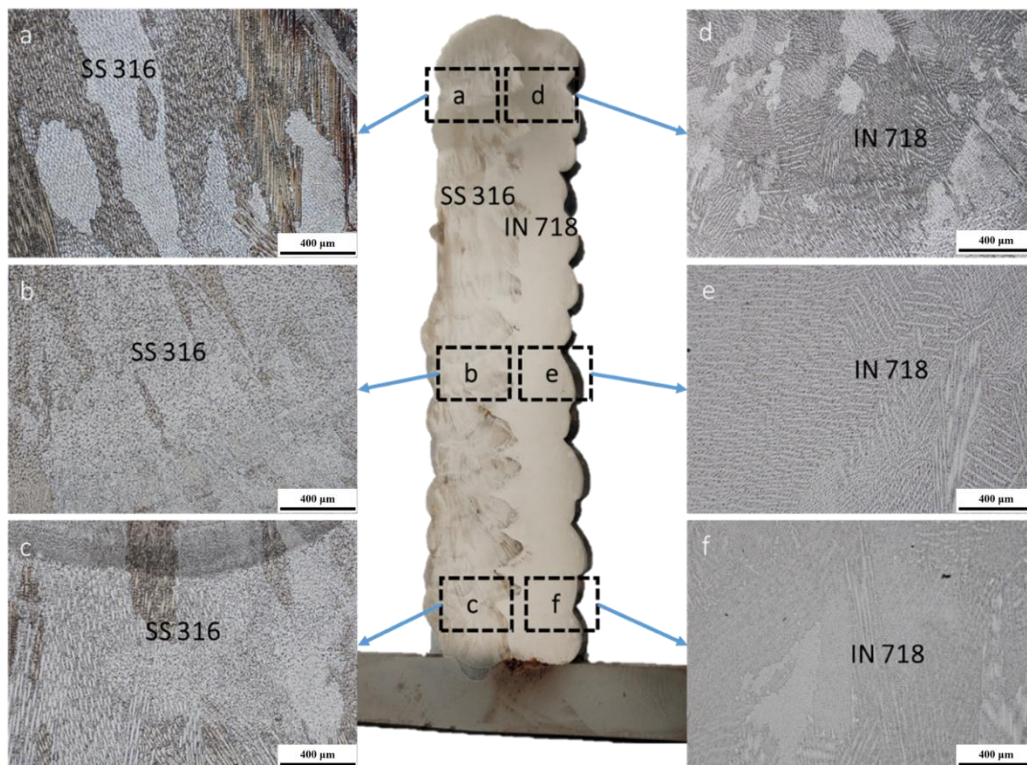


Figure 5.3.2. The representative microstructure in both SS316 and IN716 sides of Wall 6

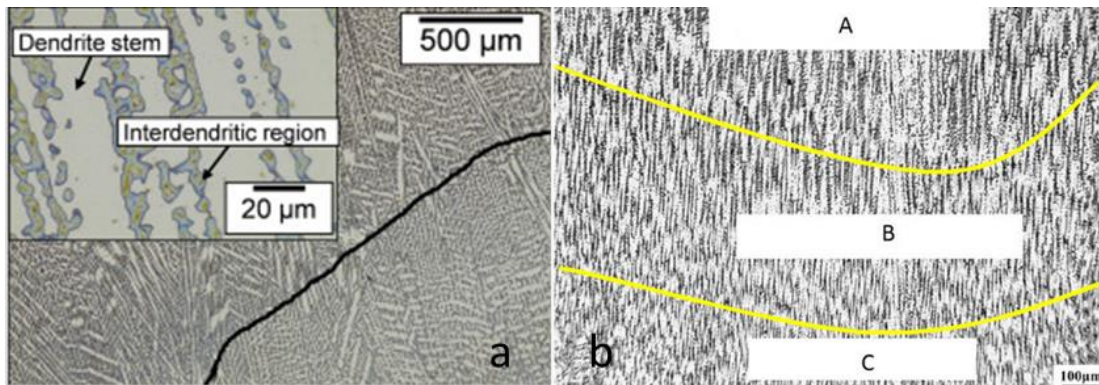


Figure 5.3.3. Microstructure of wire and arc additively manufactured (a) SS316 [237] and (b) IN718 [238].

The interface in Figure 5.3.4 displayed only dendritic microstructure with the interdendritic region in dark colour. Generally, severe segregation of elements is prone to occur in the inter-dendritic area [239]. The direct consequences include crack initiation and propagation, as well as anisotropic mechanical properties [240].

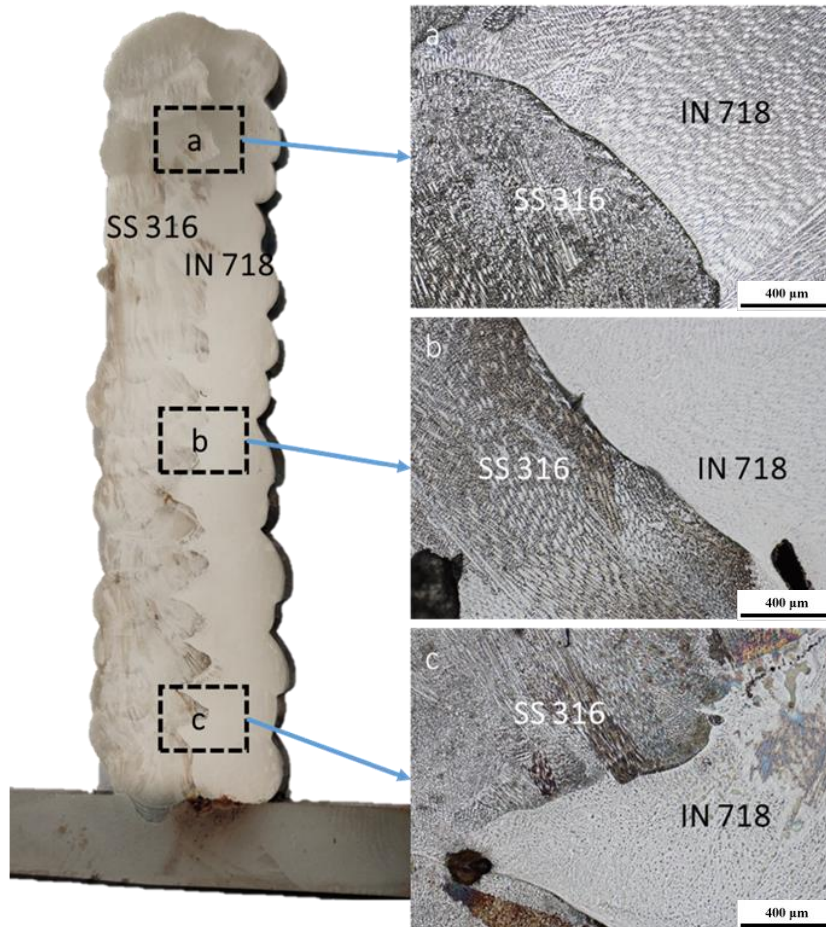


Figure 5.3.4. The representative microstructure in the interface of Wall 6.

5.3.3 Observation of hot cracks

The main object of this study is to investigate the effect of working parameters and working conditions on the generation of hot cracks in welding. The distribution of existing hot cracks (marked as “c”) and porosities (marked as “p”) on the cross-section of as-built six walls are shown in the image below (figure 5.3.5). Overall, the number of cracks of as-built six walls are 16,15,20,19,10,7 from wall 1 to wall 6, respectively. A few porosities are generated generally at the upper half of the bimetallic walls.

The effect of working parameters on microcracks based on the number and distribution of cracks in as-built walls with different welding parameters have been analysed. Wall 1 & 2 (different building sequence) shows a similar number of cracks (16 & 15 respectively), which means the building sequence of nickel and steel may not impact the number of cracks. While Wall 3 & 4 (adjusted torch angle, different interlayer temperature from each other) shows the most cracks throughout all the six groups with an almost identical number of cracks (20 & 19 respectively), the comparison between them reveals the interlayer temperature may not have a significant impact on the number of cracks. In addition, the adjusted torch angle may promote the generation of hot cracks for the IN718-SS316 bimetallic wall compared to Wall 2. Wall 5 & 6 (adjusted torch angle & cooled with pressured air, different heat inputs from each other) has the fewest cracks throughout all the six groups (10 & 7, respectively). It is concluded that the increased cooling rate results in a decreased number of cracks, and group 6 has fewer cracks than that of Wall 5, which reveals that controlling the heat input may be an effective way for reducing the number of cracks (which will be further explained in the following section).

Hot Crack Investigation

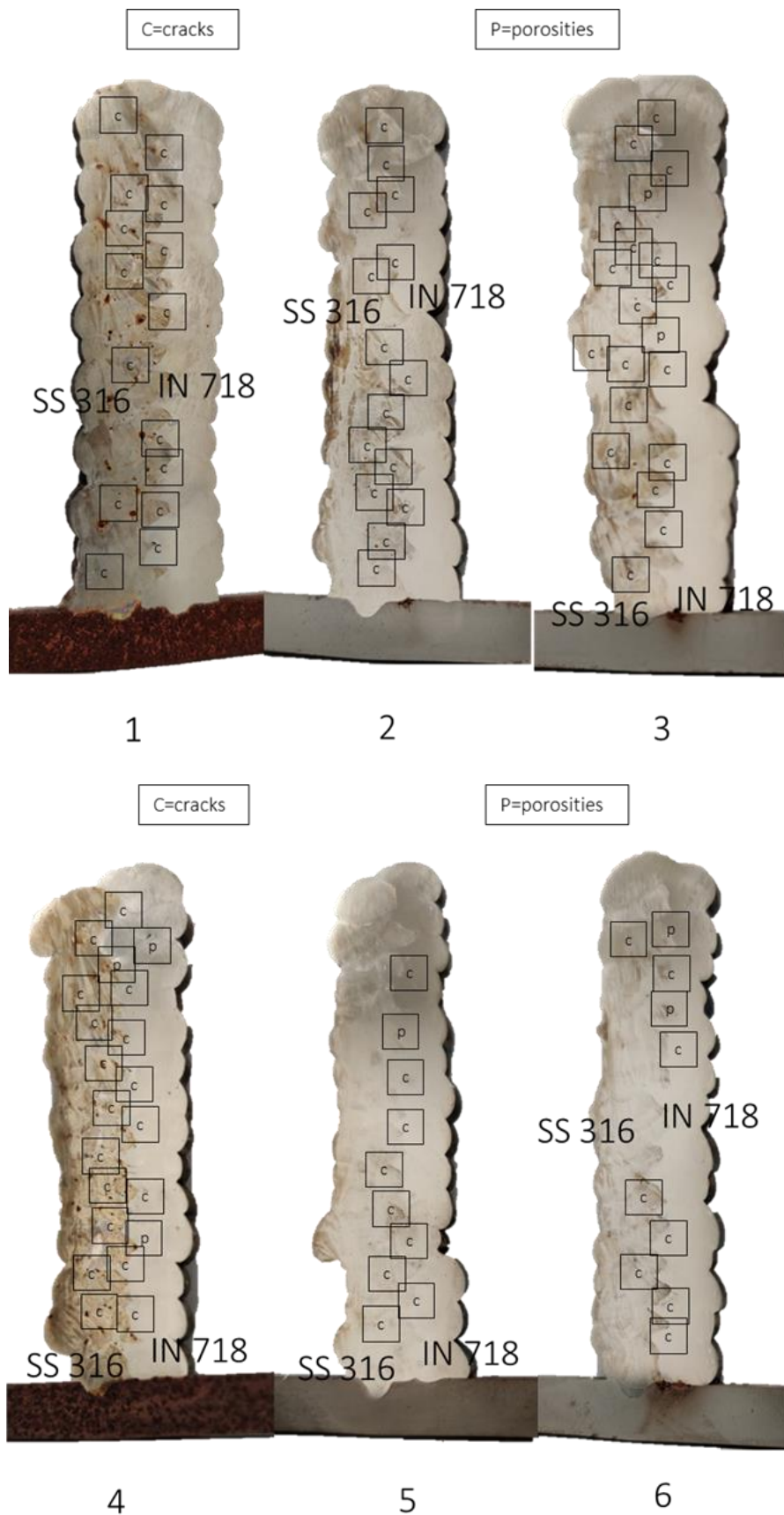


Figure 5.3.5. Distribution map of existing micro-cracks of WAAM built six walls

Hot Crack Investigation

The images below show the microstructure of hot cracks that happened in Wall 4 and Wall 6 (Figure 5.3.6 (1), (2)), a large number of hot cracks that existed in stainless steel part, which are considered as typical solidification cracking because they always happen along the grain boundaries as demonstrated in Figure 5.3.6 (1-a, c, e, f). In addition, there is also a certain number of cracks that appear near the surface between two metals. They always happen at the lower tip of the interlocking area (the “blade section” of a knife) and parallel to the intermetallic surface as shown in the image (Figure 5.3.6 (2-c, e, f)) below, so they are considered as typical liquation cracking when cracks appear at the interface, they always tend to appear on the nickel-based alloy side.

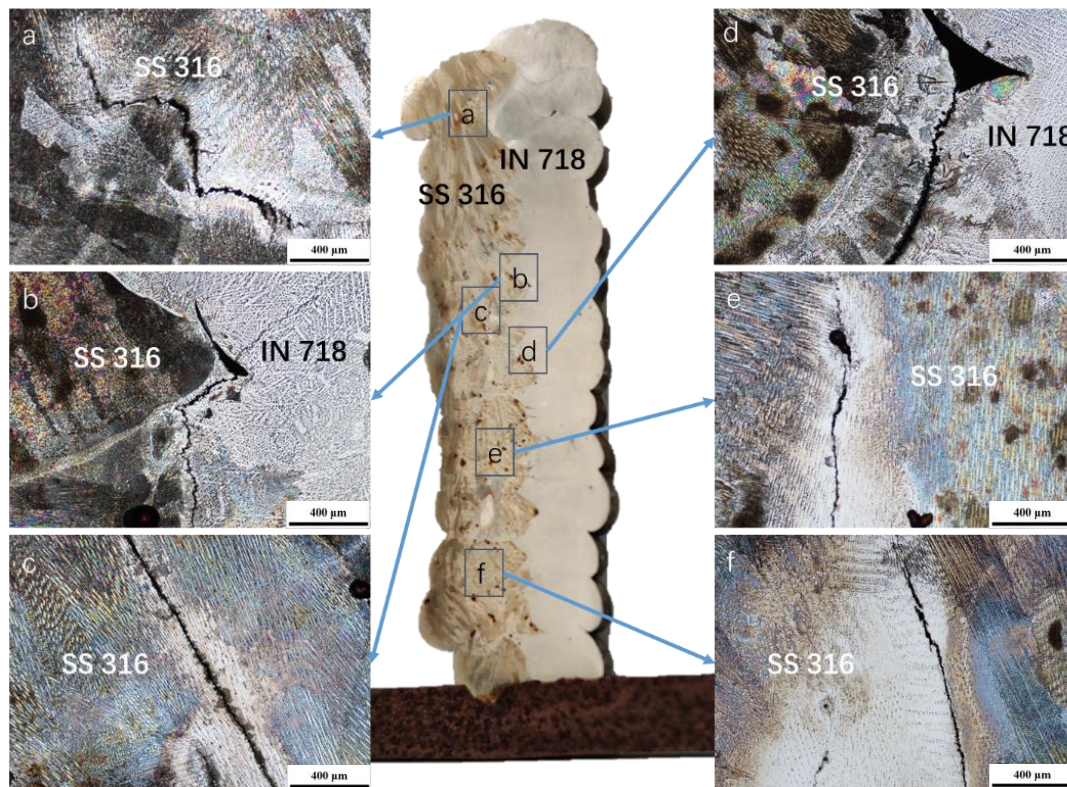


Figure 5.3.6 (1). Microstructure of hot cracks exist in Wall 4

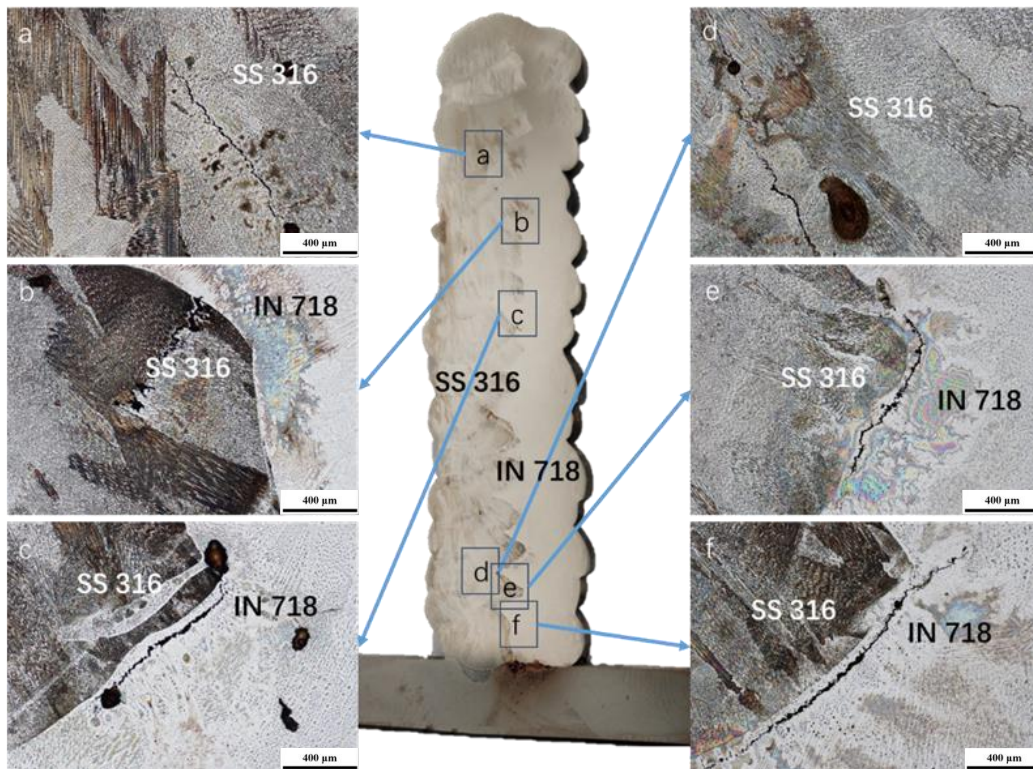


Figure 5.3.6 (2). Microstructure of hot cracks exist in Wall 6

As analysed by previous studies, the interpass temperature, cooling rate and heat input are vital in controlling the occurrence of cracks. Although welding variables can be directed to minimise the high hot-cracking susceptibility of welds, it is not always practical for all high alloying materials [241]. It would be more difficult for the more complicated additive manufacturing process. Correspondingly, the pertinence of the method and welding process parameters on the microstructure and sensitivity of joint hot cracking has been studied to control the hot cracking defects in SS316 and IN718. Heat input should be directed to moderate levels (2kJ/mm maximum) for most alloys to limit grain growth and heat-affected zone (HAZ) size. In welding of SS316, the hot cracks are always generated because of the sigma (σ) phase during the solidification process and extended along the boundary of the γ/σ interface [242]. According to Kuboň Z. et al. [243], the heat input of welding austenitic stainless steel must be restricted to a certain level (from 1100 to 1900 J/mm) and also the interlayer temperature should get controlled at 150 °C to avoid σ phase. For some nickel-based alloys, a maximum heat input of 1kJ/mm is recommended. Nevertheless, it has been

found that the low heat input welds were prone to liquation cracking in HAZ of Allvac 718Plus superalloy, while the welds with higher heat input were free from the liquation cracking [244]. Montazeri, M. et al. [245] has also stated that the susceptibility to liquation cracking in IN738 nickel-based superalloy decreased with increasing heat input in Laser welding.

It is also worth noticing that the fewest cracks in Wall 6 should be attributed to either a slightly higher heat input or reduced wire feeding rate and travel speed. However, the fastest welding speed is usually recommended, not always confirmed on site. Several researchers [247-249] reported that the travel speed influences solidification cracking's formation through thermal and metallurgical effects. Increasing travel speed results in opposing impacts. It enhances the formation of solidification cracking by decreasing the centreline temperature gradient, reducing the time to feed shrinkage, and generating centreline grain segregation. On the other hand, increasing travel speed hinders solidification cracking formation by shifting the compression cell to the mushy zone, which was caused by the non-uniform thermal distribution while welding, reducing the time exposed to strain, and refining weld metal grains.

Moreover, the morphology and composition of the detrimental laves phase in the welding of IN718 strongly depended on the weld cooling rate, with fast weld cooling rates found to be beneficial in lower amounts of laves phases with less interconnectivity [246]. The consideration of interpass temperatures is also of prime importance. Interpass temperature is the temperature of the weld area between passes, which also affects the weld cooling rate. It can also affect the micro-segregation, and the morphology of the laves phase.

5.3.4 SEM-EDS observation

The interface of the fewest cracks existed bimetallic wall (Wall 6) is observed via SEM and analysed via EDS for investigating the elemental distribution and further determine the mechanism of crack generation—cracks can generate from detrimental

phases (normally laves phase), which can be revealed via EDS with a dramatic change of the elemental peak (normally Nb and Ni) near the crack because of the elemental segregation, or the cracks may simply be generated by insufficient working parameters, whose EDS analytical image will show a direct drop on the elemental peaks because of the vacuum of atoms. Figure 5.3.7 (1) shows SEM/EDS mapping of elemental distribution at SS316/IN718 interface in Wall 6 of this study. A distinctive interlocking interface is expected in the elemental maps for Fe, Ni, Nb and Mo due to different alloying elements in SS316 and IN718. Other elements are found to distribute uniformly through the interface. This is attributed to the similar composition of some elements in the two alloys, such as 16-18% Cr in SS316 and 17-22% Cr in IN718. It is noticeable that there is no apparent elemental segregation near the crack. The line analysis in Figure 5.3.7 (2) also shows the simultaneous and direct decrease of all the elements across the crack, which is most likely to be generated by unsuitable welding parameters rather than the formation of detrimental phase due to elemental segregation.

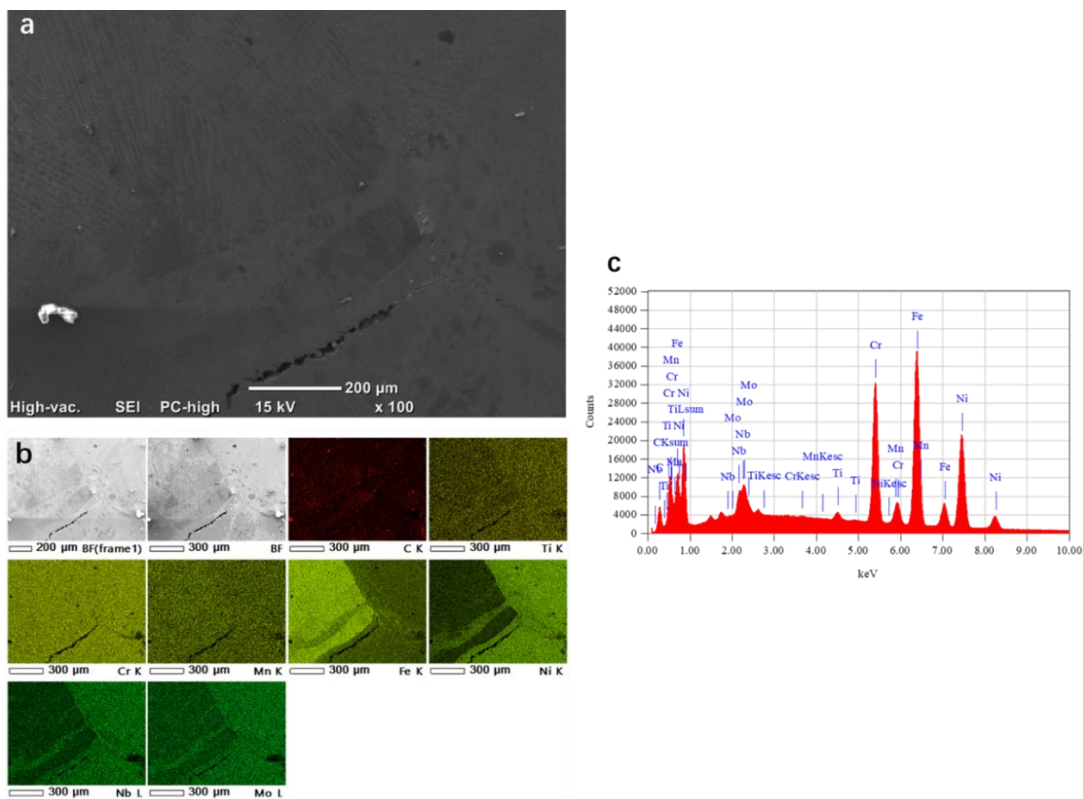


Figure 5.3.7 (1). (a) SEM image of the observed interface area in Wall 6; (b) SEM-

EDS elemental maps—elemental distribution at the interface in Wall 6; (c)
Composition of elements in the observed interface area in Wall 6.

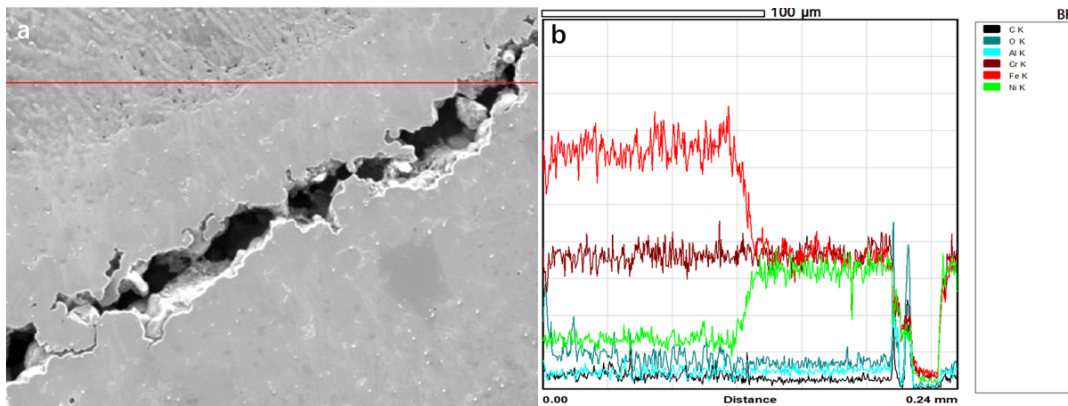


Figure 5.3.7 (2). Line analysis of the elemental distribution near the crack existed at the interface.

5.3.5 Mechanical properties

The mechanical properties of as-built walls are displayed via the Vickers hardness test and small punch test (SPT); the testing results are listed and analysed in the following sections.

Vickers hardness

The Vickers hardness value of Wall 5 and Wall 6 are demonstrated in the figure below (Figure 5.3.8 (1), (2)). As shown in the figure, the hardness curve from SS316 to IN718 shows a relative average hardness value with a slight fluctuation owing to different phases and defects. A sudden drop of the hardness value happens in the interface area, and the average hardness of nickel (about 240) is higher than that of steel (about 180), which is similar to that of the typical WAAM built materials separately [233]. In addition, the hardness value from top to bottom did not change exaggeratedly for the same part, while the average hardness of Wall 5 is slightly lower than that of Wall 6, which might be because of the influence of a larger number of hot cracks that existed in Wall 5 (the hardness value will show a sudden drop when the tester goes through defects).

Hot Crack Investigation

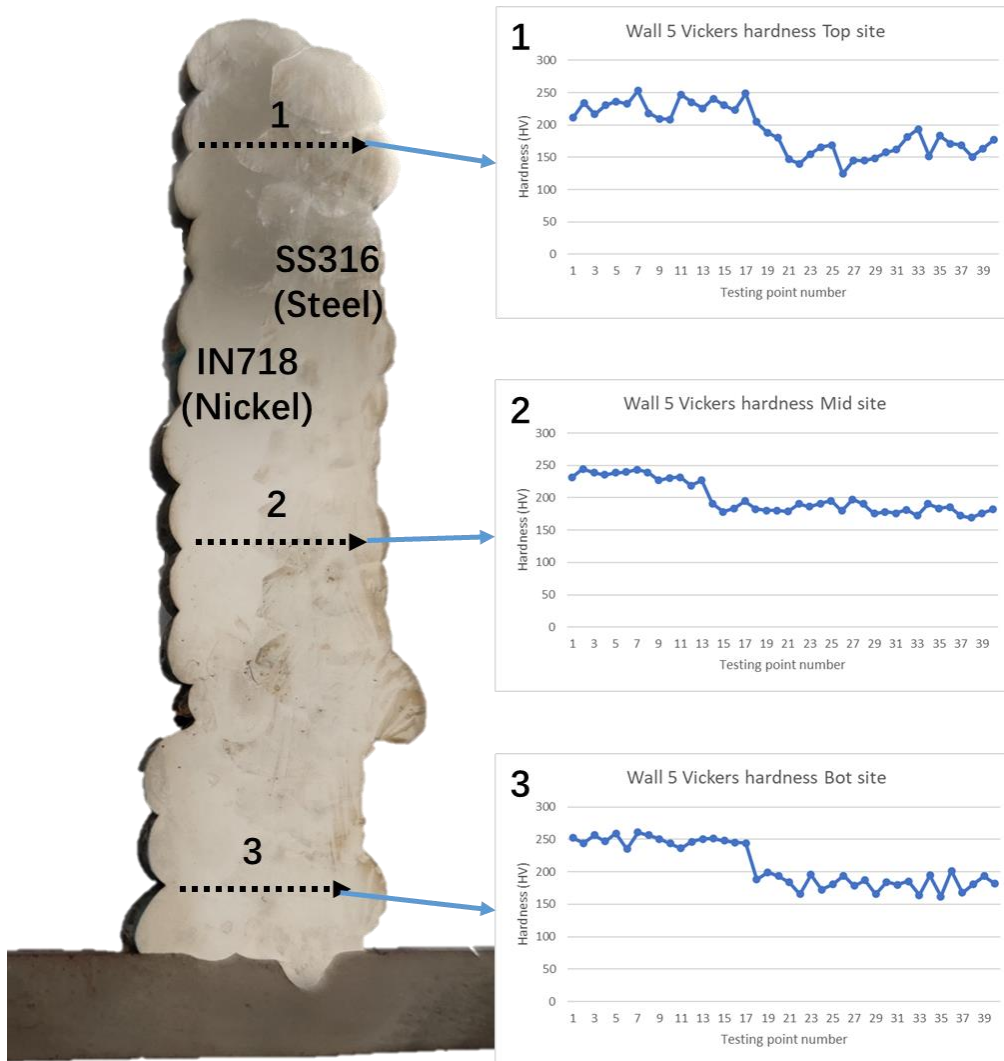


Figure 5.3.8 (1). Vickers hardness comparison from top to bottom of Wall 5

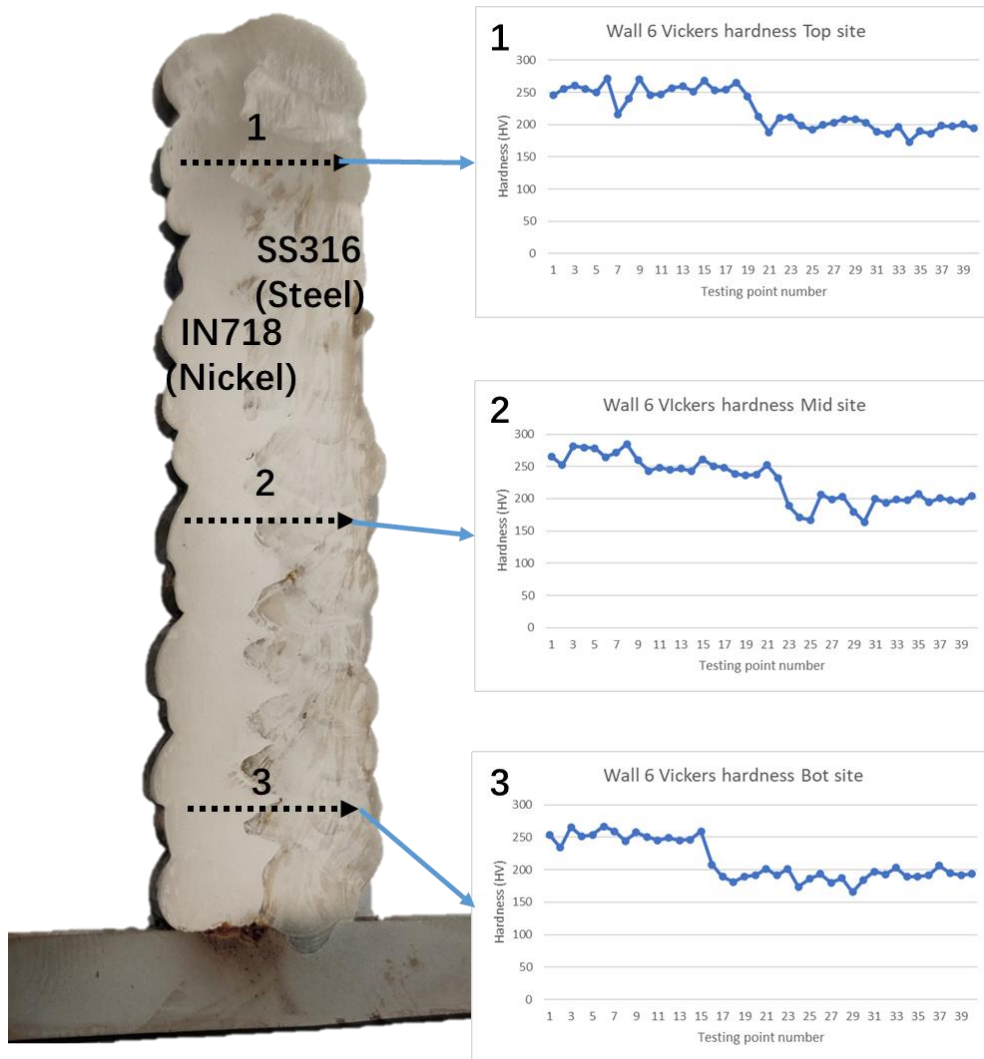


Figure 5.3.8 (2). Vickers hardness comparison from top to bottom of Wall 6

Small punch test

As introduced by previous sections, small disks are sent to ANSTO for small punch testing at four specimens per group. In this study, the fewest cracking behaved walls from groups 5 & 6 are prepared and tested.

The SPT data diagrams are shown in figure 5.3.9 below. As revealed in the diagram, the maximum force (F_m) values of specimens from both Wall 5 and Wall 6 are different but approximately at the same level. The average value is calculated as 1164.29 N and 814.87 N, respectively.

Hot Crack Investigation

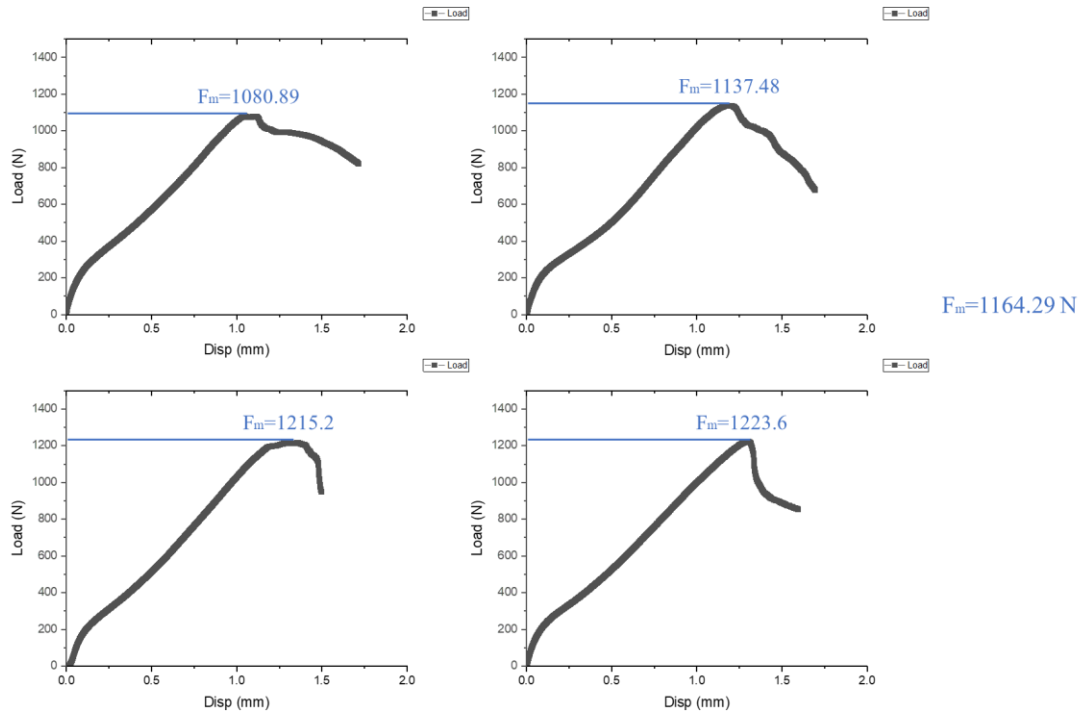


Figure 5.3.9 (1). Diagram of SPT data of specimens from Wall 5.

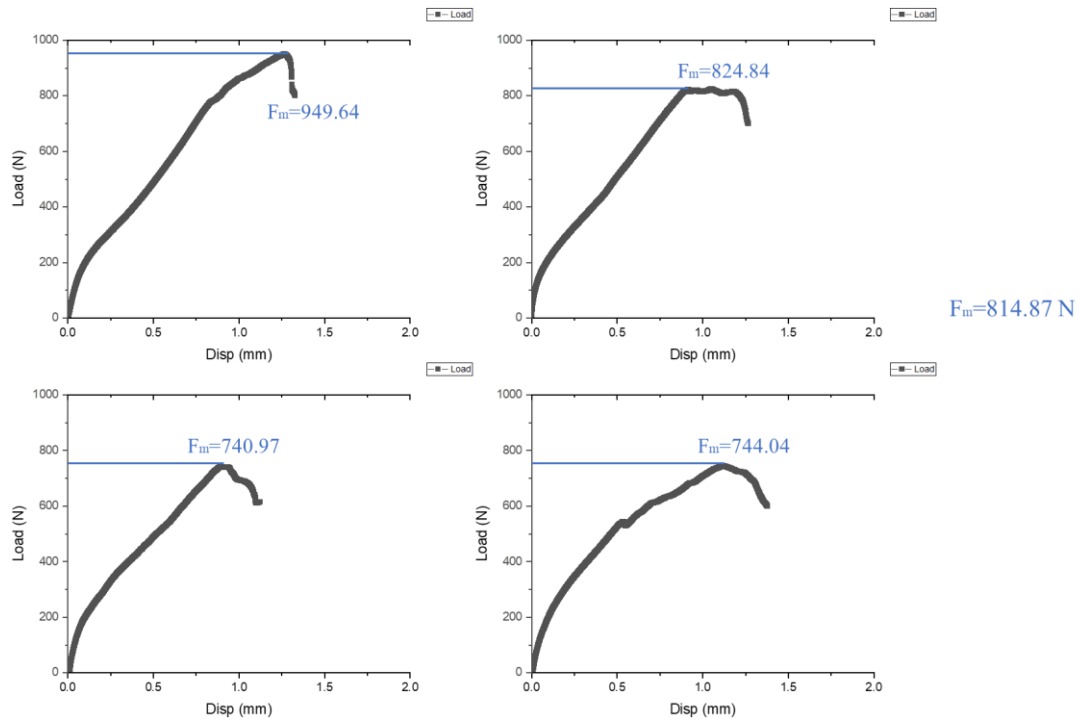


Figure 5.3.9 (2). Diagram of SPT data of specimens from Wall 6.

Another critical data is elastic-plastic transition force (F_e), which can be determined via establishing bilinear function $f(v)$ through origin and data points (as revealed in the

formula below) [247].

$$f(v) = \begin{cases} \frac{f_A \cdot v}{u_A} & \text{for } 0 \leq v \leq v_A \\ \frac{f_B - f_A}{u_B - u_A} (v - v_A) + f_A & \text{for } v_A \leq v \leq v_B \end{cases}$$

In this equation, B is taken from the point that the displacement equals origin thickness (0.5mm), for experimental transition force, point A is determined via the x value of two linear function's cross point that located in the raw data curve (as shown in the figure below).

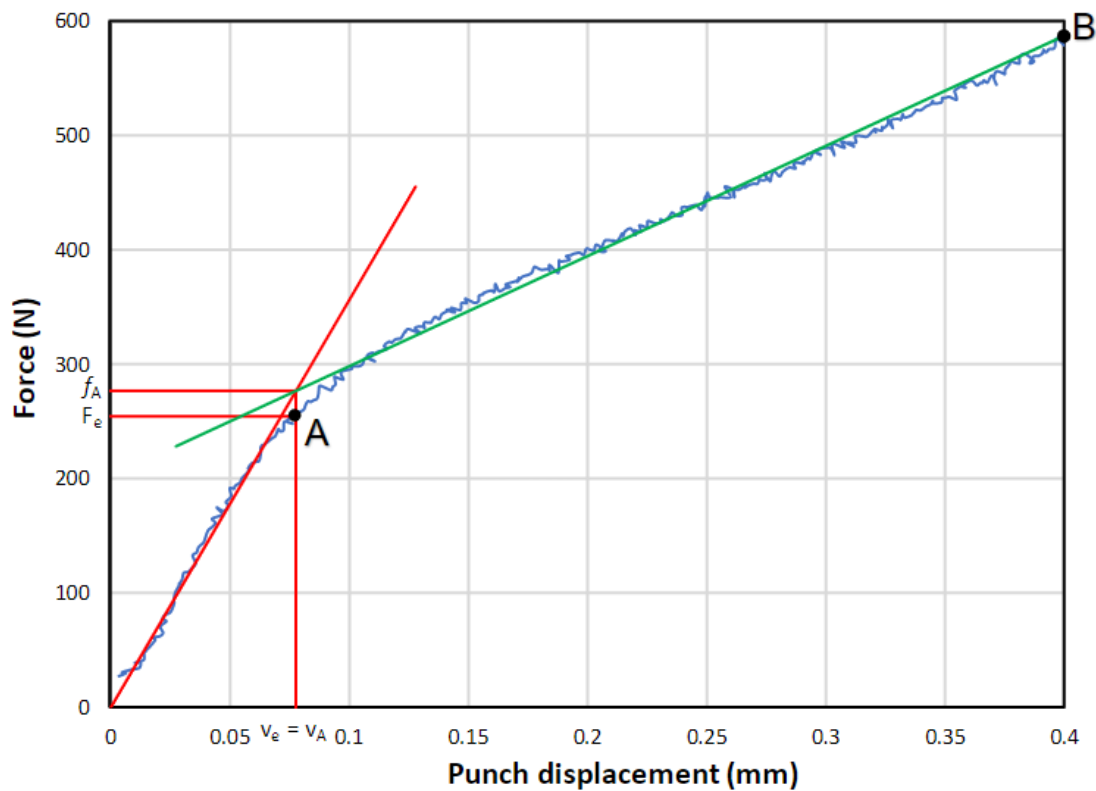


Figure 5.3.10. Determination of elastic-plastic force

After calculation, the average F_e for Walls 5 & 6 is determined at 199.46 N and 146.78 N.

According to Bruchhausen et al. [248], the equation of calculating yield strength is as the formula below shows:

$$R_{p0.2} = \beta_{Rp0.2} \frac{F_e}{h_0^2}$$

Where the $\beta_{Rp0.2}$ is correlation coefficient that depends on the geometry of the test rig, in this study, the value is 0.346 [248], and h_0 as the initial specimen thickness,

which is 0.5mm in this study.

So, the estimated yield strength can be calculated as 276.05 Mpa and 203.14 Mpa for Wall 5 & 6 respectively, both of them showed a comparable value compared to the yield strength of stainless steel 316 (>205 Mpa), but far lower than that of the Inconel 718 (>1034 Mpa), which is might because of the Ni-Fe bimetallic structure—nickel enhances the yield strength of steel but reduces that of themselves on the contrary. In addition, the yield strength of Wall 5 is slightly higher than that of Wall 6. The only difference between them is the heat input of Wall 6 is marginally lower than Wall5. However, according to Hossein Eskandari Sabzi et al. [249], the yield strength of IN718 decreases dramatically with the increment of heat input, but that of the SS 316 increases slightly with the increasing heat input in the laser powder bed fusion AM method, which is contrasting to the conclusion we get from this study, further examinations and theoretically analyses are required for explaining this irregular phenomenon.

Also, according to the formula below, the estimated ultimate tensile strength can be calculated using the F_m value observed before:

$$R_m = \beta_{Rm} \frac{F_m}{h_0 u_m}$$

Where the β_{Rm} is another geometry dependent correlation coefficient, which is 0.277 in this study, u_m is the displacement value in F_m point, the values are 1.186 and 1.051 for Wall 5 & 6 respectively.

The average estimated ultimate tensile strength is calculated as 543.85 Mpa and 429.53 Mpa, respectively, which are also similar to that of the SS316 (>515Mpa) but far lower than that of the IN718 (>1241Mpa), which might be because of the combination between two materials are not strong enough, same as Li et al. research [250], poor intermetallic bonding between IN718 and SS316L is also shown in their study, there shows a high possibility of ductile fracture happened in the bimetallic interface by conventional tensile testing method, so the unsatisfactory tensile results in this study are ordinary.

Another mechanical property of the specimens that can be calculated via SPT

Hot Crack Investigation

testing data is elongation to failure (%), which is demonstrated in the formula below:

$$\varepsilon = 12.57 * u_m$$

The elongation values of specimens are determined as 14.91 % and 13.21 %, respectively, which are more than half below either SS316 (>40%) or IN718 (>30%) commercial materials in a room temperature. However, several research studies have shown a similar elongation of fracture than commercial materials, but both used a layer-by-layer building strategy (different materials for different layers). It is estimated that the interweaving structure greatly affected the ductility of the material. Further examinations and analysis should be done to investigate the effect of interweaving structure on the elongation rate of IN718-SS316 bimetallic material.

5.4 Conclusion

In this study, six IN718-SS316 bimetallic walls with different welding parameters were successfully built for investigating the effect of welding parameters on hot cracking. The cracks in the cross-section of as-built walls are observed via optical microscopy and SEM to analyse the quantity and cause of formation. The following conclusions can be drawn based on the result analysis:

- 1) The microstructural observation shows a similar dendritic structure in all the bimetallic walls compared with the sample in the preliminary study (Section 4), and similar distribution of cracks are found in newly built samples, which means the changing of parameters in this study does not impact the microstructural behaviour of IN718-SS316 bimetallic material.
- 2) An application of a 30°-degree torch angle provides flexibility to welding, however, it can also increase the number of cracks, while other parameters—application of pressured air and lower WFS & TS reduce the possibility of crack generation. It is considered that a balance of welding parameters and cracks should be drawn in future studies.
- 3) Although the number of cracks strongly relates to the variation of some of the welding parameters in this study, some welding parameters like welding sequence or a slight change of interlayer temperature do not play a critical role in affecting the cracks' generation.
- 4) SEM-EDS observation proves the cracks found near the interface are not caused by detrimental phases (which are generally difficult to eliminate in welding) generated by elemental segregation. It is highly likely that interface cracking can be prevented by optimising welding parameters.
- 5) The hardness values of specimens are relatively uniform on either IN718 or SS316 side, but there is a clear demarcation at the interface. These hardness values are similar to commercially produced monolithic alloys, indicating comparable strengths

Chapter 6 Summary and Future Research

In summary, nickel alloy-stainless steel bimetallic walls were successfully fabricated via WAAM with an interweaving fabrication strategy. Based on the outcome from the preliminary study, a material combination of IN718-SS316 has been selected for detailed investigation, the mechanical properties of the as-built bimetallic wall have been tested, the result shows the hardness value of as-built IN718-SS316 is very close to that of the commercial materials. However, cracks are common defects found at the cross-section surface of as-built walls. The SEM and EDS analysis reveal there is no obvious evidence that proves the cracks are generated by elemental segregation. The degree of cracking appears to be welding parameter dependent. Systematic trials were conducted with various welding parameters to eliminate defects, including building sequence, interpass temperature, cooling rate, heat input, travel speed, and wire feed rate. The outcome provided valuable information in establishing an optimal operation window for manufacturing quality IN 718-SS316 components.

In feasibility study, a cylindrical IN718-SS316 part has been successfully produced, as shown in figure 6.1 below, which has relative smooth outer and inner surfaces with no visible distortion. Therefore, it is demonstrated that WAAM has excellent potential in fabricating bimetallic components with complex geometry.



Figure 6.1. The as-fabricated IN718-SS316 bimetallic cylinder.

Future research aims to identify the suitable welding parameters for producing

Summary and Future Research

defect-free IN718-SS316 bimetallic walls, manufacturing more complex geometry bimetallic parts such as cylinders or tees, and characterising microstructure, mechanical properties, oxidation resistance, etc.

Reference

- [1] C. T. Sims, "A history of superalloy metallurgy for superalloy metallurgists," *Superalloys*, vol. 1984, pp. 399-419, 1984.
- [2] H. S. Mali and D. R. Unune, "Machinability of Nickel-Based Superalloys: An Overview," in *Reference Module in Materials Science and Materials Engineering*: Elsevier, 2017.
- [3] T. Nagayama, T. Yamamoto, and T. Nakamura, "Thermal expansions and mechanical properties of electrodeposited Fe–Ni alloys in the Invar composition range," *Electrochimica Acta*, vol. 205, pp. 178-187, 2016/07/01/ 2016, doi: <https://doi.org/10.1016/j.electacta.2016.04.089>.
- [4] G. Sushko, "Atomistic molecular dynamics approach for channeling of charged particles in oriented crystals," 2015.
- [5] M. J. Donachie, S. Donachie, M. Donachie, and S. Donachie, *Superalloys : A Technical Guide*. Materials Park, UNITED STATES: A S M International, 2002.
- [6] "12 - Superalloys for gas turbine engines," in *Introduction to Aerospace Materials*, A. P. Mouritz Ed.: Woodhead Publishing, 2012, pp. 251-267.
- [7] Brandon. mstudent. (accessed).
- [8] C. Cui, D. Ping, Y. Gu, and H. Harada, "A New Co-Base Superalloy Strengthened by γ' Phase," *MATERIALS TRANSACTIONS*, vol. 47, no. 8, pp. 2099-2102, 2006, doi: 10.2320/matertrans.47.2099.
- [9] D. Coutsouradis, A. Davin, and M. Lamberigts, "Cobalt-based superalloys for applications in gas turbines," *Materials Science and Engineering*, vol. 88, pp. 11-19, 1987/04/01/ 1987, doi: [https://doi.org/10.1016/0025-5416\(87\)90061-9](https://doi.org/10.1016/0025-5416(87)90061-9).
- [10] N. Mohammed Dawood and A. Mishaal Salim, "A Review on Characterization, Classifications, and Applications of Super Alloys," *Journal of University of Babylon for Engineering Sciences*, vol. 29, no. 1, pp. 53 - 62, 04/21 2021. [Online]. Available: <https://www.journalofbabylon.com/index.php/JUBES/article/view/3505>.
- [11] Y. Yamamoto *et al.*, "Development of creep-resistant, alumina-forming ferrous alloys for high-temperature structural use," in *ASME 2018 Symposium on Elevated Temperature Application of Materials for Fossil, Nuclear, and Petrochemical Industries, ETAM 2018*, 2018, doi: 10.1115/ETAM2018-6727. [Online]. Available: <https://www.scopus.com/inward/record.uri?eid=2-s2.0-85068510470&doi=10.1115%2fETAM2018-6727&partnerID=40&md5=646f1c68bc8972c5289ad7e55efb132b>
- [12] H. Zhang, X. Qin, X. Li, and L. Zhou, "Incipient Melting Behavior and Its Influences on the Mechanical Properties of a Directionally Solidified Ni-Based Superalloy with High Boron Content," *Jinshu Xuebao/Acta Metallurgica Sinica*, Article vol. 53, no. 6, pp. 684-694, 2017, doi: 10.11900/0412.1961.2016.00495.
- [13] J. L. Caron and J. W. Sowards, "6.09 - Weldability of Nickel-Base Alloys," in *Comprehensive Materials Processing*, S. Hashmi, G. F. Batalha, C. J. Van Tyne, and B. Yilbas Eds. Oxford: Elsevier, 2014, pp. 151-179.

- [14] J. Belan, "GCP and TCP Phases Presented in Nickel-base Superalloys," *Materials Today: Proceedings*, vol. 3, no. 4, pp. 936-941, 2016/01/01/ 2016, doi: <https://doi.org/10.1016/j.matpr.2016.03.024>.
- [15] W. O. Soboyejo, *Mechanical properties of engineered materials*. New York: Marcel Dekker (in English), 2003.
- [16] H. Ur-Rehman, "Solid Solution Strengthening and Diffusion in Nickel- and Cobalt-based Superalloys Mischkristallhärtung und Diffusion in Nickel- und Kobaltbasissuperlegierungen," FAU University Press, Erlangen, 2016. [Online]. Available: <https://opus4.kobv.de/opus4-fau/frontdoor/index/index/docId/7407>
<https://nbn-resolving.org/urn:nbn:de:bvb:29-opus4-74073>
- [17] A. Thakur. "What is the difference between Solid solution strengthening and precipitation strengthening?" (accessed.
- [18] W. D. Callister, *Fundamentals of materials science and engineering*. Wiley London, 2000.
- [19] A. H. Chokshi, "Grain Boundary Processes in Strengthening, Weakening, and Superplasticity," *Advanced Engineering Materials*, vol. 22, no. 1, p. 1900748, 2020, doi: <https://doi.org/10.1002/adem.201900748>.
- [20] J. W. Martin, *Precipitation hardening: theory and applications*. Butterworth-Heinemann, 2012.
- [21] T. Gladman, "Precipitation hardening in metals," *Materials Science and Technology*, vol. 15, no. 1, pp. 30-36, 1999/01/01 1999, doi: 10.1179/026708399773002782.
- [22] R. M. German, "1 - Metal powder injection molding (MIM): Key trends and markets," in *Handbook of Metal Injection Molding (Second Edition)*, D. F. Heaney Ed.: Woodhead Publishing, 2019, pp. 1-21.
- [23] "1 - Introduction to aerospace materials," in *Introduction to Aerospace Materials*, A. P. Mouritz Ed.: Woodhead Publishing, 2012, pp. 1-14.
- [24] K. Horke, A. Meyer, and R. F. Singer, "24 - Metal injection molding (MIM) of nickel-base superalloys," in *Handbook of Metal Injection Molding (Second Edition)*, D. F. Heaney Ed.: Woodhead Publishing, 2019, pp. 575-608.
- [25] R. C. Reed, *The Superalloys : Fundamentals and Applications*. Cambridge, UNITED KINGDOM: Cambridge University Press, 2006.
- [26] "2 - Aerospace materials: past, present and future," in *Introduction to Aerospace Materials*, A. P. Mouritz Ed.: Woodhead Publishing, 2012, pp. 15-38.
- [27] J. N. DuPont, S. D. Kiser, and J. C. Lippold, *Welding metallurgy and weldability of nickel-base alloys*. Hoboken, N.J: John Wiley & Sons, 2009.
- [28] A. Jena and M. Chaturvedi, "The role of alloying elements in the design of nickel-base superalloys," *Journal of Materials Science*, vol. 19, no. 10, pp. 3121-3139, 1984.
- [29] V. Sikka, S. Deevi, S. Viswanathan, R. Swindeman, and M. Santella, "Advances in processing of Ni₃Al-based intermetallics and applications," *Intermetallics*, vol. 8, no. 9-11, pp. 1329-1337, 2000.

- [30] A. Wagner, B. Shollock, and M. McLean, "Grain structure development in directional solidification of nickel-base superalloys," *Materials Science and Engineering: A*, vol. 374, no. 1-2, pp. 270-279, 2004.
- [31] M. T. Jovanović, B. Lukić, Z. Mišković, I. Bobić, I. Cvijović, and B. Dimčić, "Processing and some applications of nickel, cobalt and titanium-based alloys," *Association of Metallurgical Engineers of Serbia*, 2007.
- [32] G. R. Thellaputta, P. S. Chandra, and C. S. P. Rao, "Machinability of Nickel Based Superalloys: A Review," *Materials Today: Proceedings*, vol. 4, no. 2, Part A, pp. 3712-3721, 2017/01/01/ 2017, doi: <https://doi.org/10.1016/j.matpr.2017.02.266>.
- [33] E. P. DeGarmo, J. T. Black, and R. A. Kohser, *Materials and Processes in Manufacturing*. Wiley, 2003.
- [34] Matmatch. "Superalloys: Properties, Processing, and Applications." (accessed.
- [35] R. Schlatter, "Vacuum induction melting," *JOM*, vol. 24, no. 5, pp. 17-25, 1972.
- [36] R. L. Boxman, D. Sanders, and P. J. Martin, *Handbook of vacuum arc science & technology: fundamentals and applications*. William Andrew, 1996.
- [37] D. A. Melgaard, R. G. Erdmann, J. J. Beaman, and R. L. Williamson, "Monitoring the vacuum arc remelting process," Sandia National Laboratories, 2007.
- [38] Y. Tanaka, "5 - Production of creep-resistant steels for turbines," in *Creep-Resistant Steels*, F. Abe, T.-U. Kern, and R. Viswanathan Eds.: Woodhead Publishing, 2008, pp. 174-214.
- [39] C. Sommitsch, R. Radis, A. Krumphals, M. Stockinger, and D. Huber, "12 - Microstructure control in processing nickel, titanium and other special alloys," in *Microstructure Evolution in Metal Forming Processes*, J. Lin, D. Balint, and M. Pietrzyk Eds.: Woodhead Publishing, 2012, pp. 337-383.
- [40] Electroslag Remelting Process: Part One
- [41] R. SIDALL, "Comparison of the Attributes of VIM+ ESR," *Superalloys 718, 625 and Various Derivatives*, pp. 29-41, 1991.
- [42] T. Rajan, T. S. Rajan, C. Sharma, and A. Sharma, *Heat treatment: principles and techniques*. PHI Learning Pvt. Ltd., 2011.
- [43] "Heat Treating Nickel Alloys." (accessed 21/12, 2021).
- [44] J. R. Davis, *Nickel, cobalt, and their alloys*. ASM international, 2000.
- [45] J. D. Verhoeven, *Fundamentals of physical metallurgy*. Wiley, 1975.
- [46] "SOLUTION ANNEALING HEAT TREATMENT." (accessed 22/12, 2021).
- [47] W. Akhtar, J. Sun, P. Sun, W. Chen, and Z. Saleem, "Tool wear mechanisms in the machining of Nickel based super-alloys: A review," *Frontiers of Mechanical Engineering*, vol. 9, no. 2, pp. 106-119, 2014.
- [48] S. Sun, M. Brandt, and M. Dargusch, "Machining Ti-6Al-4V alloy with cryogenic compressed air cooling," *International Journal of Machine Tools and Manufacture*, vol. 50, no. 11, pp. 933-942, 2010.
- [49] E. Ezugwu, Z. Wang, and A. Machado, "The machinability of nickel-based alloys: a review," *Journal of Materials Processing Technology*, vol. 86, no. 1-3,

- pp. 1-16, 1999.
- [50] D. Dudzinski, A. Devillez, A. Moufki, D. Larrouquère, V. Zerrouki, and J. Vigneau, "A review of developments towards dry and high speed machining of Inconel 718 alloy," *International Journal of Machine Tools and Manufacture*, vol. 44, no. 4, pp. 439-456, 2004/03/01/ 2004, doi: [https://doi.org/10.1016/S0890-6955\(03\)00159-7](https://doi.org/10.1016/S0890-6955(03)00159-7).
- [51] E. Cui, J. Zhao, X. Wang, and S. Song, "Cutting performance, failure mechanisms and tribological properties of GNPs reinforced Al₂O₃/Ti(C,N) ceramic tool in high speed turning of Inconel 718," *Ceramics International*, vol. 46, no. 11, Part B, pp. 18859-18867, 2020/08/01/ 2020, doi: <https://doi.org/10.1016/j.ceramint.2020.04.206>.
- [52] A. Seleznev, N. W. S. Pinargote, and A. Smirnov, "Ceramic Cutting Materials and Tools Suitable for Machining High-Temperature Nickel-Based Alloys: A Review," *Metals*, vol. 11, no. 9, p. 1385, 2021. [Online]. Available: <https://www.mdpi.com/2075-4701/11/9/1385>.
- [53] S. Pervaiz, A. Rashid, I. Deiab, and M. Nicolescu, "Influence of tool materials on machinability of titanium-and nickel-based alloys: a review," *Materials and Manufacturing Processes*, vol. 29, no. 3, pp. 219-252, 2014.
- [54] V. Cassidy. (2008, February 1) Taming the 'Nastalloys'. *Cutting Tool Engineering*.
- [55] G.-J. Tzou, D.-Y. Chen, and C.-Y. Hsu, "Application of Taguchi method in the optimization of cutting parameters for turning operations Application of Taguchi method in the optimization of cutting parameters for turning operations," 12/24 2021.
- [56] B. Satyanarayana, G. R. Janardhana, and D. H. Rao, "Optimized high speed turning on Inconel 718 using Taguchi method based Grey relational analysis," 2013.
- [57] A. Aggarwal, H. Singh, P. Kumar, and M. Singh, "Optimization of multiple quality characteristics for CNC turning under cryogenic cutting environment using desirability function," *Journal of materials processing technology*, vol. 205, no. 1-3, pp. 42-50, 2008.
- [58] E. Oberg, F. Jones, H. Horton, and H. Ryffel, "Machinery's Handbook & Guide to Machinery's Handbook, 2008," ed: Industrial Press.
- [59] A. Shokrani, V. Dhokia, and S. T. Newman, "Environmentally conscious machining of difficult-to-machine materials with regard to cutting fluids," *International Journal of Machine Tools and Manufacture*, vol. 57, pp. 83-101, 2012/06/01/ 2012, doi: <https://doi.org/10.1016/j.ijmachtools.2012.02.002>.
- [60] W. Grzesik, *Advanced machining processes of metallic materials: theory, modelling and applications*. Elsevier, 2008.
- [61] V. P. Astakhov, "Tribology of metal cutting," 2006.
- [62] M. El Baradie, "Cutting fluids: Part I. characterisation," *Journal of materials processing technology*, vol. 56, no. 1-4, pp. 786-797, 1996.
- [63] L. C. Brandão, R. T. Coelho, and A. R. Rodrigues, "Experimental and theoretical

Reference

- study of workpiece temperature when end milling hardened steels using (TiAl) N-coated and PcBN-tipped tools," *Journal of materials processing Technology*, vol. 199, no. 1-3, pp. 234-244, 2008.
- [64] S. Y. Hong, I. Markus, and W.-c. Jeong, "New cooling approach and tool life improvement in cryogenic machining of titanium alloy Ti-6Al-4V," *International journal of machine tools and manufacture*, vol. 41, no. 15, pp. 2245-2260, 2001.
- [65] E. C. Jameson, *Electrical discharge machining*. Society of Manufacturing Engineers, 2001.
- [66] J. P. Davim, *Machining: fundamentals and recent advances*. Springer Science & Business Media, 2008.
- [67] D. B. Moulton, "Wire EDM the fundamentals," *Sugar Grove, IL: EDM network (www.notebookmanuals.bestmanualguide.Com)*, 1999.
- [68] P. Sharma, D. Chakradhar, and S. Narendranath, "Evaluation of WEDM performance characteristics of Inconel 706 for turbine disk application," *Materials & Design*, vol. 88, pp. 558-566, 2015/12/25/ 2015, doi: <https://doi.org/10.1016/j.matdes.2015.09.036>.
- [69] J. S. Binoj, N. Manikandan, P. Thejasree, K. C. Varaprasad, N. Prem Sai, and M. Manideep, "Machinability studies on wire electrical discharge machining of Nickel alloys using multiple regression analysis," *Materials Today: Proceedings*, vol. 39, pp. 155-159, 2021/01/01/ 2021, doi: <https://doi.org/10.1016/j.matpr.2020.06.407>.
- [70] R. Niemi, "Integrity prediction," *SME Technical Paper*, 1971.
- [71] C. H. Lund, *Oxidation of nickel-and cobalt-base superalloys*. Defense Metals Information Center, Battelle Memorial Institute, 1965.
- [72] A. Hart and R. Leach, *Review of methods for cleaning surfaces prior to surface texture measurement*. 2001.
- [73] S. Yang, W. Li, and H. Chen, *Surface finishing theory and new technology*. Springer, 2018.
- [74] S. Hashmi, *Comprehensive materials processing*. Newnes, 2014.
- [75] B. Choudhury and M. Chandrasekaran, "Investigation on welding characteristics of aerospace materials – A review," *Materials Today: Proceedings*, vol. 4, no. 8, pp. 7519-7526, 2017/01/01/ 2017, doi: <https://doi.org/10.1016/j.matpr.2017.07.083>.
- [76] C. Radhakrishna and K. P. Rao, "The formation and control of Laves phase in superalloy 718 welds," *Journal of Materials Science*, vol. 32, no. 8, pp. 1977-1984, 1997.
- [77] S. Manikandan, D. Sivakumar, K. P. Rao, and M. Kamaraj, "Effect of weld cooling rate on Laves phase formation in Inconel 718 fusion zone," *Journal of Materials Processing Technology*, vol. 214, no. 2, pp. 358-364, 2014.
- [78] X. Ye, X. Hua, M. Wang, and S. Lou, "Controlling hot cracking in Ni-based Inconel-718 superalloy cast sheets during tungsten inert gas welding," *Journal of Materials Processing Technology*, vol. 222, pp. 381-390, 2015.

Reference

- [79] N. Richards, R. Nakkalil, and M. Chaturvedi, "The influence of electron-beam welding parameters on heat-affected-zone microfissuring in INCOLOY 903," *Metallurgical and Materials Transactions A*, vol. 25, no. 8, pp. 1733-1745, 1994.
- [80] G. Peng, K.-f. ZHANG, B.-g. ZHANG, S.-s. JIANG, and B.-w. ZHANG, "Microstructures and high temperature mechanical properties of electron beam welded Inconel 718 superalloy thick plate," *Transactions of Nonferrous Metals Society of China*, vol. 21, pp. s315-s322, 2011.
- [81] M. Agilan, T. Venkateswaran, D. Sivakumar, and B. Pant, "Effect of heat input on microstructure and mechanical properties of inconel-718 EB Welds," *Procedia Materials Science*, vol. 5, pp. 656-662, 2014.
- [82] A. Chamanfar, M. Jahazi, A. Bonakdar, E. Morin, and A. Firoozrai, "Cracking in fusion zone and heat affected zone of electron beam welded Inconel-713LC gas turbine blades," *Materials Science and Engineering: A*, vol. 642, pp. 230-240, 2015.
- [83] S. Gobbi, L. Zhang, J. Norris, K. Richter, and J. Loreau, "High powder CO₂ and Nd YAG laser welding of wrought Inconel 718," *Journal of materials processing technology*, vol. 56, no. 1-4, pp. 333-345, 1996.
- [84] A. V. Reddy, K. P. Rao, and G. Reddy, "JK Sarin Sundar GD Janaki Ram," Microstructure and tensile properties of Inconel 718 pulsed Nd-YAG laser welds," *Journal of Materials Processing Technology*, vol. 167, no. 1, pp. 73-82, 2005.
- [85] Z. Hou, J. Sheikh-Ahmad, F. Jarrar, and F. Ozturk, "Residual stresses in dissimilar friction stir welding of AA2024 and AZ31: experimental and numerical study," *Journal of Manufacturing Science and Engineering*, vol. 140, no. 5, 2018.
- [86] Y. Sato, P. Arkom, H. Kokawa, T. Nelson, and R. Steel, "Effect of microstructure on properties of friction stir welded Inconel Alloy 600," *Materials Science and Engineering: A*, vol. 477, no. 1-2, pp. 250-258, 2008.
- [87] K. Song, H. Fujii, and K. Nakata, "Effect of welding speed on microstructural and mechanical properties of friction stir welded Inconel 600," *Materials & Design*, vol. 30, no. 10, pp. 3972-3978, 2009.
- [88] Y. Pardhi, *Metallurgy: Advances in Materials and Processes*. BoD–Books on Demand, 2012.
- [89] M. Sundararaman, S. Banerjee, and H. Mori, "The stability of gamma-double-prime and gamma-prime phases in Alloy 718 under electron irradiation," *Superalloys 718, 625, 706 and various derivatives*, pp. 379-387, 2001.
- [90] X. Z. Qin, J. Guo, C. Yuan, G. Yang, L. Zhou, and H. Ye, "A mu-Phase behavior in a cast Ni-base superalloy," *Journal of Materials Science*, vol. 44, pp. 4840-4847, 09/01 2009, doi: 10.1007/s10853-009-3738-7.
- [91] M. Sundararaman, P. Mukhopadhyay, and S. Banerjee, "Carbide precipitation in nickel base superalloys 718 and 625 and their effect on mechanical properties," *Superalloys*, vol. 718, pp. 625-706, 1997.
- [92] A. Szczotok and K. Rodak, "Microstructural studies of carbides in MAR-M247

Reference

- nickel-based superalloy," *IOP Conference Series: Materials Science and Engineering*, vol. 35, p. 012006, 2012/05/02 2012, doi: 10.1088/1757-899x/35/1/012006.
- [93] C. Rowolt, B. Milkereit, P. Andrezza, and O. Kessler, "Quantitative high temperature calorimetry on precipitation in steel and nickel alloys," *Thermochimica Acta*, vol. 677, 02/01 2019, doi: 10.1016/j.tca.2019.01.026.
- [94] A. Lavakumar, P. Singh, S. Srivastava, S. A. Kori, and L. A. Kumar, "Gamma Prime Coarsening Behavior of Nickel Super alloy Super cast 247 A after Prolonged Thermal Exposures," 2013.
- [95] N. El-Bagoury, "Microstructure and Mechanical Properties of Aged Nickel Base Superalloy," *Archives of Applied Science Research*, vol. 3, p. 266, 01/01 2011.
- [96] N. El-Bagoury and Q. Mohsen, "Gamma prime and TCP phases and mechanical properties of thermally exposed nickel-base superalloy," *Phase Transitions*, vol. 84, no. 11-12, pp. 1108-1122, 2011/11/01 2011, doi: 10.1080/01411594.2011.582379.
- [97] H. Kitaguchi, "Microstructure-property relationship in advanced Ni-based superalloys, Metallurgy–Advances in Materials and Processes," *InTech, DOI*, vol. 10, p. 52011, 2012.
- [98] H. Kitaguchi, *Microstructure-property relationship in advanced Ni-based superalloys*. chapter, 2012.
- [99] "Monel, Inconel, Nickel, and Nickel Alloys.," *Development and Research Division: International Nickel Company.*, 1947.
- [100] I. Monel, Nickel, and Nickel Alloys. Development and Research Division: International Nickel Company. 1947. (accessed.
- [101] ""Special Metals Corporation: History"." (accessed Archived from the original on April 21, 2008. Retrieved 2012-05-18.).
- [102] J. C. Lippold, S. D. Kiser, and J. N. DuPont, *Welding Metallurgy and Weldability of Nickel-Base Alloys*. Wiley, 2011.
- [103] W. S. Tait, "Chapter 27 - Controlling Corrosion of Chemical Processing Equipment," in *Handbook of Environmental Degradation of Materials (Third Edition)*, M. Kutz Ed.: William Andrew Publishing, 2018, pp. 583-600.
- [104] AEETHER. "Clearly Understand the 4 Roles of Chromium in Superalloys." (accessed.
- [105] P. Kontis, Z. Li, D. M. Collins, J. Cormier, D. Raabe, and B. Gault, "The effect of chromium and cobalt segregation at dislocations on nickel-based superalloys," *Scripta Materialia*, vol. 145, pp. 76-80, 2018/03/01/ 2018, doi: <https://doi.org/10.1016/j.scriptamat.2017.10.005>.
- [106] S. M. Corporation. "INCONEL® Alloy 617." (accessed.
- [107] S. M. Corporation. "INCONEL® Alloy 625." (accessed.
- [108] S. M. Corporation. "INCONEL® Alloy 718." (accessed.
- [109] D. Agarwal, "Nickel and nickel alloys," *Handbook of Advanced Materials*, p. 217, 2004.
- [110] X. Wang, Y. Ding, Y. Gao, Y. Ma, J. Chen, and B. Gan, "Effect of grain

- refinement and twin structure on the strength and ductility of Inconel 625 alloy," *Materials Science and Engineering: A*, vol. 823, p. 141739, 2021.
- [111] C. Rae, M. Karunaratne, C. Small, R. Broomfield, C. Jones, and R. Reed, "Topologically close packed phases in an experimental rhenium-containing single crystal superalloy," *Superalloys*, vol. 2000, pp. 767-776, 2000.
- [112] J. K. Tien and R. N. Jarrett, "Effects of Cobalt in Nickel-Base Superalloys," Dordrecht, 1982: Springer Netherlands, in *High Temperature Alloys for Gas Turbines 1982*, pp. 423-446.
- [113] S. M. Corporation. "INCONEL® Alloy X-750." (accessed.
- [114] G. D. Smith and N. C. Eisinger, "The effect of niobium on the corrosion resistance of nickel-base alloys," *Proceedings of the International Symposium on Niobium for High Temperature Applications*, pp. 23-34, 01/01 2004.
- [115] L. Zheng, C. P. Gu, and G. Q. Zhang, "Effect of Ta addition on microstructure of cast nickel base superalloys containing low level of Cr and high level of W," *RARE METAL MATERIALS AND ENGINEERING*, vol. 34, pp. 194-198, 02/01 2005.
- [116] G. Pigrova, S. Korkka, and T. Grebtsova, "Effect of silicon on the phase composition of nickel-base alloys," *Metal Science and Heat Treatment*, vol. 22, no. 4, pp. 274-277, 1980.
- [117] O. Sinha, M. Chatterjee, V. Sarma, and S. Jha, "Effect of residual elements on high performance nickel base superalloys for gas turbines and strategies for manufacture," *Bulletin of Materials Science*, vol. 28, no. 4, pp. 379-382, 2005.
- [118] J. Pelleg, *Mechanical properties of materials*. Springer Science & Business Media, 2012.
- [119] V. Shankar, K. Bhanu Sankara Rao, and S. L. Mannan, "Microstructure and mechanical properties of Inconel 625 superalloy," *Journal of Nuclear Materials*, vol. 288, no. 2, pp. 222-232, 2001/02/01/ 2001, doi: [https://doi.org/10.1016/S0022-3115\(00\)00723-6](https://doi.org/10.1016/S0022-3115(00)00723-6).
- [120] T. Sonar, V. Balasubramanian, S. Malarvizhi, T. Venkateswaran, and D. Sivakumar, "An overview on welding of Inconel 718 alloy - Effect of welding processes on microstructural evolution and mechanical properties of joints," *Materials Characterization*, vol. 174, p. 110997, 2021/04/01/ 2021, doi: <https://doi.org/10.1016/j.matchar.2021.110997>.
- [121] M. Balachander, *Microstructural characterization and thermal fatigue study of a coated Incoloy 909 Superalloy*. University of Manitoba (Canada), 2011.
- [122] T. Sonar, V. Balasubramanian, S. Malarvizhi, T. Venkateswaran, and D. Sivakumar, "Development of 3-Dimensional (3D) response surfaces to maximize yield strength and elongation of InterPulsed TIG welded thin high temperature alloy sheets for jet engine applications," *CIRP Journal of Manufacturing Science and Technology*, vol. 31, pp. 628-642, 2020/11/01/ 2020, doi: <https://doi.org/10.1016/j.cirpj.2020.09.003>.
- [123] G. M. Reddy, C. S. Murthy, K. S. Rao, and K. P. Rao, "Improvement of mechanical properties of Inconel 718 electron beam welds—influence of

Reference

- welding techniques and postweld heat treatment," *The International Journal of Advanced Manufacturing Technology*, vol. 43, no. 7, pp. 671-680, 2009.
- [124] G. J. Ram, A. V. Reddy, K. P. Rao, G. M. Reddy, and J. S. Sundar, "Microstructure and tensile properties of Inconel 718 pulsed Nd-YAG laser welds," *Journal of Materials Processing Technology*, vol. 167, no. 1, pp. 73-82, 2005.
- [125] G. Janaki Ram, A. Venugopal Reddy, K. Prasad Rao, and G. Madhusudhan Reddy, "Control of Laves phase in Inconel 718 GTA welds with current pulsing," *Science and technology of welding and joining*, vol. 9, no. 5, pp. 390-398, 2004.
- [126] K. Sivaprasad, S. G. S. Raman, P. Mastanaiah, and G. M. Reddy, "Influence of magnetic arc oscillation and current pulsing on microstructure and high temperature tensile strength of alloy 718 TIG weldments," *Materials Science and Engineering: A*, vol. 428, no. 1-2, pp. 327-331, 2006.
- [127] T. Sonar, V. Balasubramanian, S. Malarvizhi, T. Venkateswaran, and D. Sivakumar, "Effect of heat input on evolution of microstructure and tensile properties of gas tungsten constricted arc (GTCA) welded inconel 718 alloy sheets," *Metallography, Microstructure, and Analysis*, vol. 9, pp. 369-392, 2020.
- [128] K. Sivaprasad and S. G. S. Raman, "Influence of weld cooling rate on microstructure and mechanical properties of alloy 718 weldments," *Metallurgical and Materials Transactions A*, vol. 39, no. 9, pp. 2115-2127, 2008.
- [129] Z. Jia, X. Wan, and D. Guo, "Study on microstructure and mechanical properties of Inconel718 components fabricated by UHFP-GTAW technology," *Materials Letters*, vol. 261, p. 127006, 2020/02/15/ 2020, doi: <https://doi.org/10.1016/j.matlet.2019.127006>.
- [130] K. D. Ramkumar *et al.*, "Studies on the weldability, microstructure and mechanical properties of activated flux TIG weldments of Inconel 718," *Materials Science and Engineering: A*, vol. 639, pp. 234-244, 2015/07/15/ 2015, doi: <https://doi.org/10.1016/j.msea.2015.05.004>.
- [131] N. Anbarasan, S. Jerome, and S. G. K. Manikandan, "Hydrogen and molybdenum control on laves phase formation and tensile properties of inconel 718 GTA welds," *Materials Science and Engineering: A*, vol. 773, p. 138874, 2020/01/31/ 2020, doi: <https://doi.org/10.1016/j.msea.2019.138874>.
- [132] H. Kumar, G. N. Ahmad, and N. K. Singh, "Activated flux TIG welding of Inconel 718 super alloy in presence of tri-component flux," *Materials and Manufacturing Processes*, vol. 34, no. 2, pp. 216-223, 2019/01/25 2019, doi: 10.1080/10426914.2018.1532581.
- [133] K. Devendranath Ramkumar *et al.*, "Effect of filler wires and direct ageing on the microstructure and mechanical properties in the multi-pass welding of Inconel 718," *Journal of Manufacturing Processes*, vol. 18, pp. 23-45, 2015/04/01/ 2015, doi: <https://doi.org/10.1016/j.jmapro.2015.01.001>.
- [134] R. Cortés, E. Barragán, V. López, R. Ambriz, and D. Jaramillo, "Mechanical properties of Inconel 718 welds performed by gas tungsten arc welding," *The*

- International Journal of Advanced Manufacturing Technology*, vol. 94, no. 9, pp. 3949-3961, 2018.
- [135] A. Thomas, M. El-Wahabi, J. M. Cabrera, and J. M. Prado, "High temperature deformation of Inconel 718," *Journal of Materials Processing Technology*, vol. 177, no. 1, pp. 469-472, 2006/07/03/ 2006, doi: <https://doi.org/10.1016/j.jmatprotec.2006.04.072>.
- [136] K. Chen, J. Dong, Z. Yao, T. Ni, and M. Wang, "Creep performance and damage mechanism for Allvac 718Plus superalloy," *Materials Science and Engineering: A*, vol. 738, pp. 308-322, 2018.
- [137] P. Kontis, A. Kostka, D. Raabe, and B. Gault, "Influence of composition and precipitation evolution on damage at grain boundaries in a crept polycrystalline Ni-based superalloy," *Acta Materialia*, vol. 166, pp. 158-167, 2019.
- [138] X. Liu *et al.*, "High-temperature tensile and creep behaviour of Inconel 625 superalloy sheet and its associated deformation-failure micromechanisms," *Materials Science and Engineering: A*, vol. 829, p. 142152, 2022/01/01/ 2022, doi: <https://doi.org/10.1016/j.msea.2021.142152>.
- [139] R. Rai, J. Sahu, A. Pramanick, N. Paulose, D. Fernando, and S. Das, "Creep deformation micro-mechanisms of CM 247 DS LC Ni-base superalloy under relevant service condition," *Materials Characterization*, vol. 150, pp. 155-165, 2019.
- [140] Y. C. Lin, H. Yang, D.-G. He, and J. Chen, "A physically-based model considering dislocation–solute atom dynamic interactions for a nickel-based superalloy at intermediate temperatures," *Materials & Design*, vol. 183, p. 108122, 2019/12/05/ 2019, doi: <https://doi.org/10.1016/j.matdes.2019.108122>.
- [141] P. Ganesan, C. Renteria, and J. Crum, "Versatile Corrosion Resistance of INCONEL” alloy 625 in Various."
- [142] X. Tang, S. Wang, D. Xu, Y. Gong, J. Zhang, and Y. Wang, "Corrosion behavior of Ni-based alloys in supercritical water containing high concentrations of salt and oxygen," *Industrial & Engineering Chemistry Research*, vol. 52, no. 51, pp. 18241-18250, 2013.
- [143] H. Jang, C. Park, and H. Kwon, "Photoelectrochemical analysis on the passive film formed on Ni in pH 8.5 buffer solution," *Electrochimica Acta*, vol. 50, no. 16, pp. 3503-3508, 2005/05/30/ 2005, doi: <https://doi.org/10.1016/j.electacta.2004.12.027>.
- [144] M. A. Amin, N. El-Bagoury, M. Saracoglu, and M. Ramadan, "Electrochemical and corrosion behavior of cast re-containing inconel 718 alloys in sulphuric acid solutions and the effect of Cl," *Int. J. Electrochem. Sci*, vol. 9, no. 9, pp. 5352-5374, 2014.
- [145] T. Kurzynowski, I. Smolina, K. Kobiela, B. Kuźnicka, and E. Chlebus, "Wear and corrosion behaviour of Inconel 718 laser surface alloyed with rhenium," *Materials & Design*, vol. 132, pp. 349-359, 2017/10/15/ 2017, doi: <https://doi.org/10.1016/j.matdes.2017.07.024>.
- [146] K. D. Ramkumar *et al.*, "Effect of Mo-rich fillers in pulsed current gas tungsten

- arc welding of Inconel 718 for improved strength and hot corrosion resistance," *Journal of Materials Engineering and Performance*, vol. 26, no. 11, pp. 5620-5640, 2017.
- [147] M. Hernández-Rodríguez, M. Soria-Aguilar, J. Acevedo-Dávila, R. Ambriz-Rojas, and F. Curiel-López, "Welding input effect on the corrosion behavior and microstructure of heat treated GTAW welds of Inconel 718," *Int. J. Electrochem. Sci*, vol. 14, pp. 4083-4094, 2019.
- [148] S. Kumar, B. Satapathy, D. Pradhan, and G. S. Mahobia, "Effect of surface modification on the hot corrosion resistance of Inconel 718 at 700 °C," *Materials Research Express*, vol. 6, no. 8, p. 086549, 2019/05/10 2019, doi: 10.1088/2053-1591/ab1dc7.
- [149] C.-Y. Bai, Y.-J. Luo, and C.-H. Koo, "Improvement of high temperature oxidation and corrosion resistance of superalloy IN-738LC by pack cementation," *Surface and Coatings Technology*, vol. 183, no. 1, pp. 74-88, 2004/05/01/ 2004, doi: <https://doi.org/10.1016/j.surfcoat.2003.10.011>.
- [150] G. Wallwork, "The oxidation of alloys," *Reports on Progress in Physics*, vol. 39, no. 5, p. 401, 1976.
- [151] G. Greene and C. Finfrock, "Oxidation of Inconel 718 in air at high temperatures," *Oxidation of metals*, vol. 55, no. 5, pp. 505-521, 2001.
- [152] H. Wan *et al.*, "Effects of helium ion irradiation on the high temperature oxidation resistance of Inconel 718 alloy," *Surface and Coatings Technology*, vol. 363, pp. 34-42, 2019/04/15/ 2019, doi: <https://doi.org/10.1016/j.surfcoat.2019.02.021>.
- [153] H. M. Cobb, *The history of stainless steel*. Materials Park, Ohio: ASM International, 2010.
- [154] J. R. Davis and A. S. M. I. H. Committee, *Stainless Steels*. ASM International, 1994.
- [155] J. Davis, "Stainless steels," *Materials Park: ASM International*, 2000.
- [156] A. D. H. SERIES, "DESIGN GUIDELINES FOR THE SELECTION AND USE OF STAINLESS STEELS."
- [157] Britannica. "stainless steel." (accessed 19 January, 2022).
- [158] "Alloy 20 Datasheet." Rolled Alloys. (accessed).
- [159] T. Belesis. (2018, Winter 2018) Ferritic Stainless Steels. *Australian Stainless magazine*.
- [160] "What is Martensitic Stainless Steel and What Can It Do for Your business?," vol. 2022, ed. Ulbrich, 2020.
- [161] T. Collins. "Duplex Stainless Steels." (accessed).
- [162] "Duplex Stainless Steel, Lean Duplex and Super Duplex," vol. 2022, ed. montanstahl, 2017.
- [163] R. Brucker, "A Guide to Precipitation-Hardening Stainless Alloys," vol. 2022, ed. ulbrich, 14/Jan.
- [164] "17-7PH Stainless Steel: An Introduction to this Workhorse Stainless Alloy," vol. 2022, ed. ulbrich, 16/Sep.

- [165] *Austenitic Stainless Steels - New Aspects* (Austenitic stainless steels). IntechOpen, 2017.
- [166] K. Mukahiwa, *Microstructural Characterisation of Type 316 Austenitic Stainless Steels: Implications for Corrosion Fatigue Behaviour in PWR Primary Coolant*. The University of Manchester (United Kingdom), 2017.
- [167] M. F. McGuire, "Austenitic Stainless Steels," in *Stainless Steels for Design Engineers*: ASM International, 2008, p. 0.
- [168] M. F. McGuire, *Stainless steels for design engineers*. Materials Park, OH: ASM International, 2008.
- [169] S. Astafurov and E. Astafurova, "Phase composition of austenitic stainless steels in additive manufacturing: A review," *Metals*, vol. 11, no. 7, p. 1052, 2021.
- [170] J.-Y. Choi and W. Jin, "Strain induced martensite formation and its effect on strain hardening behavior in the cold drawn 304 austenitic stainless steels," *Scripta Materialia*, vol. 36, no. 1, pp. 99-104, 1997.
- [171] M. P. Brady, K. A. Unocic, M. J. Lance, M. L. Santella, Y. Yamamoto, and L. R. Walker, "Increasing the Upper Temperature Oxidation Limit of Alumina Forming Austenitic Stainless Steels in Air with Water Vapor," *Oxidation of Metals*, vol. 75, no. 5, pp. 337-357, 2011/06/01 2011, doi: 10.1007/s11085-011-9237-7.
- [172] outokumpu, "High temperature stainless steels," outokumpu.
- [173] M. O. Speidel, "Nitrogen containing austenitic stainless steels," *Materialwissenschaft und Werkstofftechnik: Entwicklung, Fertigung, Prüfung, Eigenschaften und Anwendungen technischer Werkstoffe*, vol. 37, no. 10, pp. 875-880, 2006.
- [174] M. Attaran, "The rise of 3-D printing: The advantages of additive manufacturing over traditional manufacturing," *Business Horizons*, Article vol. 60, no. 5, pp. 677-688, 2017, doi: 10.1016/j.bushor.2017.05.011.
- [175] B. Blakey-Milner *et al.*, "Metal additive manufacturing in aerospace: A review," *Materials and Design*, Article vol. 209, 2021, Art no. 110008, doi: 10.1016/j.matdes.2021.110008.
- [176] A. Vafadar, F. Guzzomi, A. Rassau, and K. Hayward, "Advances in metal additive manufacturing: A review of common processes, industrial applications, and current challenges," *Applied Sciences (Switzerland)*, Review vol. 11, no. 3, pp. 1-33, 2021, Art no. 1213, doi: 10.3390/app11031213.
- [177] A. Chabot, M. Rauch, and J. Y. Hascoët, "Towards a multi-sensor monitoring methodology for AM metallic processes," *Welding in the World*, Article vol. 63, no. 3, pp. 759-769, 2019, doi: 10.1007/s40194-019-00705-4.
- [178] T. Iso-Junno, K. K. Mäkelä, K. Mäntyjärvi, and T. Jokelainen. *A short glance on metal 3d am*, *Key Engineering Materials*, vol. 786 KEM, pp. 348-355, 2018.
- [179] D. Ding, Z. Pan, D. Cuiuri, and H. Li, "Wire-feed additive manufacturing of metal components: technologies, developments and future interests," *The International Journal of Advanced Manufacturing Technology*, vol. 81, no. 1, pp. 465-481, 2015.

- [180] C. Lieberwirth, A. Harder, and H. Seitz, "Extrusion based additive manufacturing of metal parts," *Journal of Mechanics Engineering and Automation*, vol. 7, no. 2, pp. 79-83, 2017.
- [181] B. Wu *et al.*, "A review of the wire arc additive manufacturing of metals: properties, defects and quality improvement," *Journal of Manufacturing Processes*, vol. 35, pp. 127-139, 2018/10/01/ 2018, doi: <https://doi.org/10.1016/j.jmapro.2018.08.001>.
- [182] L. P. Raut and R. V. Taiwade, "Wire Arc Additive Manufacturing: A Comprehensive Review and Research Directions," *Journal of Materials Engineering and Performance*, vol. 30, no. 7, pp. 4768-4791, 2021/07/01 2021, doi: 10.1007/s11665-021-05871-5.
- [183] T. A. Rodrigues, V. Duarte, R. M. Miranda, T. G. Santos, and J. P. Oliveira, "Current Status and Perspectives on Wire and Arc Additive Manufacturing (WAAM)," *Materials*, vol. 12, no. 7, p. 1121, 2019. [Online]. Available: <https://www.mdpi.com/1996-1944/12/7/1121>.
- [184] S. W. Williams, F. Martina, A. C. Addison, J. Ding, G. Pardal, and P. Colegrove, "Wire + Arc Additive Manufacturing," *Materials Science and Technology*, vol. 32, no. 7, pp. 641-647, 2016/05/02 2016, doi: 10.1179/1743284715Y.0000000073.
- [185] F. Martina, J. Ding, S. Williams, A. Caballero, G. Pardal, and L. Quintino, "Tandem metal inert gas process for high productivity wire arc additive manufacturing in stainless steel," *Additive Manufacturing*, vol. 25, pp. 545-550, 2019/01/01/ 2019, doi: <https://doi.org/10.1016/j.addma.2018.11.022>.
- [186] C. Wu, L. Wang, W. Ren, and X. Zhang, "Plasma arc welding: Process, sensing, control and modeling," *Journal of manufacturing processes*, vol. 16, no. 1, pp. 74-85, 2014.
- [187] P. Kah, "Chapter 1 - Gas metal arc welding," in *Advancements in Intelligent Gas Metal Arc Welding Systems*, P. Kah Ed.: Elsevier, 2021, pp. 1-103.
- [188] C. Pickin and K. Young, "Evaluation of cold metal transfer (CMT) process for welding aluminium alloy," *Science and Technology of Welding and Joining*, vol. 11, no. 5, pp. 583-585, 2006.
- [189] V. Dhinakaran, J. Ajith, A. F. Y. Fahmidha, T. Jagadeesha, T. Sathish, and B. Stalin, "Wire Arc Additive Manufacturing (WAAM) process of nickel based superalloys—A review," *Materials Today: Proceedings*, vol. 21, pp. 920-925, 2020.
- [190] J. Singh, K. S. Arora, and D. K. Shukla, "Dissimilar MIG-CMT weld-brazing of aluminium to steel: A review," *Journal of Alloys and Compounds*, vol. 783, pp. 753-764, 2019/04/30/ 2019, doi: <https://doi.org/10.1016/j.jallcom.2018.12.336>.
- [191] L. Marin, "Numerical solution of the Cauchy problem for steady-state heat transfer in two-dimensional functionally graded materials," *International Journal of Solids and Structures*, vol. 42, no. 15, pp. 4338-4351, 2005.
- [192] W. Pompe *et al.*, "Functionally graded materials for biomedical applications,"

Reference

- Materials Science and Engineering: A*, vol. 362, no. 1-2, pp. 40-60, 2003.
- [193] L. Lu, M. Chekroun, O. Abraham, V. Maupin, and G. Villain, "Mechanical properties estimation of functionally graded materials using surface waves recorded with a laser interferometer," *NDT & E International*, vol. 44, no. 2, pp. 169-177, 2011.
- [194] E. Mueller, Č. Drašar, J. Schilz, and W. Kaysser, "Functionally graded materials for sensor and energy applications," *Materials Science and Engineering: A*, vol. 362, no. 1-2, pp. 17-39, 2003.
- [195] R. M. Mahamood, E. T. Akinlabi, M. Shukla, and S. L. Pityana, "Functionally graded material: an overview," 2012.
- [196] B. Onuike and A. Bandyopadhyay, "Additive manufacturing of Inconel 718–Ti6Al4V bimetallic structures," *Additive Manufacturing*, vol. 22, pp. 844-851, 2018.
- [197] M. R. U. Ahsan, A. N. M. Tanvir, T. Ross, A. Elsayy, M.-S. Oh, and D. B. Kim, "Fabrication of bimetallic additively manufactured structure (BAMS) of low carbon steel and 316L austenitic stainless steel with wire+ arc additive manufacturing," *Rapid Prototyping Journal*, 2020.
- [198] B. Wu *et al.*, "Enhanced interface strength in steel-nickel bimetallic component fabricated using wire arc additive manufacturing with interweaving deposition strategy," *Journal of Materials Science & Technology*, vol. 52, pp. 226-234, 2020.
- [199] L. Liu, Z. Zhuang, F. Liu, and M. Zhu, "Additive manufacturing of steel–bronze bimetal by shaped metal deposition: interface characteristics and tensile properties," *The International Journal of Advanced Manufacturing Technology*, vol. 69, no. 9-12, pp. 2131-2137, 2013.
- [200] A. R. Kannan, S. M. Kumar, N. P. Kumar, N. S. Shanmugam, A. Vishnu, and Y. Palguna, "Process-microstructural features for tailoring fatigue strength of wire arc additive manufactured functionally graded material of SS904L and Hastelloy C-276," *Materials Letters*, vol. 274, p. 127968, 2020.
- [201] Y. Tian, J. Shen, S. Hu, J. Gou, and E. Kannatey-Asibu, "Wire and arc additive manufactured Ti–6Al–4V/Al–6.25 Cu dissimilar alloys by CMT-welding: effect of deposition order on reaction layer," *Science and Technology of Welding and Joining*, 2019.
- [202] M. R. Ahsan *et al.*, "Microstructures and mechanical behavior of the bimetallic additively-manufactured structure (BAMS) of austenitic stainless steel and Inconel 625," *Journal of Materials Science & Technology*, vol. 74, pp. 176-188, 2021.
- [203] P. A. Colegrove *et al.*, "Microstructure and residual stress improvement in wire and arc additively manufactured parts through high-pressure rolling," *Journal of Materials Processing Technology*, vol. 213, no. 10, pp. 1782-1791, 2013.
- [204] W. J. Sames, F. List, S. Pannala, R. R. Dehoff, and S. S. Babu, "The metallurgy and processing science of metal additive manufacturing," *International materials reviews*, vol. 61, no. 5, pp. 315-360, 2016.

Reference

- [205] H. Mayer, M. Papakyriacou, B. Zettl, and S. Stanzl-Tschegg, "Influence of porosity on the fatigue limit of die cast magnesium and aluminium alloys," *International journal of fatigue*, vol. 25, no. 3, pp. 245-256, 2003.
- [206] M. Kobayashi, Y. Dorce, H. Toda, and H. Horikawa, "Effect of local volume fraction of microporosity on tensile properties in Al–Si–Mg cast alloy," *Materials Science and Technology*, vol. 26, no. 8, pp. 962-967, 2010.
- [207] A. P. Boeira, I. L. Ferreira, and A. Garcia, "Alloy composition and metal/mold heat transfer efficiency affecting inverse segregation and porosity of as-cast Al–Cu alloys," *Materials & Design*, vol. 30, no. 6, pp. 2090-2098, 2009.
- [208] C. L. M. Da Silva and A. Scotti, "The influence of double pulse on porosity formation in aluminum GMAW," *Journal of materials processing technology*, vol. 171, no. 3, pp. 366-372, 2006.
- [209] F. Wang, S. Williams, P. Colegrove, and A. A. Antonysamy, "Microstructure and Mechanical Properties of Wire and Arc Additive Manufactured Ti-6Al-4V," *Metallurgical and Materials Transactions A*, vol. 44, no. 2, pp. 968-977, 2013/02/01 2013, doi: 10.1007/s11661-012-1444-6.
- [210] B. Cong, J. Ding, and S. Williams, "Effect of arc mode in cold metal transfer process on porosity of additively manufactured Al-6.3% Cu alloy," *The International Journal of Advanced Manufacturing Technology*, vol. 76, no. 9-12, pp. 1593-1606, 2015.
- [211] T. Marazani, D. M. Madyira, and E. T. Akinlabi, "Repair of Cracks in Metals: A Review," *Procedia Manufacturing*, vol. 8, pp. 673-679, 2017/01/01/ 2017, doi: <https://doi.org/10.1016/j.promfg.2017.02.086>.
- [212] R. J. Dexter and J. M. Ocel, "Manual for repair and retrofit of fatigue cracks in steel bridges," United States. Federal Highway Administration, 2013.
- [213] A. Nedoseka, "3 - Load-carrying capacity of welded structures," in *Fundamentals of Evaluation and Diagnostics of Welded Structures*, A. Nedoseka Ed.: Woodhead Publishing, 2012, pp. 183-321.
- [214] G. Pluvinage, J. Capelle, and C. Schmitt, "Chapter 3 - Methods for assessing defects leading to gas pipe failure," in *Handbook of Materials Failure Analysis with Case Studies from the Oil and Gas Industry*, A. S. H. Makhlof and M. Aliofkhazraei Eds.: Butterworth-Heinemann, 2016, pp. 55-89.
- [215] P. Hart, "Hydrogen cracking-its causes, costs and future occurrence," in *Proceedings: 1st International Conference*, 1999, pp. 1-1.
- [216] K. Yushchenko, V. Savchenko, N. Chervyakov, A. ZVYAGINTSEVA, G. MONKO, and V. PESTOV, "Investigation of cracking susceptibility of austenitic material using PVR-test procedure," *The Paton Welding J*, vol. 6, no. 7, pp. 10-13, 2014.
- [217] S. Kou, "Solidification and liquation cracking issues in welding," *Jom*, vol. 55, no. 6, pp. 37-42, 2003.
- [218] J. Borland, "Fundamentals of solidification cracking in welds.-II," *Welding and Metal Fabrication*, vol. 47, no. 2, pp. 99-107, 1979.
- [219] C. Huang and S. Kou, "Liquation cracking in full-penetration Al-Cu welds,"

- WELDING JOURNAL-NEW YORK*-, vol. 83, no. 2, pp. 50-S, 2004.
- [220] G. Agarwal, "Study of solidification cracking during laser welding in advanced high strength steels: A combined experimental and numerical approach," 2019.
- [221] R. Thavamani, V. Balusamy, J. Nampoothiri, R. Subramanian, and K. Ravi, "Mitigation of hot cracking in Inconel 718 superalloy by ultrasonic vibration during gas tungsten arc welding," *Journal of Alloys and Compounds*, vol. 740, pp. 870-878, 2018.
- [222] M. G Mousavi, "Grain refinement and elimination of hot cracks due to application of electromagnetic stirring in commercial aluminum alloy welds," in *Advanced Materials Research*, 2014, vol. 875: Trans Tech Publ, pp. 1306-1311.
- [223] T. Artaza, T. Bhujangrao, A. Suárez, F. Veiga, and A. Lamikiz, "Influence of Heat Input on the Formation of Laves Phases and Hot Cracking in Plasma Arc Welding (PAW) Additive Manufacturing of Inconel 718," *Metals*, vol. 10, no. 6, p. 771, 2020. [Online]. Available: <https://www.mdpi.com/2075-4701/10/6/771>.
- [224] J. Gu, J. Bai, J. Ding, S. Williams, L. Wang, and K. Liu, "Design and cracking susceptibility of additively manufactured Al-Cu-Mg alloys with tandem wires and pulsed arc," *Journal of Materials Processing Technology*, vol. 262, pp. 210-220, 2018.
- [225] A. A. Edidin, "38 - Development and Application of the Small Punch Test to UHMWPE," in *UHMWPE Biomaterials Handbook (Third Edition)*, S. M. Kurtz Ed. Oxford: William Andrew Publishing, 2016, pp. 739-752.
- [226] M. P. Manahan, A. S. Argon, and O. K. Harling, "The development of a miniaturized disk bend test for the determination of postirradiation mechanical properties," *Journal of Nuclear Materials*, vol. 104, pp. 1545-1550, 1981.
- [227] C. Rodríguez, J. G. Cabezas, E. Cárdenas, F. Belzunce, and C. Betegón, "Mechanical properties characterization of heat-affected zone using the small punch test," *Weld. J*, vol. 88, no. 9, pp. 188-92, 2009.
- [228] C. Haden, G. Zeng, F. Carter III, C. Ruhl, B. Krick, and D. Harlow, "Wire and arc additive manufactured steel: Tensile and wear properties," *Additive manufacturing*, vol. 16, pp. 115-123, 2017.
- [229] N. Sridharan, M. W. Noakes, A. Nycz, L. J. Love, R. R. Dehoff, and S. S. Babu, "On the toughness scatter in low alloy C-Mn steel samples fabricated using wire arc additive manufacturing," *Materials Science and Engineering: A*, vol. 713, pp. 18-27, 2018.
- [230] B. Yilbas, S. S. Akhtar, and C. Karatas, "Laser surface treatment of Inconel 718 alloy: thermal stress analysis," *Optics and Lasers in Engineering*, vol. 48, no. 7-8, pp. 740-749, 2010.
- [231] Y. Chen *et al.*, "Dendritic microstructure and hot cracking of laser additive manufactured Inconel 718 under improved base cooling," *Journal of Alloys and Compounds*, vol. 670, pp. 312-321, 2016/06/15/ 2016, doi: <https://doi.org/10.1016/j.jallcom.2016.01.250>.
- [232] V. Shankar, T. Gill, S. Mannan, and S. Sundaresan, "Solidification cracking in

- austenitic stainless steel welds," *Sadhana*, vol. 28, no. 3-4, pp. 359-382, 2003.
- [233] R. Zhang *et al.*, "Mechanical properties and microstructure of additively manufactured stainless steel with laser welded joints," *Materials & Design*, p. 109921, 2021.
- [234] M. Rafieezad, M. Ghaffari, A. V. Nemani, and A. Nasiri, "Microstructural evolution and mechanical properties of a low-carbon low-alloy steel produced by wire arc additive manufacturing," *The International Journal of Advanced Manufacturing Technology*, vol. 105, no. 5, pp. 2121-2134, 2019.
- [235] Y. Ma, D. Cuiuri, C. Shen, H. Li, and Z. Pan, "Effect of interpass temperature on in-situ alloying and additive manufacturing of titanium aluminides using gas tungsten arc welding," *Additive Manufacturing*, vol. 8, pp. 71-77, 2015.
- [236] O. Popović, R. Prokić, M. Burzić, and Z. Milutinović, "The effect of heat input on the weld metal toughness of surface welded joint," in *Faculty of Mechanical Engineering, University of Belgrade, Serbia: presented in 14th International Research/Expert Conference "Trends in the Development of Machinery and Associated Technology", Mediterranean Cruise, 2010: Citeseer*, pp. 11-18.
- [237] W. Jin, C. Zhang, S. Jin, Y. Tian, D. Wellmann, and W. Liu, "Wire arc additive manufacturing of stainless steels: a review," *Applied sciences*, vol. 10, no. 5, p. 1563, 2020.
- [238] C. E. Seow, H. E. Coules, G. Wu, R. H. Khan, X. Xu, and S. Williams, "Wire+ Arc Additively Manufactured Inconel 718: Effect of post-deposition heat treatments on microstructure and tensile properties," *Materials & Design*, vol. 183, p. 108157, 2019.
- [239] C. E. Seow *et al.*, "Effect of crack-like defects on the fracture behaviour of Wire+ Arc Additively Manufactured nickel-base Alloy 718," *Additive Manufacturing*, vol. 36, p. 101578, 2020.
- [240] M. Komarasamy, S. Shukla, S. Williams, K. Kandasamy, S. Kelly, and R. S. Mishra, "Microstructure, fatigue, and impact toughness properties of additively manufactured nickel alloy 718," *Additive Manufacturing*, vol. 28, pp. 661-675, 2019.
- [241] V. Shankar, T. Gill, S. Mannan, and P. Rodriguez, "A review of hot cracking in austenitic stainless steel weldments," 1991.
- [242] C.-C. Hsieh and W. Wu, "Overview of intermetallic sigma (σ) phase precipitation in stainless steels," *International Scholarly Research Notices*, vol. 2012, 2012.
- [243] Z. Kuboň, Š. Stejskalová, and L. Kander, "Effect of Sigma Phase on Fracture Behavior of Steels and Weld Joints of Components in Power Industry Working at Supercritical Conditions," *Austenitic Stainless Steels-New Aspects, IntechOpen*, pp. 63-92, 2017.
- [244] C. Fink, M. Zinke, and D. Keil, "Evaluation of hot cracking susceptibility of nickel-based alloys by the PVR test," *Welding in the World*, vol. 56, no. 7, pp. 37-43, 2012.
- [245] M. Montazeri, F. M. Ghaini, and O. Ojo, "Heat input and the liquation cracking

Reference

- of laser welded IN738LC superalloy," *Weld. J.*, vol. 92, no. 9, pp. 258s-264s, 2013.
- [246] Y. Mei *et al.*, "Effect of base metal and welding speed on fusion zone microstructure and HAZ hot-cracking of electron-beam welded Inconel 718," *Materials & Design*, vol. 89, pp. 964-977, 2016.
- [247] E. Lucon, E. Lucon, J. Benzing, and N. Hrabe, *Development and validation of small punch testing at NIST*. US Department of Commerce, National Institute of Standards and Technology, 2020.
- [248] M. Bruchhausen *et al.*, "European standard on small punch testing of metallic materials," in *Pressure Vessels and Piping Conference*, 2017, vol. 57908: American Society of Mechanical Engineers, p. V01AT01A065.
- [249] H. Eskandari Sabzi and P. E. J. Rivera-Díaz-del-Castillo, "Composition and process parameter dependence of yield strength in laser powder bed fusion alloys," *Materials & Design*, vol. 195, p. 109024, 2020/10/01/ 2020, doi: <https://doi.org/10.1016/j.matdes.2020.109024>.
- [250] P. Li, Y. Gong, Y. Xu, Y. Qi, Y. Sun, and H. Zhang, "Inconel-steel functionally bimetal materials by hybrid directed energy deposition and thermal milling: Microstructure and mechanical properties," *Archives of Civil and Mechanical Engineering*, vol. 19, no. 3, pp. 820-831, 2019/09/01 2019, doi: 10.1016/j.acme.2019.03.002.